Check for updates

NEUROSCIENCE

Distinct properties of glutamate-dopamine, nonglutamate-dopamine, and glutamate-only ventral tegmental area neurons

Copyright © 2026 The Authors, some rights reserved; exclusive licensee American Association for the Advancement of Science. No claim to original U.S. Government Works

Emily D. Prévost[1], Lucy A. Ward[1], Daniel Alas[1], Giulia A. Aimale[1], Sara K. Ikenberry[1], Katie Fox[1], Melissa Deming[1], Julianne Pelletier[1], Annie Ly[1], Jayson Ball[1], Zachary P. Kilpatrick[2], Kailyn Price[3], Abigail M. Polter[3], Fabio Simões de Souza[1], Suzanne Fulgham[1], Yoon Seok Kim[4]†, Lief E. Fenno[4]‡, Charu Ramakrishnan[4], Karl Deisseroth[4,5,6], David H. Root[1]*

Dopamine neurons in the ventral tegmental area (VTA) have roles in motivation, learning, and psychiatric disorders. We found that genetically defined VTA dopamine neuron subtypes had distinct electrophysiological properties, neuronal signaling dynamics in response to reward- and aversion-related stimuli, and roles in somatic optogenetically induced reward dependent on the neurotransmitters they released. Nonglutamate-dopamine neurons increased activity after reward-related stimuli and decreased activity after the omission of an expected reward (negative reward prediction error) and aversion-related stimuli. Glutamate-dopamine and glutamate-only (nonGABAergic and nondopaminergic) neurons were activated by both rewarding and aversive events, but only glutamate-dopamine neurons had sustained cue-induced reward signaling. Recordings of all dopamine neurons without considering glutamate cotransmission showed mixed population responses during prediction error and aversive stimuli that obscured the distinct signaling patterns of its constituent subpopulations. Although the examined cell types largely differ in mediolateral location, cell-type identity better accounted for functional differences than mediolateral location. Glutamate-dopamine neurons were more excitable than nonglutamate-dopamine neurons. Glutamate-dopamine and nonglutamate-dopamine axons had similar but not identical dopamine release dynamics in the nucleus accumbens. Only nonglutamate-dopamine neurons supported somatic optogenetically induced reward and reinforcement. In glutamate-dopamine neurons, the dopamine synthetic enzyme TH contributed to associative learning of aversive or less-beneficial outcomes, whereas the vesicular glutamate transporter VGLUT2 contributed to reward- and exploration-related vigor. Our results suggest that glutamate cotransmission is a distinguishing feature of VTA dopamine neuron signaling patterns and roles in natural reward- or aversion-motivated behavior.

INTRODUCTION

Dopamine neurons in the ventral tegmental area (VTA) regulate motivation-related behaviors and contribute to psychiatric disorders through their influence on attaining rewards or avoiding punishment (*1*). VTA dopamine function is crucial to several behavioral processes, including causal learning (*2*), associative learning (*3*, *4*), incentive salience (*5*), updating value-based expectations through prediction error (*6*), and more (*7*–*15*). Reflecting their diverse functions, VTA dopamine neurons are heterogeneous in their signaling patterns related to motivational valence or salience (*7*, *16*–*28*). Further, although network connectivity (*29*–*37*) and anatomical subdivisions of the VTA (*38*–*42*) influence VTA dopamine neuron function, it is less clear how molecular identity (*1*, *29*, *43*, *44*) might contribute to the multitude of functions and signaling patterns ascribed to VTA dopamine neurons.

A primary distinction between subtypes of VTA dopamine neurons is whether they cotransmit dopamine and glutamate or release dopamine without glutamate (*39*, *40*). Glutamate-dopamine cotransmitting neurons differ from the wider population of all glutamate neurons in some motivated behaviors (*45*), but it is unknown how the mutually exclusive populations of glutamate-dopamine and nonglutamate-dopamine populations differ in their contributions to motivated behaviors related to naturally rewarding or aversive outcomes and their predictors. Further, because VTA glutamate neurons can cotransmit glutamate with dopamine, cotransmit glutamate with GABA, or transmit glutamate alone, it is unclear whether glutamate-dopamine neurons differ functionally from other glutamatergic VTA subpopulations, especially the as-of-yet uncharacterized population that releases only glutamate (without GABA or dopamine cotransmission). It has been theorized that cotransmission of a fast-acting neurotransmitter (such as glutamate) together with a slow-acting monoamine (such as dopamine) can expand the computational capabilities of neuronal circuits (*46*–*48*). Nevertheless, it remains unclear how glutamate and dopamine from glutamate-dopamine cotransmitting neurons individually contribute to natural reward- or aversion-motivated behaviors.

Here, we untangled glutamate-dopamine neurons from nonglutamate-dopamine and glutamate-only (nonGABAergic and nondopaminergic) neurons and identified the roles of glutamate and dopamine release mechanisms from glutamate-dopamine cotransmitting neurons toward behaviors motivated by naturally rewarding and aversive stimuli. Our strategy leveraged intersectional and subtractive genetics

[1]Department of Psychology and Neuroscience, University of Colorado, 2860 Wilderness Pl, Boulder, CO 80301, USA. [2]Department of Applied Mathematics, University of Colorado, 1111 Engineering Center, Boulder, CO 80309, USA. [3]Department of Pharmacology and Physiology, George Washington University, Washington, DC 20052, USA. [4]Department of Psychiatry and Behavioral Sciences, Stanford University, Stanford, CA 94305, USA. [5]Department of Bioengineering, Stanford University, Stanford, CA 94305, USA. [6]Howard Hughes Medical Institute, Stanford University, Stanford, CA 94305, USA.
†Present address: Institute of Bioengineering, École Polytechnique Fédérale de Lausanne (EPFL), CH-1015 Lausanne, Switzerland.
‡Present address: Departments of Psychiatry and Neuroscience, University of Texas at Austin, Austin, TX 78701, USA.
*Corresponding author. Email: david.root@colorado.edu

Downloaded from https://www.science.org at University of Colorado Boulder on November 21, 2026

to apply cell-type precision to ex vivo whole-cell recordings, in vivo Ca^{2+} recordings, optogenetics combined with in vivo dopamine sensors or motivated behavior, and neurotransmission-related knockdown from genetically defined neurons. We found that glutamate-dopamine, nonglutamate-dopamine, and glutamate-only neurons differentially signaled cued rewards, negative reward prediction error, and cued and uncued aversive stimuli and had separable electrophysiological properties and excitability. A subset of glutamate-only neurons exhibited commonly used electrophysiological markers of dopaminergic neurons, such as presence of a hyperpolarization-induced current (I_h) and D_2/D_3 receptor inhibition, whereas glutamate-dopamine neurons largely lacked I_h. We also found that glutamate-dopamine and nonglutamate-dopamine axons in the nucleus accumbens (NAcc) had similar but not identical dopamine release dynamics. Across multiple measures, glutamate-dopamine neurons were distinguished by a more sustained pattern of neuronal activity and a higher functional limit of neuronal output compared with nonglutamate-dopamine neurons. Experiments recording all dopamine neurons without considering glutamate cotransmission yielded intermediate results between glutamate-dopamine and nonglutamate-dopamine activation patterns, suggesting that separation of glutamate-dopamine from nonglutamate-dopamine neurons is critical for identifying motivation-related VTA dopamine functions. Further, whereas glutamatergic and nonglutamatergic cell types are largely located in the medial or lateral VTA, motivation-related signaling dynamics were better explained by the neurotransmitter identity of VTA cell types than by their mediolateral anatomical location within the sampled range. Somatic optogenetic stimulation of nonglutamate-dopamine neurons supported reward and reinforcement but was not observed with glutamate-dopamine or glutamate-only neurons. Further, we found that in glutamate-dopamine neurons, the vesicular glutamate transporter 2 (VGluT2) was necessary for the vigor of attaining rewards without affecting natural reward intake or reward learning, whereas the dopamine synthetic enzyme tyrosine hydroxylase (TH) was necessary for associative learning related to negative or aversive events without affecting avoidance behaviors or responses to nonassociative aversive stimuli. We also present a neural population model incorporating dopaminergic subtypes that recapitulated the roles of distinct neurotransmitters from glutamate-dopamine cotransmitting neurons. We interpret these results such that glutamate cotransmission is a key distinguishing feature of VTA dopamine neuron function in natural reward- or aversion-motivated behavior.

RESULTS

Intersectional and subtractive cell-type targeting strategies

To genetically access glutamate-dopamine, nonglutamate-dopamine, and glutamate-only neurons (defined as glutamatergic neurons that are nonGABAergic and nondopaminergic) in the VTA, we generated two double transgenic mouse lines. For dopamine subtypes, *Vglut2::Cre* mice were crossed with *Th::Flp* mice. Double transgenic *Vglut2::Cre*/*Th::Flp* offspring were injected in the VTA with INTRSECT adeno-associated viruses (AAVs) that expressed GCaMP6m in neurons expressing both Cre and Flp (Cre-ON/Flp-ON[Con/Fon]-GCaMP) to label glutamate-dopamine neurons or in neurons expressing Flp without Cre (Cre-OFF/Flp-ON[Coff/Fon]-GCaMP) to label nonglutamate-dopamine neurons (Fig. 1A) as previously shown (*37*). To compare dopamine subpopulation results with those of all dopamine neurons, a separate group of single recombinase *Th::Flp* mice were injected in the VTA with Coff/Fon-GCaMP to label all dopamine neurons without taking into account whether these neurons release dopamine alone or together with glutamate (Fig. 1A). To select glutamate-only neurons, we crossed *Vgat::Cre* mice with *Th::Flp* mice. Double transgenic *Vgat::Cre*/*Th::Flp* offspring were injected in the VTA with AAVs that expressed GCaMP6m in an INTRSECT Cre-Or-Flp-Off (COFO-GCaMP6m) process-of-elimination strategy to label nonGABAergic/nondopaminergic glutamatergic VTA neurons incapable of cotransmitting GABA or dopamine (Fig. 1A). INTRSECT vectors have been used to discriminate glutamate-GABA cotransmitting neurons from nonGABA-glutamate neurons and nonglutamate-GABA neurons in the VTA (*42*, *49*, *50*), but the subtractive COFO strategy uniquely enables isolation of glutamate-only neurons in the VTA. Consistent with prior localizations of *Vglut2*- and TH-expressing VTA neurons (*38*, *39*, *51*–*54*), nonglutamate-dopamine neurons were found laterally (Fig. 1, B to F), glutamate-dopamine neurons were near the midline, and both nonglutamate-dopamine and glutamate-dopamine neurons comingled at the boundary of the medial and lateral VTA (Fig. 1, G to K). We profiled the GCaMP-labeled neurons for the expression of transcripts encoding *Slc17a6* (*Vglut2*) and *Th*. In *Vglut2::Cre*/*Th::Flp* mice injected in the VTA with Con/Fon vectors targeting glutamate-dopamine neurons, 96.02 ± 1.9% of GCaMP-labeled neurons expressed both *Vglut2* and *Th* mRNA, and very few neurons (3.42 ± 1.7%) expressed *Th* mRNA without *Vglut2* mRNA (Fig. 1L). In contrast, for *Vglut2::Cre*/*Th::Flp* mice injected in the VTA with Coff/Fon vectors targeting nonglutamate-dopamine neurons, 97.4 ± 0.72% of GCaMP-labeled neurons expressed *Th* mRNA without *Vglut2* mRNA, and very few neurons (2.49 ± 0.69%) expressed both *Vglut2* and *Th* mRNAs (Fig. 1L). In a separate group of *Vglut2::Cre*/*Th::Flp* mice, we coinjected in the VTA AAVs encoding Coff/Fon-GCaMP6m with Con/Fon-SRGECO and determined TH protein coexpression. We found that both cell types were immunoreactive for TH in ~90% of labeled VTA neurons (fig. S1, A to E).

For *Vgat::Cre*/*Th::Flp* mice injected in the VTA with AAVs encoding COFO-GCaMP6m to target glutamate-only neurons, labeled neurons were most often observed around the midline, consistent with prior literature (*38*, *39*, *51*) (Fig. 1, M to R). We profiled the GCaMP-labeled neurons for the expression of transcripts encoding *Vglut2* and *Vgat*, as well as for TH immunoreactivity. Of GCaMP-labeled neurons, 89.9 ± 0.59% expressed *Vglut2* mRNA without *Vgat* mRNA or TH immunoreactivity coexpression (Fig. 1S). Other cell types labeled were sparse, varying between 0 and 3.15% of GCaMP-labeled neurons, which likely reflects a small population of Cre- or Flp-lacking VTA neurons in the *Vgat::Cre*/*Th::Flp* line. In separate groups of mice, we labeled glutamate-dopamine, nonglutamate-dopamine, and glutamate-dopamine neurons with ChRmine-oScarlet and show representative distributions across three anterior-posterior planes (fig. S2). Together, INTRSECT vectors effectively targeted nonglutamate-dopamine neurons, glutamate-dopamine neurons, all dopamine neurons, and glutamate-only neurons.

Ex vivo electrophysiological properties among cell types

Features such as I_h, high capacitance, electrophysiological response to dopamine D_2/D_3 receptor agonism, and pacemaker firing with broad action potentials have been used as electrophysiological markers of dopamine neurons, although the reliability of these markers has been called into question (*32*, *55*). We therefore examined distribution

Downloaded from https://www.science.org at University of Colorado Boulder on November 21, 2026

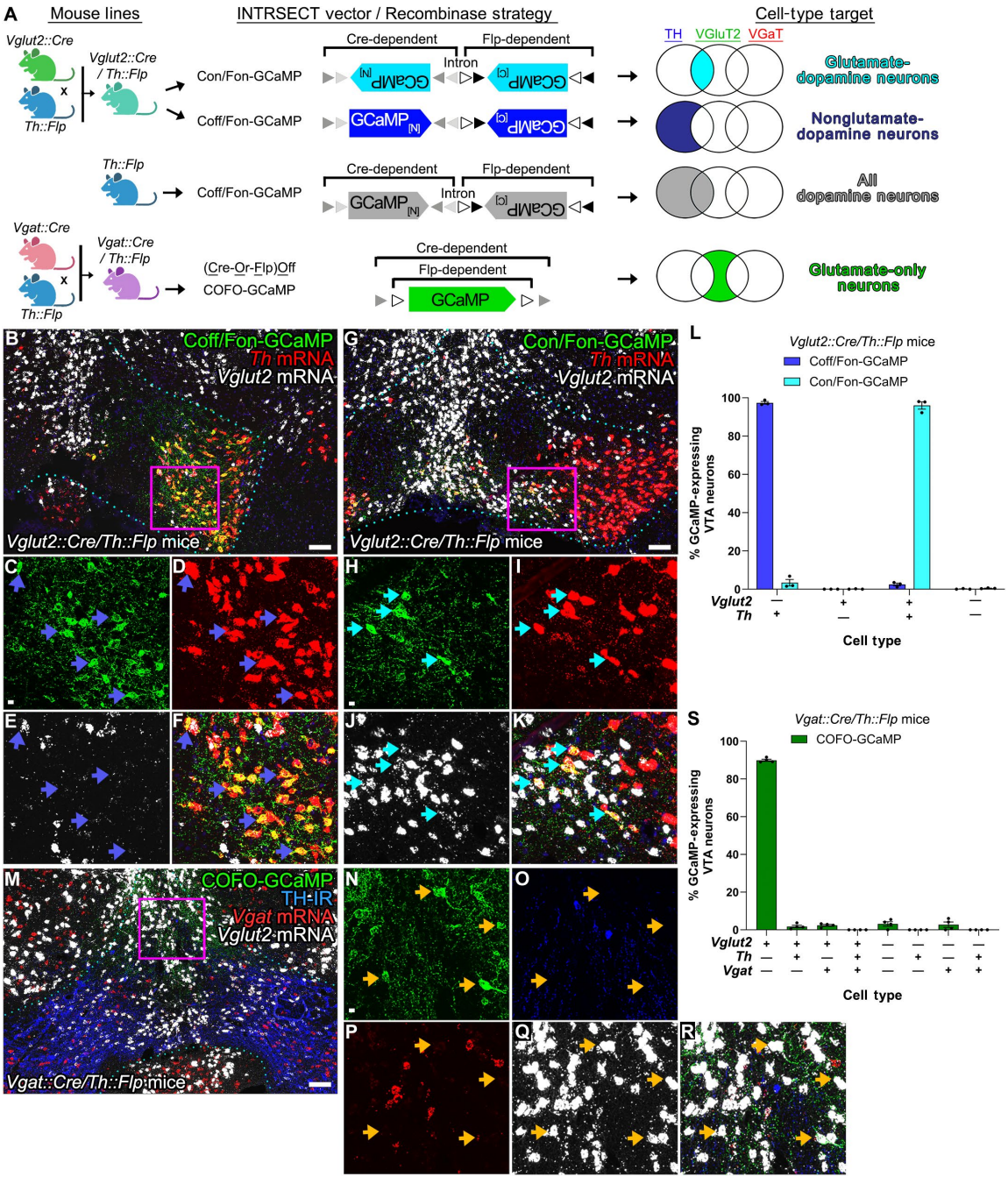


Fig. 1. Genetic access to dopaminergic and glutamatergic cell types in the VTA. (**A**) Neuronal targeting strategies. *Vglut2::Cre* mice were crossed with *Th::Flp* mice. *Vglut2::Cre/Th::Flp* offspring were injected in the VTA with INTRSECT AAVs encoding GCaMP6m in a Cre AND Flp manner (Con/Fon) to target glutamate-dopamine neurons or a NOT Cre AND Flp manner (Coff/Fon) to target nonglutamate-dopamine neurons. In *Th::Flp* mice, Coff/Fon vectors target all dopamine neurons (glutamate-dopamine neurons and nonglutamate-dopamine neurons). To target glutamate-only neurons, *Vgat::Cre* mice were crossed with *Th::Flp* mice. *Vgat::Cre/Th::Flp* offspring were injected in the VTA with an INTRSECT AAV encoding GCaMP6m in a NOT(Cre or Flp) manner to select neurons that do not release GABA or dopamine, which in the VTA selects neurons that only release glutamate. C, Cre; F, Flp; on, must express; off, must not express. [N], N terminus; [C], C terminus. Gray triangles, Cre recognition targets loxP (light) and lox2722 (dark). Black triangles, Flp recognition targets F3 (black outline) and F5 (solid black). (**B** to **F**) Coff/Fon GCaMP neurons were examined for *Th* mRNA (red) and *Vglut2* mRNA (white). Blue arrows indicate GCaMP *Vglut2*$^{-}$/*Th*$^{+}$ neurons. Images are representative of $N = 5$ to 7 VTA sections per mouse from three mice per group. Bregma = −3.28 mm. (**G** to **K**) Con/Fon-GCaMP6m neurons were examined for *Th* mRNA (red) and *Vglut2* mRNA (white). Cyan arrows indicate GCaMP-expressing *Vglut2*$^{+}$/*Th*$^{+}$ neurons. Images are representative of $N = 7$ to 9 VTA sections per mouse from three mice. Bregma = −3.16 mm. (**L**) Quantification of GCaMP expression. $N = 5$ to 9 VTA sections per mouse from three mice per group (one male and five female). (**M** to **R**) *Vgat::Cre/Th::Flp* mice were injected in the VTA with COFO-GCaMP6m. GCaMP-labeled neurons were examined for TH protein immunoreactivity (blue), *Vgat* mRNA (red), and *Vglut2* mRNA (white). Orange arrows indicate GCaMP *Vglut2*$^{+}$/TH^{-}/*Vgat*$^{-}$ neurons. Images are representative of $N = 4$ to 6 VTA sections per mouse from four mice. Bregma = −3.40 mm. (**S**) Quantification of GCaMP expression. $N = 4$ to 6 VTA sections per mouse from four mice (three male and one female). Scale bars in (B), (G), and (M), 100 μm. Scale bars in (C), (H), and (N), 10 μm, which also apply to (D) to (F), (I) to (K), and (O) to (R), respectively.

Downloaded from https://www.science.org at University of Colorado Boulder on November 21, 2026

of these and other electrophysiological properties in VTA glutamate-dopamine, nonglutamate-dopamine, and glutamate-only neurons ex vivo (Fig. 2A). *Vglut2::Cre*/*Th::Flp* mice were injected in the VTA with a mixture of AAVs encoding Con/Fon-eYFP and Coff/Fon-mCherry to label glutamate-dopamine neurons in eYFP and nonglutamate-dopamine neurons in mCherry. *Vgat::Cre*/*Th::Flp* mice were injected in the VTA with an AAV encoding COFO-oScarlet to label glutamate-only neurons in oScarlet. Capacitance and input resistance did not differ between the three cell types, whereas the resting membrane potential was more hyperpolarized in glutamate-only neurons relative to the other two dopaminergic cell types (table S1). I_h was observed in about 61.5% of glutamate-only neurons and in 35.7% of nonglutamate-dopamine neurons (Fig. 2, B to D). However, detectable I_h was found in very few glutamate-dopamine neurons (11.1%). Whole-cell spontaneous action potentials also differed between the three cell types. Action potential half-width was broadest in nonglutamate-dopamine neurons and narrowest in glutamate-only neurons, whereas glutamate-dopamine neurons showed intermediate half-widths (Fig. 2, E and F). The magnitude of the afterhyperpolarization (AHP) was significantly smaller in glutamate-dopamine neurons than nonglutamate-dopamine or glutamate-only neurons (Fig. 2G). Spontaneous cell-attached firing rates were highest in glutamate-only neurons and lowest in nonglutamate-dopamine neurons, with firing rates of glutamate-dopamine neurons again intermediate between the two (Fig. 2, H and I). Although cell-attached firing of at least some cells from each cell type was inhibited in response to bath application of the dopamine D_2/D_3 receptor agonist quinpirole, D_2/D_3 receptor sensitivity was universal among nonglutamate-dopamine neurons but only found in 55 to 60% of glutamate-dopamine and glutamate-only neurons (Fig. 2J). In response to hyperpolarization (Fig. 2K), 78% of glutamate-only neurons showed rebound firing of action potentials, whereas 8% or no cells exhibited this property among glutamate-dopamine or nonglutamate-dopamine neurons, respectively (Fig. 2L). Last, glutamate-only and glutamate-dopamine neurons showed more sustained and robust excitability compared with nonglutamate-dopamine neurons in response to increasing depolarizing current injections (Fig. 2, K and M). Together, these data suggest that glutamate-only and glutamate dopamine neurons have several features that allow for sustained firing across a linear range of frequencies, such as faster action potentials and smaller after hyperpolarizations. In contrast, nonglutamate-dopamine neurons have a more limited range of excitability, predominantly firing at low frequencies, even when depolarized. Although dopaminergic neurons rarely burst in slice preparations, it is possible that these nonglutamate-dopamine neurons may exhibit the more canonical dopaminergic firing pattern of slow tonic firing punctuated by stimulus-driven bursts in vivo.

We then performed dimensionality reduction and cluster analysis to determine whether electrophysiological profiles clustered better with anatomical location or molecular cell type of the recorded cell. Whole-cell recorded neurons were categorized according to both molecular cell type and whether they were located proximally (medial) or distally (lateral) to 0.40 mm from the midline. We used Uniform Manifold Approximation and Projection (UMAP) to reduce all whole-cell electrophysiological properties of individual neurons (Fig. 2N) into a two-dimensional projection (Fig. 2, O and P). Neurons with similar electrophysiological profiles clustered more closely to one another. Silhouette scores, a measure of clustering quality, were calculated according to whether neurons were classified by mediolateral location (Fig. 2O) or molecular cell type (Fig. 2P). We found that both mediolateral categorization (silhouette score = −0.02) and cell-type categorization (silhouette score = −0.08) produced clusters of poor quality (Fig. 2Q). Together, VTA glutamate-dopamine, nonglutamate-dopamine, and glutamate-only subpopulations differed considerably in single measures of electrophysiological characteristics, but their multidimensional repertoires of electrophysiological properties were not predicted by cell type or anatomical location in the VTA.

In vivo signaling dynamics during natural reward- and aversion-motivated behaviors differ among cell types

To determine whether VTA cell types differed in signaling of motivated behaviors, we expressed GCaMP6m in either VTA glutamate-dopamine neurons (fig. S3A), nonglutamate-dopamine neurons (fig. S3B), all dopamine neurons (fig. S3C), or glutamate-only neurons (fig. S3D) and implanted an optic fiber in the VTA (fig. S3E). Mice were trained to associate an auditory stimulus (CS+) with sucrose reward delivery and a different auditory stimulus (CS−) with no reward delivery (Fig. 3A). All groups learned to increase reward port entries during the CS+ (CS+ hits) (Fig. 3B) and decrease reward port entries during the CS− (CS− hits) (Fig. 3C). Although some statistically significant differences were observed between groups during the earliest training days, there were no group differences in CS+ hits or CS− hits during the last 4 days of training before neuronal recordings (Fig. 3B). After reaching training criteria, GCaMP mice were recorded in a single session under the same paradigm, with the exception that 11% of trials presented the CS+ cue but the reward was omitted to probe for negative reward prediction error signaling. Negative reward prediction error was defined as suppression of neuronal activity below baseline at the time of reward omission and is a critical component of the wider reward prediction error hypothesis (*13*). We otherwise compared pretrial baseline neuronal activity with cue- and outcome-related neuronal activity in each cell type. When cue- or outcome-related activity was greater than baseline, we compared maximum normalized dF values at each event (to identify activation peaks). When cue- or outcome-related activity was lower than baseline, we compared minimum values (to identify suppressions in activity).

All cell types showed an increase in neuronal activity from baseline after both the reward-predictive CS+ and reward delivery (Fig. 3, D to G). Two types of VTA dopamine neurons are distinguished by transient or sustained cued reward-related activity (*56*). Here, we found that transient and sustained activity in cued reward was cell type specific. Glutamate-dopamine neurons showed sustained activity, in which activity was statistically indistinguishable between CS+ and just before reward delivery. In contrast, transient activity was observed in glutamate-only neurons, nonglutamate-dopamine neurons, and all dopamine neurons, consisting of a statistically significant reduction in activity between CS+ and just before reward delivery (Fig. 3, H and I).

Prediction error signaling is thought to be a critical function of VTA dopamine neurons (*6*, *13*, *57*). We probed each cell type for negative reward prediction error signaling by omitting reward during a subset of CS+ trials (Fig. 3J). We found that negative reward prediction error signaling was cell type specific. In part mediated by their transient CS+ activation pattern, nonglutamate-dopamine neurons showed significantly suppressed activity from baseline during reward omission, reflective of negative reward prediction error. In contrast, by virtue of the neurons' sustained CS+ activation pattern, glutamate-

Downloaded from https://www.science.org at University of Colorado Boulder on November 21, 2026

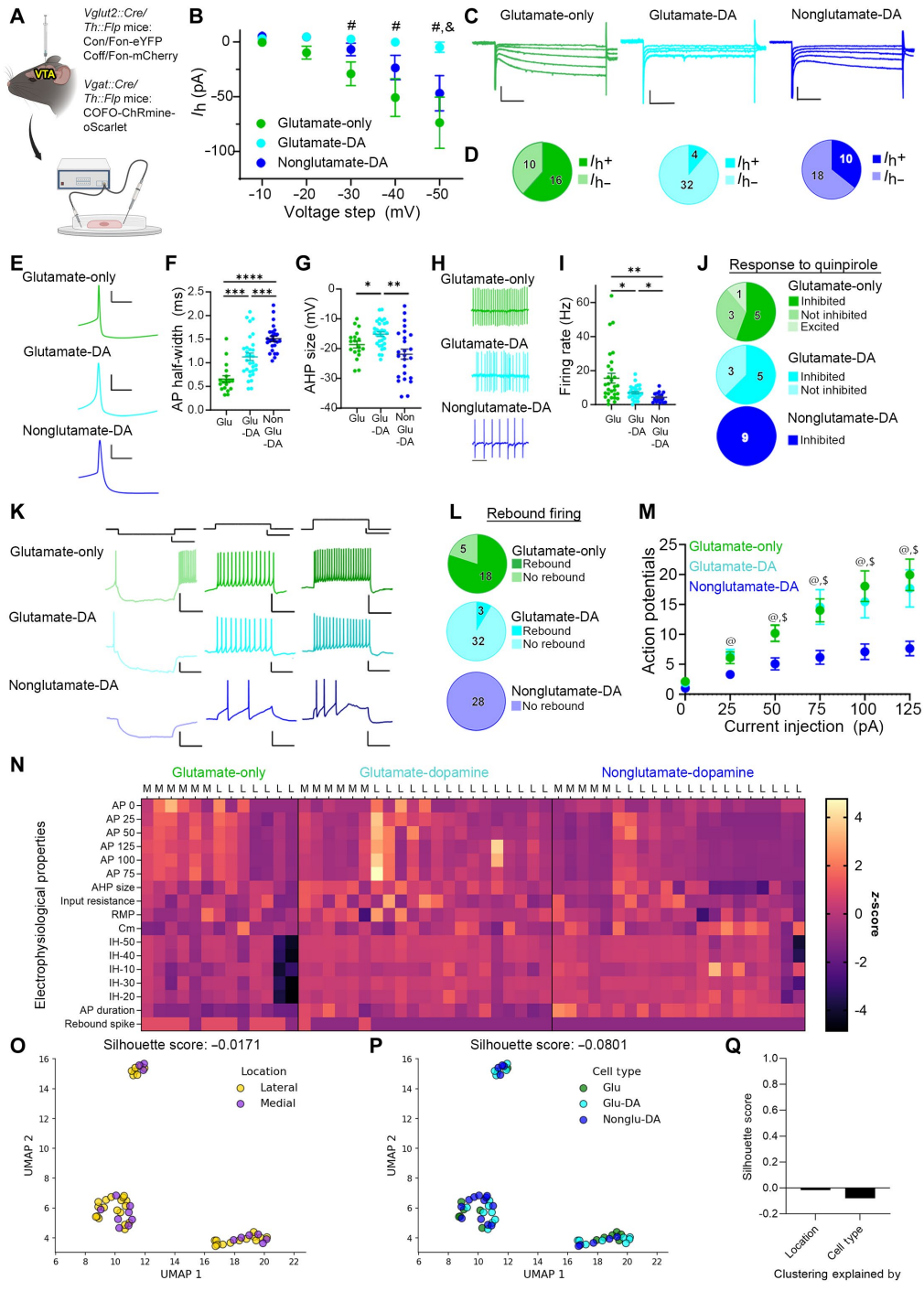


Fig. 2. Electrophysiological properties of dopaminergic and glutamatergic cell types in the VTA. (**A**) Schematic of INTRSECT viral targeting and fluorescence-guided electrophysiological recordings. (**B**) I_h in VTA neurons across a range of hyperpolarizing steps. Two-way repeated measures ANOVA, cell type × voltage step: $F(8,360) = 5.57$, $P < 0.001$. Tukey's multiple comparisons test: #$P < 0.05$, glutamate-only compared with glutamate-dopamine; $P < 0.05$ for nonglutamate-dopamine compared with glutamate-dopamine. $N = 29$ to 37 VTA neurons from six to nine mice per group (eight male and six female). (**C**) Representative traces of hyperpolarization-induced currents from each cell type. Scale bars: 100 pA, 100 ms. (**D**) Pie charts representing the number of cells that were I_h+ (maximal current >25 pA) or I_h- (maximal current <25 pA). Inset numbers represent the number of cells in each category. χ^2 test (17.38,2): $P < 0.001$. $N = 26$ to 36 VTA neurons from six to nine mice per group (eight male and six female). (**E**) Representative averages of 20 spontaneous action potentials. Scale bars: 20 mV, 10 ms. (**F**) Action potential duration (half-width of spontaneous action potentials) measured in whole-cell configuration. One-way ANOVA: $F(2,71) = 29.34$, $P < 0.0001$. Tukey's multiple comparisons test: ***$P < 0.001$; ****$P < 0.0001$. $N = 18$ to 31 VTA neurons from six to nine mice per group (eight male and six female). (**G**) AHP magnitude of spontaneous action potentials measured in whole-cell configuration. Welch's ANOVA test $W(2,39.18) = 7.98$, $P = 0.001$. *$P < 0.05$; **$P < 0.01$ by Dunnett's multiple comparisons test. $N = 18$ to 31 VTA neurons from six to nine mice per group (eight male and six female). (**H**) Representative traces of cell-attached action potential firing from each cell type. Scale bar, 500 ms. (**I**) Cell-attached firing rate. Welch's ANOVA test: $W(2,47.04) = 10.05$. Dunnett's multiple comparisons test: $P < 0.001$. *$P < 0.05$; **$P < 0.01$. $N = 21$ to 29 VTA neurons from five to eight mice per group (seven male and six female). (**J**) Pie charts representing the number of cells in which the cell-attached firing rate was inhibited, excited, or unaffected by bath application of 1 μM quinpirole. Inset numbers represent the number of cells in each category. Fisher's exact test: $P = 0.100$. $N = 8$ or 9 VTA neurons from five to seven mice per group (six male and six female). (**K**) Representative traces of evoked action potentials in response to −50 pA, 50 pA, and 100 pA current injections. Scale bars, 50 pA, 100 ms (top row); 10 mV, 100 ms (bottom three rows). (**L**) Pie charts showing the number of cells that exhibited rebound firing of action potentials after hyperpolarization. Inset numbers indicate the number of cells in each category. Fisher's exact test: $P < 0.001$. $N = 23$ to 35 VTA neurons from six to nine mice per group (eight male and six female). (**M**) Input-output function of action potentials generated by depolarizing current injections. Mixed-effects model: $F(10,369) = 4.37$, $P < 0.001$. Tukey post hoc tests: @$P < 0.05$, glutamate-dopamine compared with nonglutamate-dopamine; \$$P < 0.05$, glutamate-only compared with nonglutamate-dopamine. $N = 20$ to 28 VTA neurons from six to nine mice per group (eight male and six female). (**N**) Heatmap of electrophysiological characteristics of whole-cell recorded neurons. Each column represents one neuron, grouped by molecular cell type and labeled with medial "M" or lateral "L" VTA location. Electrophysiological measurements were *z*-scored for heatmap visualization only. The rebound spike variable is reported as 1 = rebound spike present or −1 = rebound spike absent. AP 0 to 125, input-output function of action potentials generated by depolarizing current injections from 0 to 125 pA. Cm, specific membrane capacitance. IH-10 to IH-50, hyperpolarization-induced currents from voltage steps −10 to −50 mV. RMP, resting membrane potential. $N = 18$ to 21 VTA neurons from six to nine mice per group (eight male and six female). (**O** to **Q**) UMAP projections of electrophysiological characteristics in (N) for recorded neurons clustered by anatomical location (O) or molecular cell type (P). Silhouette scores (Q) quantify the quality of clustering.

Downloaded from https://www.science.org at University of Colorado Boulder on November 21, 2026

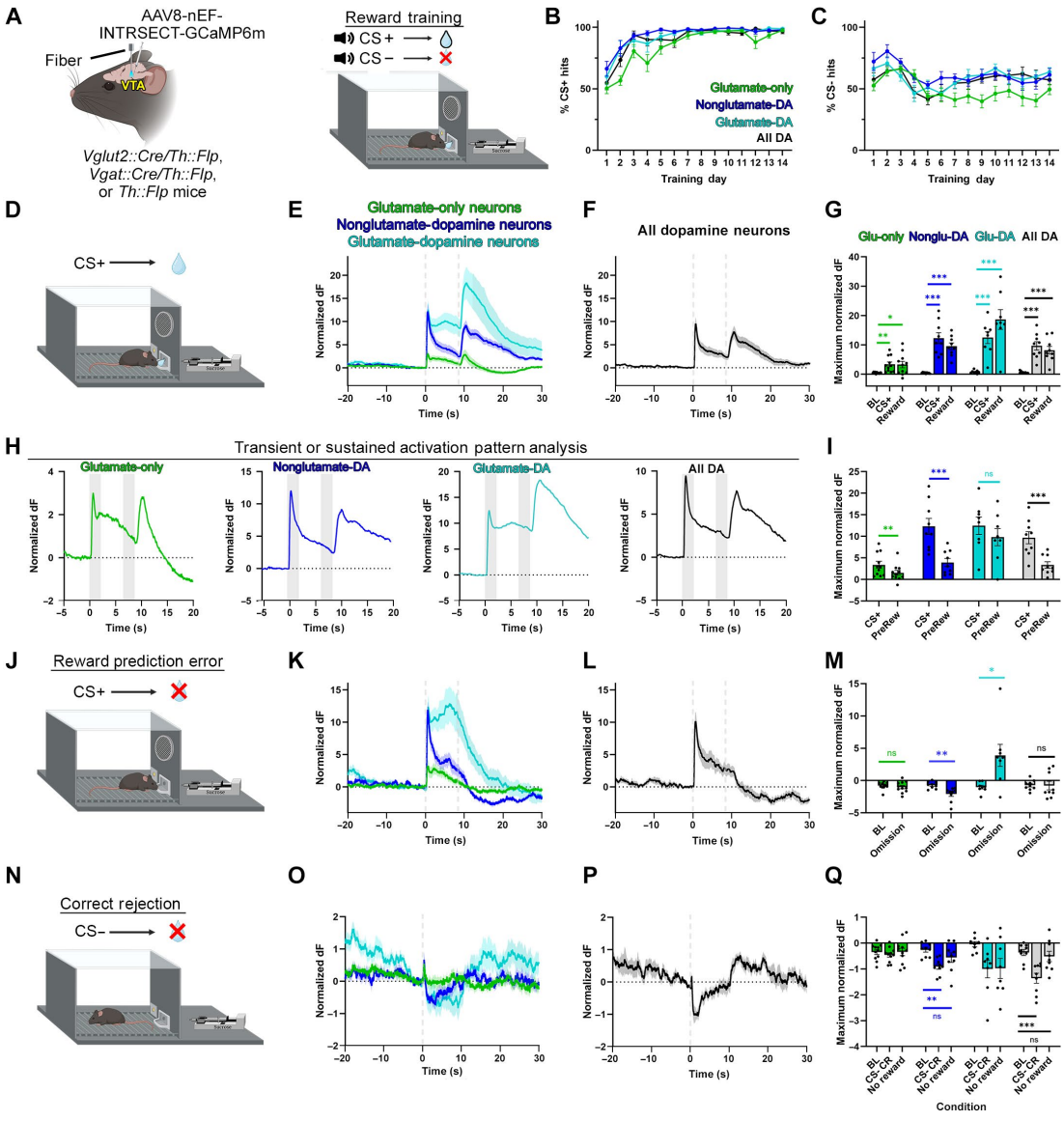


Fig. 3. Cell type–specific cued reward-related signaling. (**A**) Mice were tested on a Pavlovian reward task. $N = 8$ to 11 mice per group (17 male and 11 female). (**B**) Average (±SEM) percentage of reward port entries during CS+ trials or CS− trials over training days across groups. CS+ hits: two-way repeated measures ANOVA, day × group interaction $F(39,429) = 2.06$, $P = 0.020$. (**C**) Average (±SEM) percentage of reward port entries during CS− trials over training days across groups. CS− hits: two-way repeated measures ANOVA, day × group interaction $F(39,429) = 1.68$, $P = 0.008$. (**D**) GCaMP neuronal activity was assessed during CS+ hit trials. (**E**) CS+ hit–related neuronal activity for glutamate-only (green), nonglutamate-dopamine (dark blue), and glutamate-dopamine (cyan) neurons. (**F**) CS+ hit–related neuronal activity for all dopamine neurons. (**G**) Comparison of maximum neuronal activity between baseline, CS+, and reward epochs. Glutamate-only neurons: repeated measures ANOVA, effect of epoch $F(2,20) = 8.27$, $P = 0.012$, post hoc simple contrast tests: BL × CS+ $F(1,10) = 13.64$, $P = 0.004$; BL × reward $F(1,10) = 6.81$, $P = 0.026$. Nonglutamate-dopamine neurons: repeated measures ANOVA, effect of epoch $F(2,16) = 40.17$, $P < 0.001$, post hoc simple contrast tests: BL × CS+ $F(1,8) = 41.52$, $P < 0.001$; BL × reward $F(1,8) = 62.11$, $P < 0.001$. Glutamate-dopamine neurons: repeated measures ANOVA, effect of epoch $F(2,14) = 22.65$, $P < 0.001$, post hoc simple contrast tests: BL × CS+ $F(1,7) = 37.67$, $P < 0.001$; BL × reward $F(1,7) = 29.52$, $P < 0.001$. All dopamine neurons: repeated measures ANOVA, effect of epoch $F(2,16) = 34.13$, $P < 0.001$, post hoc simple contrast tests: BL × CS+ $F(1,8) = 42.19$, $P < 0.001$; BL × reward $F(1,8) = 33.45$, $P < 0.001$. (**H**) Analysis of cell type–specific transient and sustained cued reward signaling. Traces of normalized, averaged neuronal activity in (E) and (F) with *y* axes adjusted to depict transient or sustained activation patterns. Gray bars indicate CS+ and prereward epochs. (**I**) Comparison of maximum neuronal activity between CS+ and prereward epochs. Glutamate-only neurons: paired samples *t* test, $t(10) = 3.71$, $P = 0.004$. Nonglutamate-dopamine neurons: paired samples *t* test, $t(8) = 8.47$, $P < 0.001$. Glutamate-dopamine neurons: paired samples *t* test, $t(7) = 1.39$, $P = 0.207$. All dopamine neurons: paired samples *t* test, $t(8) = 6.56$, $P < 0.001$. (**J**) Neuronal activity during CSe and reward omission trials in which mice entered the reward port. For reward omission, minimum normalized dF values were taken from 1 to 3 s after normal reward offset in CS+ trials. Paired samples *t* tests compared minimum normalized dF at baseline and at reward omission to identify suppressions in activity indicative of negative reward prediction error. (**K**) Reward omission related neuronal activity for glutamate-only (green), nonglutamate-dopamine (dark blue), and glutamate-dopamine (cyan) neurons. (**L**) Reward omission–related neuronal activity for all dopamine neurons. (**M**) Comparison of minimum neuronal activity between baseline and reward omission. Glutamate-only neurons: paired samples *t* test, $t(10) = 0.69$, $P = 0.507$. Nonglutamate-dopamine neurons: paired samples *t* test, $t(8) = 4.55$, $P = 0.002$. Glutamate-dopamine neurons: paired samples *t* test, $t(7) = -2.30$, $P = 0.020$. All dopamine neurons: paired samples *t* test, $t(8) = 0.08$, $P = 0.938$. (**N**) Neuronal signaling during correct rejection trials in which mice did not enter the reward port during CS− trials. Minimum normalized dF values were taken from 0 to 2 s surrounding each event. (**O**) Correct rejection–related neuronal activity for glutamate-only (green), nonglutamate-dopamine (dark blue), and glutamate-dopamine (cyan) neurons. (**P**) Correct rejection–related neuronal activity for all dopamine neurons. (**Q**) Comparison of maximum neuronal activity between baseline, CS−, and correct rejection. Glutamate-only neurons: repeated measures ANOVA, no effect of epoch. Nonglutamate-dopamine neurons: repeated measures ANOVA, effect of epoch $F(2,16) = 6.46$, $P = 0.009$, post hoc simple contrast tests BL × CS− $F(1,8) = 22.74$, $P = 0.001$, BL × no reward $F(1,8) = 2.08$, $P = 0.187$. Glutamate-dopamine neurons: repeated measures ANOVA, no effect of epoch. All dopamine neurons: repeated measures ANOVA, effect of epoch $F(2,16) = 17.74$, $P < 0.001$; post hoc simple contrast tests BL × CS− $F(1,8) = 44.17$, $P < 0.001$, BL × no reward $F(1,8) = 0.77$, $P = 0.405$. BL, baseline epoch; CSe, CS error/CS+ epoch in reward omission trials; CR, correct rejection; PreRew, prereward epoch. Dashed lines on peri-event time histograms represent onset of respective cues and reward/nonreward events. Bar graphs represent group averages (±SEM) of maximum or minimum neuronal activity during baseline, cue, and reward/nonreward event epochs. Symbols represent individual mice. ns, not significant, *$P < 0.05$, **$P < 0.01$, and ***$P < 0.001$.

Downloaded from https://www.science.org at University of Colorado Boulder on November 21, 2026

dopamine neuronal activity remained elevated above baseline at the time of reward omission. When recording from all dopamine neurons without consideration for glutamate cotransmission, we observed variable responses at reward omission that were statistically indistinguishable from baseline activity, likely reflecting the opposing activity of suppressed (transient) nonglutamate-dopamine neurons and elevated (sustained) glutamate-dopamine neurons. Glutamate-only neurons showed a small but statistically nonsignificant decrease in activity during reward omission (Fig. 3, K to M).

Signaling related to the CS− that predicted no reward delivery was also cell type specific. We examined the majority of CS− trials in which mice did not enter the reward port (correct rejections) (Fig. 3N). Nonglutamate-dopamine neurons and all dopamine neurons showed significantly suppressed activity from baseline at the CS− during correct rejection trials, followed by a return to baseline during the time of no reward delivery. Together with their negative prediction error signaling, suppressed activity in nonglutamate-dopamine neurons appeared to coincide with the recognition that reward was not forthcoming. Glutamate-only and glutamate-dopamine neurons showed no significant changes in CS-related signaling (Fig. 3, O to Q).

The responses of VTA dopamine neurons to naturally aversive stimuli can vary widely (*16*–*20*, *23*, *28*, *58*). Therefore, we next determined cell type–specific signaling related to naturally aversive conditions in both cued and uncued tasks. Mice were first trained to associate a CS+ with footshock delivery and a CS− with no footshock delivery. We found that neuronal signaling at the aversion-predictive CS+ and at footshock itself was cell type specific (Fig. 4A). Both glutamate-only and glutamate-dopamine neurons showed increased activity after CS+ and shock compared with baseline, with glutamate-dopamine neurons showing elevated activity at both events (Fig. 4, B to D). In contrast, nonglutamate-dopamine neurons showed suppressed activity during the CS+ and shock relative to baseline (Fig. 4, B and E). When recording from all dopamine neurons without consideration for glutamate cotransmission, we observed intermediate activity levels between nonglutamate-dopamine neurons and glutamate-dopamine neurons consisting of significantly increased activity at CS+ and shock (Fig. 4, C and D). Thus, the all-dopamine population is a mixed population that obscures the distinct aversion-related signaling dynamics of its constituent glutamate-dopamine and nonglutamate-dopamine subpopulations. On the basis of our observation of cell type–specific sustained or transient cued reward signaling, we next examined whether the footshock-predicting CS+ led to cell type–specific sustained or transient responses. Glutamate-only neuron activity was sustained between CS+ and immediately before footshock. Glutamate-dopamine neurons showed significantly reduced activity between CS+ and shock peaks but were significantly elevated from baseline at both CS+ and immediately before footshock, indicative of a largely sustained pattern (data file S1). In contrast, nonglutamate-dopamine neurons and all dopamine neurons showed transient changes in neuronal activity between CS+ and footshock (Fig. 4F). In response to the CS− (Fig. 4G), only glutamate-dopamine neurons showed a change in activity, consisting of a small but statistically significant suppression at the time of no shock delivery (Fig. 4, H to J).

To determine whether VTA neurons respond to uncued aversive events in a cell type–specific manner, mice were randomly administered unsignaled footshocks of different intensities (fig. S4, A to T). Afterwards, mice were administered 0-mA footshocks accompanied by an audible click that was present during all prior footshocks (fig. S4, U to Y). Glutamate-only neurons were activated by all shock intensities except the 0-mA click. Glutamate-dopamine neurons showed strong activation after each footshock intensity and after the audible click during 0-mA footshocks. In contrast, nonglutamate-dopamine neurons were suppressed at each current intensity except the 0-mA click. When recording from all dopamine neurons, we again observed intermediate activity levels between nonglutamate-dopamine neurons and glutamate-dopamine neurons, which consisted of significantly increased activity at shock relative to baseline across all intensities and the 0-mA audible click. Together, VTA glutamate-dopamine, nonglutamate-dopamine, and glutamate-only subpopulations had distinct signaling patterns of cued rewards, negative reward prediction error, and cued and uncued aversive stimuli. Nonglutamate-dopamine neurons bidirectionally signaled reward and aversion and signaled negative reward prediction error. Glutamate subtypes unidirectionally signaled reward and aversion, with glutamate-dopamine neurons uniquely sustaining their response between cue and reward.

Signaling dynamics during natural reward- and aversion-related motivated behaviors are better explained by cell type than anatomical location

Although each genetically defined VTA cell type is observed in every VTA subdivision, glutamate-dopamine and glutamate-only neurons are located predominantly in the medial VTA, whereas nonglutamate-dopamine neurons are predominantly in the lateral VTA (*38*–*42*, *51*). We targeted our recording fibers to the areas where each cell type was densest, raising the possibility that the observed differences in natural reward- and aversion-related signals could be explained either by the anatomical location of the recordings or by the molecularly defined cell type. We hypothesized that cell type better explained neuronal activation patterns, and we tested this hypothesis in four ways.

First, we leveraged the natural variation in the locations of recording fibers in our GCaMP experiments (fig. S3E) to determine whether mediolateral fiber position correlated with neuronal activity in response to any measured behavioral event. Across rewarding and aversive Pavlovian behavioral paradigms, neuronal activity did not correlate with mediolateral position of the recording fiber. The only significant finding was a weak negative correlation between mediolateral position and neuronal activity at the CS− during correct rejection trials (fig. S5, A to F).

Second, we binarily categorized GCaMP mice according to whether their recording fibers were situated in the medial or lateral VTA, irrespective of molecular cell type (fig. S5G). Using this anatomical categorization, we repeated our analysis of neuronal activity in response to naturally rewarding or aversive events (fig. S5, H to M). Some patterns of neuronal activity recapitulated the above results using cell-type categorization. First, medial and lateral groups were both activated at reward cues and events. Second, the lateral group exhibited transient signaling between reward cue and event. Third, the medial group was activated at shock cues and events. However, some activation patterns crucially differed between anatomical and cell-type categorization. We previously observed that glutamate-dopamine neurons showed sustained signaling between reward cue and event, but this pattern was obscured when only anatomical categorization was used. Likewise, the negative reward prediction error signaling of nonglutamate-dopamine neurons was obscured using anatomical categorization. The lateral group exhibited activation in

Downloaded from https://www.science.org at University of Colorado Boulder on November 21, 2026

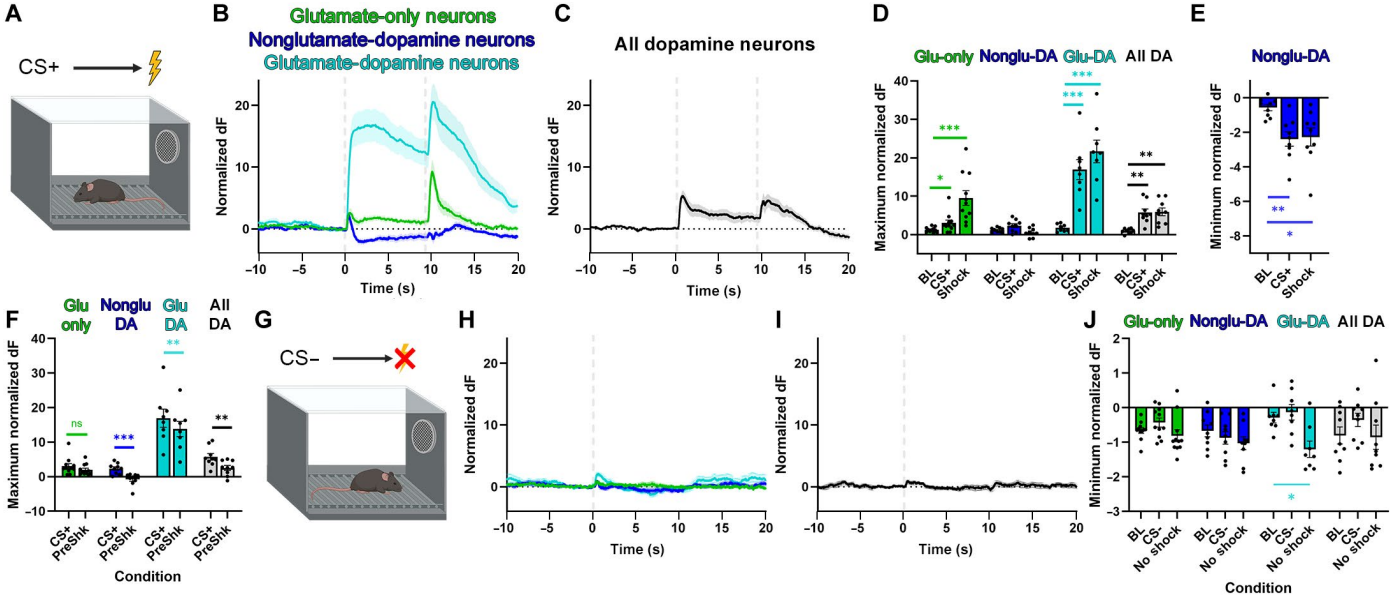


Fig. 4. Cell type–specific cued aversion-related signaling. (**A**) Mice were trained on a Pavlovian reward task. $N = 8$ to 11 mice per group (17 male and 11 female). (**B**) CS+ and footshock-related neuronal activity in glutamate-only (green), nonglutamate-dopamine (dark blue), and glutamate-dopamine (cyan) neurons. (**C**) CS+ and footshock-related neuronal activity in all dopamine (black) neurons. (**D**) Comparison of maximum normalized dF at behavioral events identifying activated neuronal populations during CS+ trials. Glutamate-only neurons: repeated measures ANOVA, effect of epoch $F(2,20) = 17.52$, $P < 0.001$, post hoc simple contrast tests BL × CS+ $F(1,10) = 6.66$, $P = 0.027$; BL × shock $F(1,10) = 22.94$, $P < 0.001$. Nonglutamate-dopamine neurons: repeated measures ANOVA, effect of epoch $F(2,16) = 5.96$, $P = 0.012$, post hoc simple contrast tests BL × CS+ $F(1,8) = 3.91$, $P = 0.083$; BL × shock $F(1,8) = 1.69$, $P = 0.230$. Glutamate-dopamine neurons: repeated measures ANOVA, effect of epoch $F(2,14) = 38.12$, $P < 0.001$, post hoc simple contrast tests BL × CS+ $F(1,7) = 33.95$, $P < 0.001$; BL × shock $F(1,7) = 48.12$, $P < 0.001$. All dopamine neurons: repeated measures ANOVA, effect of epoch $F(2,16) = 15.28$, $P < 0.001$, post hoc simple contrast tests BL × CS+ $F(1,8) = 21.48$, $P = 0.002$; BL × shock $F(1,8) = 19.23$, $P = 0.002$. (**E**) Comparison of minimum normalized dF at behavioral events in nonglutamate-dopamine neurons identifying suppressions during CS+ trials. Repeated measures ANOVA, effect of epoch $F(2,16) = 9.38$, $P = 0.002$, post hoc simple contrast tests BL × CS+ $F(1,8) = 13.71$, $P = 0.006$; BL × shock $F(1,8) = 8.36$, $P = 0.020$. (**F**) Analysis of cell type–specific transient and sustained cued aversion signaling by comparing maximum neuronal activity between CS+ and preshock epochs. Glutamate-only neurons: paired samples t test, $t(10) = 1.50$, $P = 0.163$. Nonglutamate-dopamine neurons: paired samples t test, $t(8) = 5.33$, $P < 0.001$. Glutamate-dopamine neurons: paired samples t test, $t(7) = 3.64$, $P = 0.008$; All dopamine neurons: paired samples t test, $t(8) = 4.76$, $P = 0.001$. (**G**) Neuronal activity during CS− and no footshock trials. (**H**) CS− related neuronal activity for glutamate-only (green), nonglutamate-dopamine (dark blue), and glutamate-dopamine (cyan) neurons. (**I**) CS− related neuronal activity for all dopamine neurons. (**J**) Comparison of minimum normalized dF at baseline, CS-, and footshock absence. Glutamate-only neurons: repeated measures ANOVA, no effect of epoch. Nonglutamate-dopamine neurons: repeated measures ANOVA, no effect of epoch. Glutamate-dopamine neurons: repeated measures ANOVA, effect of epoch $F(2,14) = 8.57$, $P = 0.004$, post hoc simple contrast tests: BL × CS− $F(1,7) = 0.32$, $P = 0.588$; BL × no shock $F(1,7) = 12.51$, $P = 0.010$. All dopamine neurons: repeated measures ANOVA, no effect of epoch. BL, baseline epoch; PreShk, preshock epoch. ns, not significant, $^*P < 0.05$, $^{**}P < 0.01$, $^{***}P < 0.001$. Dashed lines on peri-event time histograms represent onset of respective cues and shock events. Bar graphs represent group averages (±SEM) of maximum or minimum neuronal activity during baseline, cue, and shock/nonshsock event epochs. Symbols represent individual mice.

response to both shock cues and events, whereas the nonglutamate-dopamine cell type was suppressed at both events. Together, substantial differences can be found between medial and lateral recordings of VTA neurons irrespective of molecular cell type, but such classification obscures the distinct activation patterns of VTA subpopulations as defined by molecular cell type.

Third, we performed dimensionality reduction and cluster analysis to determine whether GCaMP activation patterns clustered better with anatomical location or molecular cell type. We used UMAP to reduce all event-related GCaMP responses of individual mice (Fig. 5A) into two-dimensional projections (Fig. 5, B and C). Mice with similar GCaMP response profiles clustered more closely to one another. Silhouette scores, a measure of clustering quality, were calculated according to whether neurons were classified by anatomical location of the recording fiber or molecular cell type of the recorded neurons. Because all dopamine neurons are a mixed population of dopaminergic neurons, these neurons were excluded from analysis. We found that anatomical categorization produced poor quality clusters, with animals from medial and lateral groups localized to both identified clusters (Fig. 5B). In comparison, cell-type categorization (Fig. 5C) produced high-quality clusters (Fig. 5D). Nonglutamate-dopamine neurons were reliably sorted into a separate cluster, but glutamate-only and glutamate-dopamine neurons were less reliably separated, reflecting similarities in their reward- and aversion-related GCaMP responses. To examine whether GCaMP responses clustered with anatomical or cell-type categorization among only dopaminergic VTA populations, we repeated the analysis without glutamate-only mice (Fig. 5, E to G). Cluster quality of anatomical categorization remained poor, whereas cell-type categorization again produced clusters of comparatively higher quality (Fig. 5G), such that every mouse was reliably sorted according to dopaminergic subcell type. When the analysis was repeated among only glutamatergic VTA populations (Fig. 5, H to J), we found that cell-type categorization was less reliable than that among all cell types or among dopaminergic populations, but was still of moderately high quality, and again of higher quality than anatomical categorization (Fig. 5J). Together, molecular cell type

Downloaded from https://www.science.org at University of Colorado Boulder on November 21, 2026

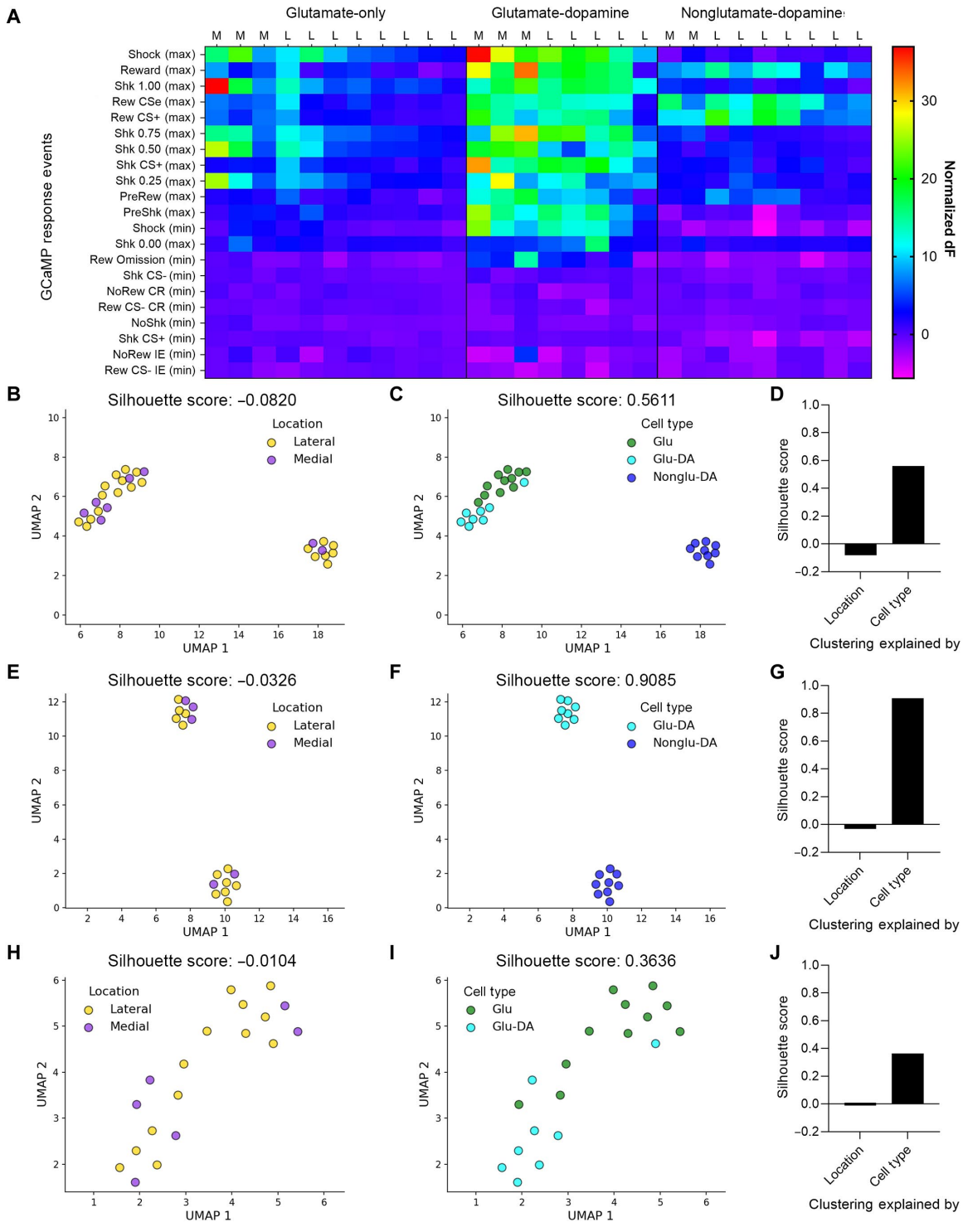


Fig. 5. Reward- and aversion-related Ca^{2+} signaling dynamics map onto cell type but not anatomical recording location. (**A**) Heatmap of GCaMP responses across rewarding and aversive events. Each column represents one animal, grouped by molecular cell type and labeled with medial "M" or lateral "L" recording fiber location. Parentheses indicate whether maximum or minimum normalized dF surrounding each event was calculated. *N* = 8 to 11 mice per group (17 male and 11 female). (**B** to **J**) UMAP projections and silhouette scores of GCaMP response dynamics in (A) for animals categorized by anatomical location of the recording fiber [(B), (E), and (H)] or molecular cell type [(C), (F), and (I)]. Silhouette scores [(D), (G), and (J)] quantify the quality of clustering. Clustering was analyzed among all cell types [(B) to (D)], among only dopaminergic subtypes [(E) to (G)], and among only glutamatergic subtypes [(H) to (J)]. CSe, CS error/CS+ epoch in reward omission trials; CR, correct rejection; IE, incorrect entry; NoRew, epoch of no reward in CS− trials; NoShk, epoch of no shock in CS− trials; PreRew, prereward epoch; PreShk, preshock epoch; Rew, reward trials; Shk, shock trials; min, minimum neuronal response; max, maximum neuronal response.

Downloaded from https://www.science.org at University of Colorado Boulder on November 21, 2026

predicted neuronal activation profiles, especially between dopaminergic subtypes, whereas anatomical location did not.

Fourth, we directly tested our hypothesis with simultaneous Ca^{2+} imaging in glutamate-dopamine and nonglutamate-dopamine neurons from a single VTA location. We expressed GCaMP6m in nonglutamate-dopamine neurons and a red-shifted Ca^{2+} sensor (sRGECO (*59*)) in glutamate-dopamine neurons (Fig. 6A). The optic fiber was positioned at the boundary of medial and lateral VTA where both cell types comingle (Fig. 6B). Because aversive events produced opposite neuronal responses in our prior GCaMP experiments, mice were trained on Pavlovian fear conditioning as described above. In accordance with our prior results, glutamate-dopamine neurons increased activity during both CS+ and footshock, whereas nonglutamate-dopamine neurons were suppressed during both CS+ and footshock compared with baseline (Fig. 6, C to E). In a separate recording session, mice were administered uncued footshocks of different intensities. Glutamate-dopamine neurons were activated at every intensity and the 0-mA click, whereas nonglutamate-dopamine neurons were suppressed (Fig. 6F). Thus, glutamate-dopamine and nonglutamate-dopamine neurons at the same VTA location signal aversion-related stimuli in opposite manners, supporting that cell type is a key distinguishing factor of VTA dopamine neuron signaling of motivated behaviors.

Optogenetically elicited dopamine signaling dynamics between cell types

We next assessed whether activation of glutamate-dopamine neurons or nonglutamate-dopamine axons in NAcc resulted in similar or

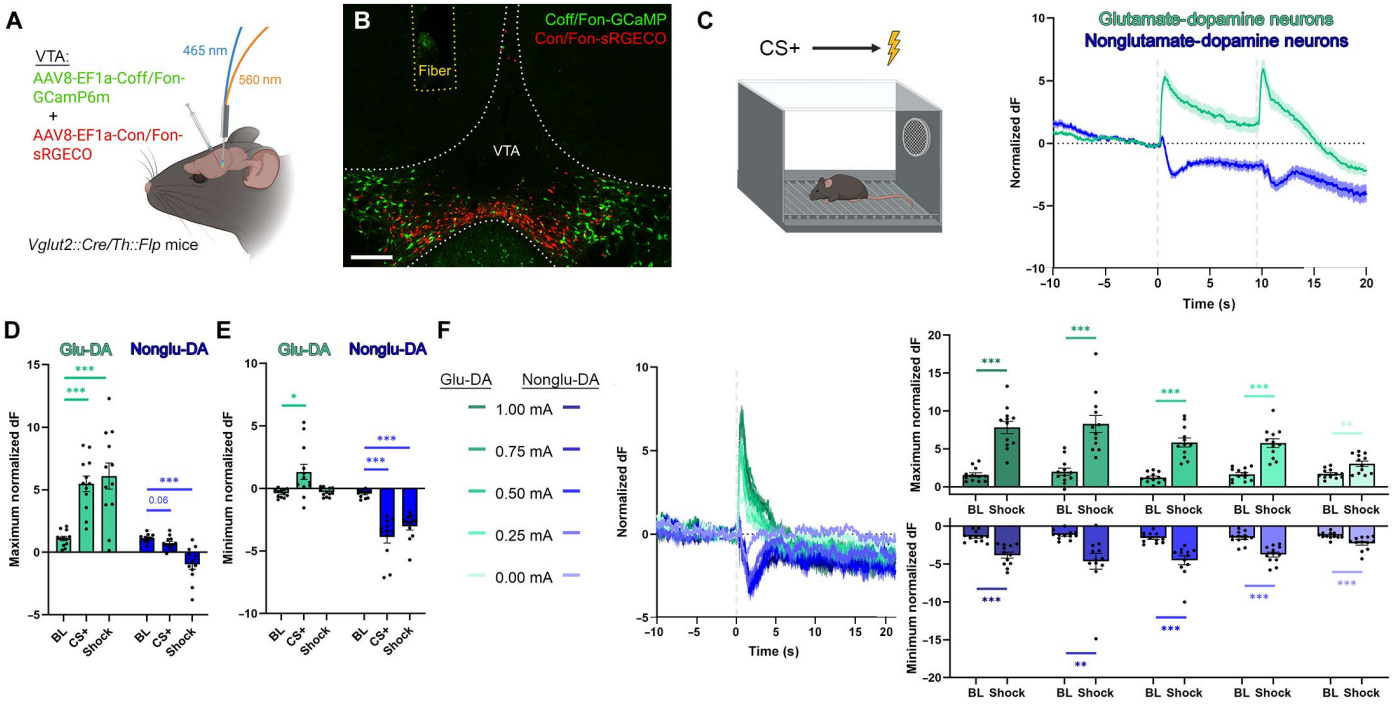


Fig. 6. Dopaminergic subtypes in the same anatomical location exhibit opposite Ca^{2+} signaling dynamics to aversive events. (**A**) *Vglut2::Cre/Th::Flp* mice were coinjected in the VTA with AAVs encoding Coff/Fon-GCaMP to target nonglutamate-dopamine neurons and Con/Fon-sRGECO to target glutamate-dopamine neurons. The two spectrally separated Ca^{2+} sensors were simultaneously excited and recorded through a single optic fiber. $N = 12$ mice (6 male and 6 female). (**B**) Example optic fiber placement and viral expression of Coff/Fon-GCaMP and Con/Fon-sRGECO in the VTA. Scale bar, 200 μm. Image is representative of 12 mice. (**C**) Left: Neuronal activity was recorded during fear conditioning where a CS+ predicted footshock (0.5 sec, 0.5 mA). Right: CS+ and footshock-related neuronal activity in nonglutamate-dopamine (dark blue) and glutamate-dopamine (green) neurons. Dashed lines represent onset of CS+ and shock. (**D**) Comparison of maximum neuronal activity during baseline, CS+, and shock event epochs. Maximum normalized dF from 0 to 2 s surrounding each event. Glutamate-dopamine neurons: repeated measures ANOVA, effect of epoch $F(2,22) = 21.12$, $P < 0.001$, post hoc simple contrast tests BL × CS+ $F(1,11) = 39.32$, $P < 0.001$; BL × shock $F(1,11) = 19.96$, $P < 0.001$. Nonglutamate-dopamine neurons: repeated measures ANOVA, effect of epoch $F(2,22) = 23.03$, $P = 0.001$, post hoc simple contrast tests BL × CS+ $F(1,11) = 4.38$, $P = 0.060$; BL × shock $F(1,11) = 25.54$, $P < 0.001$. (**E**) Comparison of minimum neuronal activity during baseline, CS+, and shock event epochs. Minimum normalized dF from 0 to 2 s surrounding each event. Glutamate-dopamine neurons: repeated measures ANOVA, effect of epoch $F(2,22) = 6.87$, $P = 0.022$, post hoc simple contrast tests BL × CS+ $F(1,11) = 6.44$, $P = 0.028$; BL × shock $F(1,11) = 0.41$, $P = 0.535$. Nonglutamate-dopamine neurons: repeated measures ANOVA, effect of epoch $F(2,22) = 44.24$, $P < 0.001$, post hoc simple contrast tests BL × CS+ $F(1,11) = 47.19$, $P < 0.001$; BL × shock $F(1,11) = 59.38$, $P < 0.001$. (**F**) Left: Neuronal activity during uncued footshocks of scaling intensity. Dashed line on peri-event time histogram represents onset of shock. Right: Bar graphs represent group averages (±SEM) of maximum or minimum neuronal activity during baseline and shock event epochs. Symbols represent individual mice. Glutamate-dopamine neurons, maximum normalized dF values: two-way repeated measures ANOVA, main effect of current $F(4,44) = 10.02$, $P = 0.001$; main effect of epoch $F(1,11) = 54.17$, $P < 0.001$; current × epoch interaction $F(4,44) = 26.04$, $P < 0.001$; Šidák-adjusted pairwise comparisons BL × 1.00 mA $P < 0.001$, BL × 0.75 mA $P < 0.001$, BL × 0.50 mA $P < 0.001$, BL × 0.25 mA $P < 0.001$, BL × 0.00 mA $P = 0.005$. Nonglutamate-dopamine neurons, minimum normalized dF values: two-way repeated measures ANOVA, main effect of epoch $F(1,11) = 176.37$, $P < 0001$; current × epoch interaction $F(4,44) = 4.36$, $P < 0.043$; Šidák-adjusted pairwise comparisons BL × 1.00 mA $P < 0.001$, BL × 0.75 mA $P = 0.003$, BL × 0.50 mA $P < 0.001$, BL × 0.25 mA $P < 0.001$, BL × 0.00 mA $P = 0.005$. *$P < 0.05$, **$P < 0.01$, ***$P < 0.001$. BL, baseline epoch.

Downloaded from https://www.science.org at University of Colorado Boulder on November 21, 2026

different dopamine release dynamics in vivo. On the basis of VTA glutamate-dopamine neurons projecting preferentially to the medial NAcc shell and VTA nonglutamate-dopamine neurons projecting preferentially to the NAcc core (*34*, *36*, *37*, *42*, *60*–*62*), *Vglut2::Cre/Th::Flp* mice were injected in the shell/core border of the NAcc with an AAV encoding the dopamine sensor $GRAB_{DA1h}$. One group of mice was also injected in the VTA with an AAV encoding the red-shifted optogenetic actuator ChRmine-oScarlet in a Cre- and Flp-dependent manner to target glutamate-dopamine neurons (figs. S6, A to D). In a separate group of mice, ChRmine-oScarlet was delivered in a Coff/Fon manner to target nonglutamate-dopamine neurons (figs. S6, E to H). ChRmine stimulation of both nonglutamate-dopamine and glutamate-dopamine axons significantly increased the magnitude of dopamine release above baseline at every stimulation pulse train (fig. S7, A to E). Magnitude of dopamine release scaled curvilinearly with stimulation pulse number in both nonglutamate-dopamine and glutamate-dopamine axons (fig. S7F). We next measured the duration of the ChRmine-evoked dopamine release by identifying the time at which the magnitude of dopamine release decreased by 50% from the maximum value, termed the half-maximum duration (fig. S7, G and H). Dopamine release differed between dopaminergic axon types such that nonglutamate-dopamine axons scaled curvilinearly with stimulation pulse number, whereas glutamate-dopamine axons scaled linearly with stimulation pulse number (*63*) (fig. S7I). Thus, optically elicited NAcc dopamine release from nonglutamate-dopamine and glutamate-dopamine axons scaled similarly in magnitude, but dopamine release from glutamate-dopamine axons scaled linearly in duration. In control mice, laser stimulation of mCherry terminals had no effect on NAcc $GRAB_{DA1h}$ fluorescence (fig. S7, J to M), indicating that increased $GRAB_{DA1h}$ activity resulted from ChRmine actuation rather than an artifact of 589-nm excitation (*64*).

Nonglutamate-dopamine neurons support reward and reinforcement

We next optogenetically stimulated the somata of each cell type to determine whether any supported optogenetically elicited reward or reinforcement. *Vglut2::Cre/Th::Flp* mice were injected in the VTA with AAVs encoding Con/Fon-ChRmine-oScarlet to target glutamate-dopamine neurons or Coff/Fon-ChRmine-oScarlet to target nonglutamate-dopamine neurons. *Vgat::Cre/Th::Flp* mice were injected in the VTA with AAVs encoding COFO-ChRmine-oScarlet to target glutamate-only neurons. Control mice consisted of fluorescent reporters in *Vglut2::Cre/TH::Flp* mice and *Vgat::Cre/Th::Flp* mice. All mice were implanted with bilateral fiber optics dorsal to VTA (Fig. 7A and fig. S8). To examine reward-related behavior, mice were placed in a three-chamber maze where time spent in the stimulation chamber resulted in the delivery of 589-nm light to the VTA of different, randomly determined frequencies over days (Fig. 7B). There were no differences in time spent in the stimulation chamber during the baseline unstimulated day. However, across all frequencies tested (5, 10, 20, and 40 Hz), only mice with somatically stimulated nonglutamate-dopamine neurons showed a preference for the stimulation chamber (Fig. 7C). To examine reinforcement-related behavior, mice were placed in an open field with two small squares between the center and perimeter of the field (Fig. 7D). Entry into the active square resulted in delivery of a 1-s train of 589-nm light at 40 Hz, whereas entry into the inactive square resulted in no consequence. There were no differences in active or inactive responses during the baseline unstimulated day. However, across the 3 days of training, only mice somatically stimulating nonglutamate-dopamine neurons showed self-stimulation behavior (Fig. 7E). On the final day, active and inactive squares were reversed. Mice somatically stimulating nonglutamate-dopamine neurons reversed to self-stimulate on the previously inactive square (Fig. 7F) and continued to respond more than all other groups on the previously active square (Fig. 7E). These results are consistent with nonglutamate-dopamine neuronal activity patterns whereby increased activity is selectively associated with reward. The lack of reward or reinforcement with glutamate-dopamine and glutamate-only neurons is also consistent with their neuronal activity patterns that are elevated in both rewarding and aversive conditions.

Glutamate and dopamine from cotransmitting neurons have different behavioral roles in natural reward and aversion

Given that glutamate-dopamine neurons increased neuronal activity after both naturally rewarding and aversive events and their learned predictors, we next sought to determine the behavioral functions of dopamine and glutamate release from glutamate-dopamine neurons. We used short hairpin RNA (shRNA) and green fluorescent protein (GFP)–encoding Cre- or Flp-inducible AAVs (*65*–*68*) to manipulate the molecular synthesis or release machineries for dopamine (*Th* shRNA), glutamate (*Vglut2* shRNA), or GABA (*Vgat* shRNA) in VTA neurons (fig. S9, A to D). To test effectiveness and specificity, we injected the Cre-dependent shRNA vectors in the VTA of *Vglut2::Cre* mice and analyzed GFP-expressing VTA neurons after 4 weeks. In mice expressing scramble control sequence shRNA, 97.3 ± 0.8% of GFP neurons expressed *Vglut2* mRNA, of which 19.5 ± 1.2% expressed *Slc32a1* (*Vgat*) mRNA, and 21.2 ± 1.2% were TH immunoreactive. In *Vglut2* shRNA mice, 4.9 ± 0.7% of GFP neurons expressed *Vglut2* mRNA, whereas *Vgat* mRNA expression or TH immunoreactivity remained about 20% each, similar to scramble controls. In *Vgat* shRNA mice, 96.6 ± 1.5% of GFP neurons expressed *Vglut2* mRNA, of which 20.3 ± 0.1% were immunoreactive for TH, but only 2.8 ± 0.3% expressed *Vgat* mRNA. In *Th* shRNA mice, 98.6 ± 0.2% GFP neurons expressed *Vglut2* mRNA, of which 17 ± 0.7% expressed *Vgat* mRNA but only 0.1 ± 0.1% had TH immunoreactivity (fig. S9E). We also examined a Flp-dependent *Vglut2* shRNA vector in the VTAs of *Th::Flp* mice. Of the total neurons, 85.84 ± 0.86% were immunoreactive for TH without detectable *VGluT2* mRNA (fig. S10, A to F). The remaining neurons either coexpressed *Vglut2* mRNA and TH immunoreactivity (6.29 ± 0.79%) or expressed other combinations of markers at about 2% each, totaling 7.88 ± 0.17% of labeled neurons (cell types: TH^- $Vglut2^+$ $Vgat^-$, TH^- $Vglut2^+$ $Vgat^+$, TH^- $Vglut2^-$ $Vgat^+$, and TH^- $Vglut2^-$ $Vgat^-$) (fig. S10F). These results demonstrate the successful knockdown of intended neurotransmission-specific transcripts in VTA $Vglut2^+$ neurons without affecting untargeted transcripts of cotransmitters.

We next performed a series of experiments examining the role of dopamine or glutamate release machineries from VTA glutamate-dopamine neurons by injecting *Vglut2::Cre* mice in the VTA with AAVs encoding Cre-dependent *Th* shRNA (to knock down *Th* from glutamate neurons), in *Th::Flp* mice with AAVs encoding Flp-dependent *Vglut2* shRNA (to knock down *Vglut2* from dopamine neurons), or in *Vglut2::Cre* mice with a Cre-dependent scrambled-sequence shRNA control (Fig. 8A). Mice were trained on a cued Pavlovian reward task in which a CS+ predicted sucrose reward and a CS− predicted no sucrose delivery. *Th* knockdown did not affect the percentage of reward port entries during CS+ trials (Fig. 8B) or latency to enter the reward port during CS+ trials (Fig. 8C). However, *Th* knockdown

Downloaded from https://www.science.org at University of Colorado Boulder on November 21, 2026

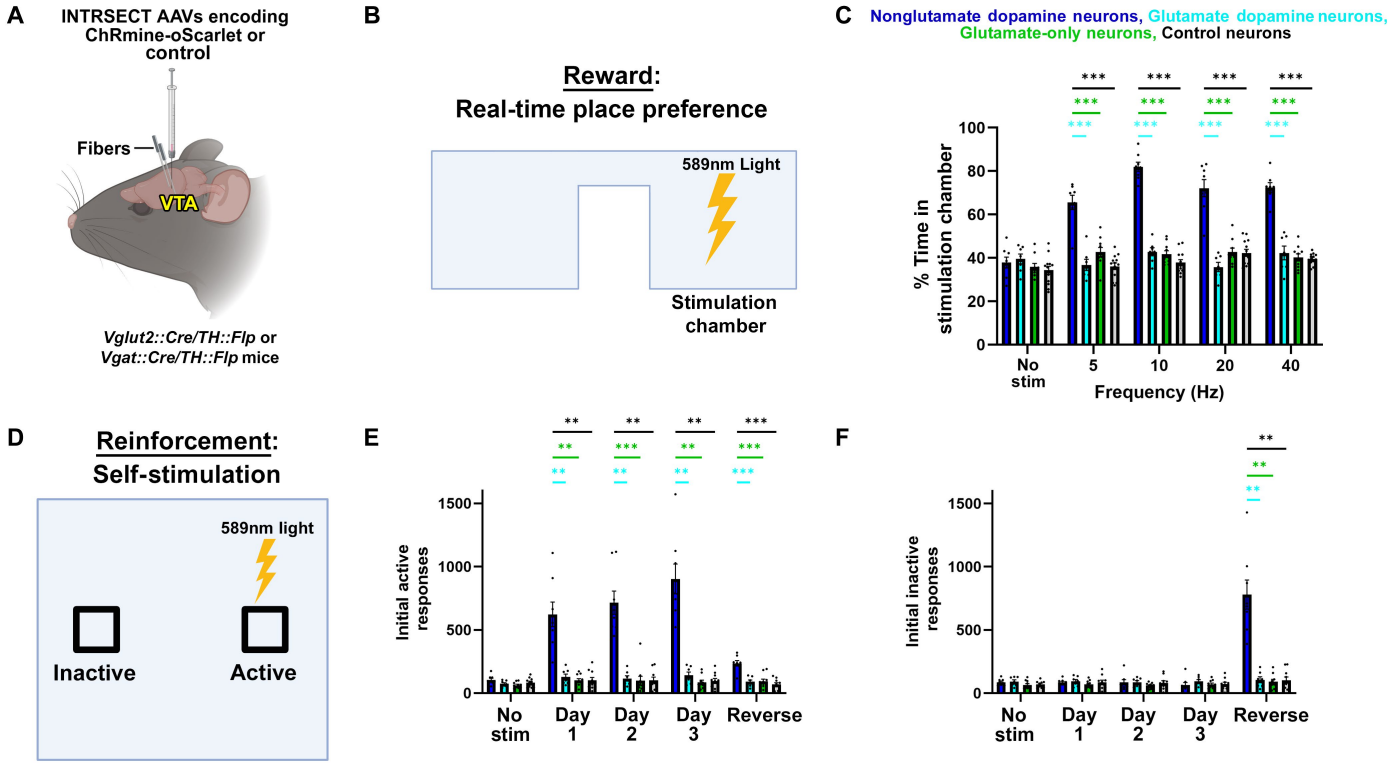


Fig. 7. Nonglutamate-dopamine neurons support reward and reinforcement. (**A**) Experimental setup. *Vglut2::Cre/Th::Flp* mice were injected with AAVs encoding Con/Fon-ChRmine-oScarlet or Coff/Fon-ChRmine-oScarlet. *Vgat::Cre/Th::Flp* mice were injected with AAVs encoding COFO-ChRmine-oScarlet. Control mice were mixed across cellular targets consisting of Vglut2::Cre/TH::Flp mice injected with AAVs encoding either Coff/Fon-mCherry or Con/Fon-EYFP or in Vgat::Cre/Th::Flp mice injected with AAVs encoding COFO-oScarlet or DIO-GFP. (**B**) Real-time place conditioning. When mice were in the stimulation chamber, they were delivered 589-nm light of different frequencies across days. (**C**) Percentage of time spent in the stimulation chamber across frequency conditions. Nonglutamate-dopamine neurons are in blue, glutamate-dopamine neurons are in cyan, glutamate-only neurons are in green, and controls are in black. Mixed ANOVA frequency × cell type interaction $F(9.286,105.2) = 15.33$, $P < 0.001$ (Greenhouse-Geisser corrected). Šidák's multiple comparison tests: 5 Hz (NongluDA compared with GluDA $P < 0.0001$, NongluDA compared with Glu $P = 0.0005$, NongluDA compared with control $P < 0.0001$), 10 Hz (NongluDA compared with GluDA $P < 0.0001$, NongluDA compared with Glu $P < 0.0001$, NongluDA compared with control $P < 0.0001$), 20 Hz (NongluDA compared with GluDA $P < 0.0001$, NongluDA compared with Glu $P = 0.0003$, NongluDA compared with control $P < 0.0003$), 40 Hz (NongluDA compared with GluDA $P < 0.0001$, NongluDA compared with Glu $P < 0.0001$, NongluDA compared with control $P < 0.0001$). $N = 7$ to 13 mice per group (19 male and 19 female). (**D**) Self-stimulation. When mice entered into the active square, they were delivered a second train of 589-nm light. On the last day, active and inactive squares were reversed. (**E**) Responses on the initially active square. Mixed ANOVA day × cell type interaction $F(4.654,48.10) = 26.85$, $P < 0.0001$ (Greenhouse-Geisser corrected). Šidák's multiple comparison tests: day 1 (NongluDA compared with GluDA $P = 0.0073$, NongluDA compared with Glu $P = 0.0059$, NongluDA compared with control $P < 0.0053$), day 2 (NongluDA compared with GluDA $P < 0.0016$, NongluDA compared with Glu $P = 0.0009$, NongluDA compared with control $P < 0.0013$), day 3 (NongluDA compared with GluDA $P < 0.0016$, NongluDA compared with Glu $P = 0.0012$, NongluDA compared with control $P < 0.0012$), reversal (NongluDA compared with GluDA $P < 0.0007$, NongluDA compared with Glu $P = 0.0008$, NongluDA compared with control $P < 0.0002$). $N = 7$ to 10 mice per group (15 male and 20 female). (**F**) Responses on the initially inactive square. Mixed ANOVA day × cell type interaction $F(3.335,34.46) = 33.09$, $P < 0.0001$ (Greenhouse-Geisser corrected). Šidák's multiple comparison tests: Reversal (NongluDA compared with GluDA $P = 0.0032$, NongluDA compared with Glu $P = 0.0030$, NongluDA compared with control $P < 0.0030$). $N = 7$ to 10 mice per group (15 male and 20 female). $^*P < 0.05$, $^{**}P < 0.01$, and $^{***}P < 0.001$.

significantly increased unrewarded entries into the reward port during the CS− in the second week of training (Fig. 8D). *Vglut2* knockdown did not affect reward port entries during the CS+ (Fig. 8E). However, *Vglut2* knockdown increased the latency of mice to enter the reward port during CS+ trials relative to scramble controls during the second week of training (Fig. 8F). *Vglut2* knockdown did not affect reward port entries during the CS− (Fig. 8G).

Mice then began extinction training in which the CS+ resulted in no sucrose delivery (Fig. 8H). Compared with scramble controls, *Th* knockdown mice were slower to extinguish reward port entries during the CS+ over days (Fig. 8I). In contrast, *Vglut2* knockdown accelerated extinction learning compared with scramble controls (Fig. 8J). To identify whether learning-related differences were influenced by changes in reward intake, mice consumed free sucrose for 1 hour. Neither *Th* knockdown nor *Vglut2* knockdown influenced free sucrose consumption (fig. S11, A to C).

To determine whether differences in CS+ hits or CS+ latency were due to differences in baseline locomotor activity, mice explored an open field. *Th* knockdown had no effect on distance traveled, whereas *Vglut2* knockdown resulted in significantly reduced distance traveled (fig. S11, D to F). The reduction in distance traveled in *Vglut2* knockdown mice was driven by a significant increase in the total time spent immobile and in the number of immobile episodes (fig. S11, G and H). We also analyzed locomotor activity in the center zone of the open field arena to assess whether these locomotor differences were driven by an anxious phenotype. After normalizing to

Downloaded from https://www.science.org at University of Colorado Boulder on November 21, 2026

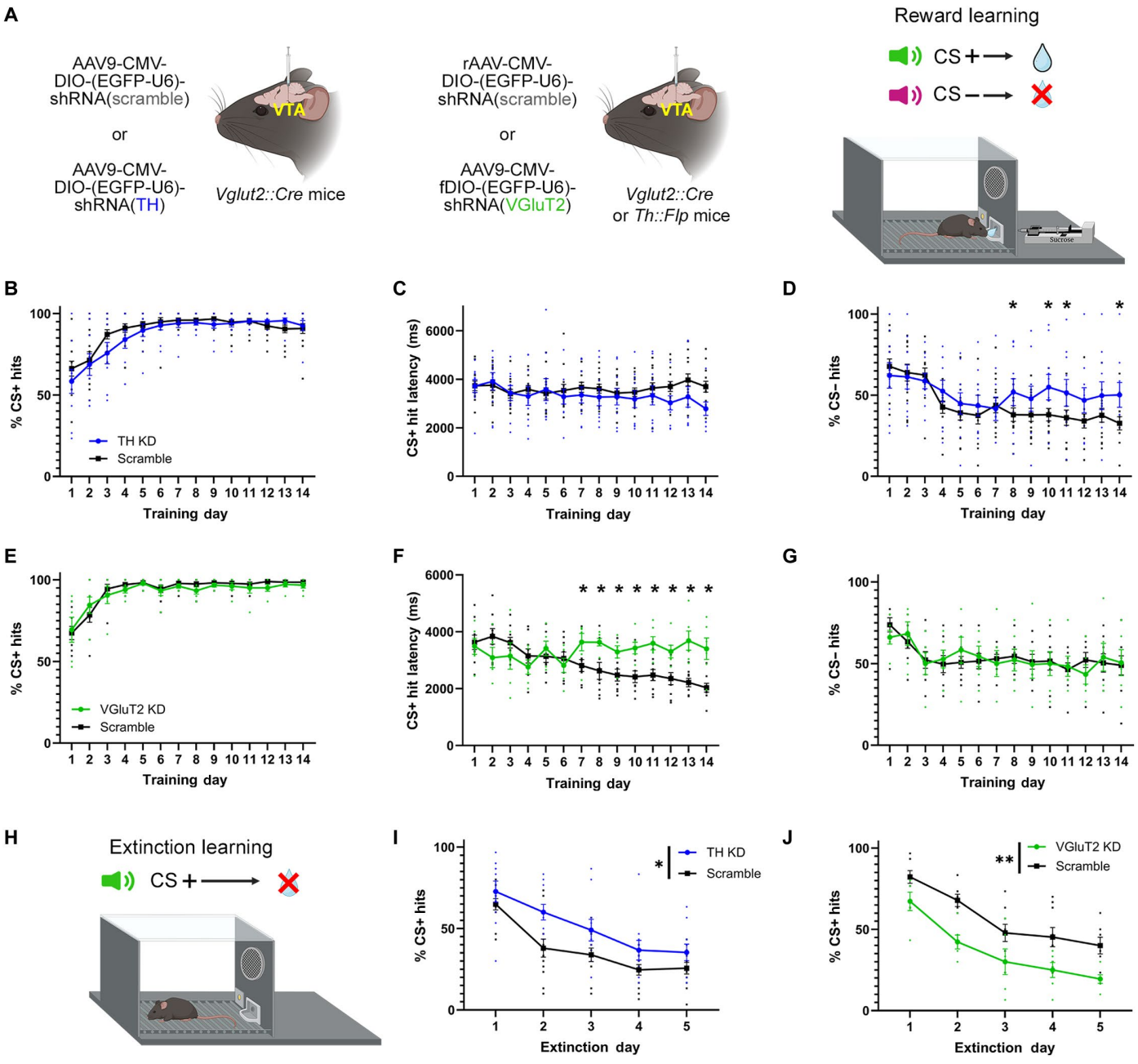


Fig. 8. Neurotransmitter-specific knockdown from VTA glutamate-dopamine neurons alters reward-related learning and extinction of conditioned reward-seeking. (**A**) *Vglut2::Cre* mice were injected in the VTA with AAVs encoding Cre-dependent *Th* shRNA (TH KD) or scramble control shRNA (Scramble). *Th::Flp* mice were injected in the VTA with an AAV encoding Flp-dependent *Vglut2* shRNA (VGluT2 KD), and *Vglut2::Cre* mice received Cre-dependent scramble control (Scramble). Mice then underwent Pavlovian reward training. (**B**) CS+ reward port entries for *Th* knockdown and scramble control groups. Mixed model ANOVA, no main effect of group or interaction. (**C**) CS+ hit latency for *Th* knockdown and scramble control groups. Mixed model ANOVA, no main effect of group or interaction. (**D**) CS− reward port entries for *Th* knockdown and scramble control groups. Mixed model ANOVA, day × group interaction $F(13,260) = 3.02$, $P < 0.001$, Šidák pairwise comparison day 8 $P = 0.039$, day 10 $P = 0.021$, day 11 $P = 0.029$, day 14 $P = 0.040$. For (B) to (D), $N = 10$ to 13 mice per group (14 male and 9 female). (**E**) CS+ reward port entries for *Vglut2* knockdown and scramble control groups. Two-way repeated measures ANOVA, no main effect of group or interaction. (**F**) CS+ hit latency for *Vglut2* knockdown and scramble control groups. Two-way repeated measures ANOVA, day × group interaction $F(13,169) = 8.70$, $P < 0.001$, Šidák pairwise comparison day 7 $P = 0.038$, day 8 $P = 0.021$, day 9 $P = 0.021$, day 10 $P = 0.0055$, day 11 $P = 0.0028$, day 12 $P = 0.010$, day 13 $P = 0.00056$, day 14 $P = 0.0021$. (**G**) CS− reward port entries for *Vglut2* knockdown and scramble control groups. Two-way repeated measures ANOVA, no main effect of group or interaction. For (E) to (G), $N = 6$ to 9 mice per group (7 male and 8 female). (**H**) Mice were trained to associate the CS+ with no reward delivery over five extinction sessions. (**I**) CS+ hits between *Th* knockdown and control mice: two-way repeated measures ANOVA, main effect of group $F(1,21) = 5.50$, $P = 0.029$. $N = 10$ to 13 mice per group (14 male and 9 female). (**J**) CS+ hits between *Vglut2* knockdown and control mice: two-way repeated measures ANOVA, main effect of group $F(1,13) = 13.29$, $P = 0.003$. $N = 6$ to 9 mice per group (7 male and 8 female). Between-group effects and day-by-group interactions indicated by $*P < 0.05$, $**P < 0.01$, and $***P < 0.001$.

Downloaded from https://www.science.org at University of Colorado Boulder on November 21, 2026

total distance traveled, *Vglut2* knockdown mice did not differ from scramble control mice in distance traveled in the center, number of entries to the center, or time spent in the center (fig. S11, I to K). To determine whether gait coordination abnormalities underlie motor suppression in the open field test, we recorded ambulatory paw sequences and time to cross a Plexiglas catwalk. *Vglut2* knockdown mice had no deficits in paw sequence regularity index (RI) or time to cross the catwalk relative to scramble controls (fig. S11, L to N). To further assess motor deficits in *Vglut2* knockdown mice, we tested mice on the RotaRod assay. *Vglut2* knockdown mice were not different from scramble controls in average latency to fall from the rod (fig. S11, O and P). We also investigated whether a stimulus that induces active avoidance would reveal deficits in aversion-related vigor and locomotor responses. To do so, we tested *Vglut2* knockdown mice in the visual loom paradigm that mimics an imminent threat from an avian predator (*69*). *Vglut2* knockdown did not affect the number of trials resulting in freezing to avoid detection by the simulated predator, escaping to the shelter, or freezing then escaping (fig. S11, Q and R). *Vglut2* knockdown likewise did not affect the latency to freeze or latency to enter the shelter after loom onset (fig. S11, S and T), indicating that locomotor deficits in *Vglut2* knockdown mice were specific to rewarding contexts and exploratory behavior.

Mice were next trained on a cued Pavlovian aversion task in which a CS+ predicted footshock and a CS− predicted no footshock (Fig. 9A). This paradigm results in more fear-related freezing behavior in response to the CS+ compared with the CS− (*70*), so mice were examined for freezing during CS+ and CS−. *Th* knockdown decreased CS+ freezing and had no effect on CS− freezing (Fig. 9, B and C). *Vglut2* knockdown had no effect on CS+ or CS− freezing (Fig. 9, D and E). We also examined whether groups differentially discriminated CS+ and CS− by normalizing the cued data in discrimination scores such that values above 0 reflected more freezing to CS+ and values below zero reflected more freezing to CS−. Scramble control mice had significantly higher discrimination scores than TH knockdown mice (fig. S12A), whereas discrimination in VGluT2 knockdown and scramble control mice did not differ (fig. S12B).

Mice then began extinction training in which neither the CS+ nor the CS− resulted in footshock (Fig. 9F). Despite less freezing induced by CS+ during acquisition, we found that extinction of freezing induced by CS+ was impaired in *Th* knockdown mice (Fig. 9, G and H). On the first day of extinction, scramble control mice continued to freeze more than *Th* knockdown mice. However, on day 2, there was no difference in freezing between groups as scramble control mice began to demonstrate extinction learning. During the next two extinction training days, scramble control mice froze less than *Th* knockdown mice as they continued to extinguish CS+-induced fear, in contrast with *Th* knockdown mice, which did not demonstrate extinction learning. There was no difference in freezing in response to the CS− between groups over days. In contrast with *Th* knockdown, *Vglut2* knockdown in VTA dopamine neurons did not affect CS+ or CS− freezing during extinction (Fig. 9, I and J).

To determine whether conditioned fear-related deficits were influenced by changes in pain sensitivity, we tested mice on a hot water tail immersion assay. Neither *Th* knockdown nor *Vglut2* knockdown affected pain sensitivity (fig. S11, U to W). To assess whether the conditioned fear- and extinction-related differences in *Th* knockdown mice were driven by general memory deficits, we assessed *Th* knockdown mice in the nonassociative memory-forming novel object recognition task. However, *Th* knockdown mice showed no differences in discrimination for novel objects (fig. S11, X and Y).

To clarify whether the observed fear- and extinction-related deficits in *Th* knockdown mice were specific to associative learning or produced an aversion-resistant reward-seeking phenotype, mice were assessed in a reward-consumption task coupled with nonassociative aversive events. Mice learned to freely consume sucrose from a bottle spout during short-access daily sessions. On a single test day, the session was interrupted by 10 noncontingent 0.20-mA footshocks delivered at randomized intershock intervals. Shocks increased in duration with each presentation, from 0.1 to 1.0 s. Licking on the sucrose spout and freezing behavior were scored in each intershock interval. Longer shocks decreased licking behavior and increased the latency to return to licking in intershock intervals, but there was no difference between *Th* knockdown and scramble control groups. Freezing behavior was not influenced by shock duration or shRNA group (fig. S13, A to E). Therefore, *Th* knockdown from glutamate-dopamine neurons produced no deficits in the suppression of reward-seeking or the expression of fear behavior in response to nonassociative aversive events. To identify potential anxiety-related deficits with *Th* knockdown, mice were assessed in the light-dark box. There were no differences between *Th* knockdown and controls in all variables tested (fig. S13, F to M). To determine whether *Th* knockdown affected threat responding in naturalistic aversive contexts, mice were tested on the visual sweep and visual loom paradigms. The visual sweep mimics a distal threat from an aerial predator that is not immediately approaching the subject, which biases mice toward passive avoidance (freezing) (*71*). In contrast, the visual loom mimics an imminent threat from an approaching aerial predator and promotes active avoidance (escape to a shelter) (*69*). Overall contingency counts of behavior at stimulus onset differed between sweep trials and loom trials, such that sweep trials elicited more freezing without escape and loom trials elicited more escape without freezing. However, in both paradigms, *Th* knockdown did not affect the likelihood of mice to freeze, escape to the shelter, freeze then escape, the latency to freeze, duration of freezing, latency to escape, or latency to re-exit the shelter after escape (fig. S13, N to Y). Together, *Vglut2* and *Th* knockdown in glutamate-dopamine neurons resulted in distinct changes in natural reward- and aversion-based learning without affecting sensitivity to naturally rewarding or aversive events, inducing motor or nonassociative memory deficits, or producing an anxious or aversion-resistant reward-seeking phenotype. Glutamatergic vesicular packaging (VGluT2) in glutamate-dopamine neurons was necessary for reward- and exploration-related vigor, whereas dopamine synthesis (TH) in glutamate-dopamine neurons supported associative learning of aversive or less-beneficial outcomes.

Neural population model of glutamate-dopamine and nonglutamate-dopamine neurons

On the basis of our results indicating several fundamental differences between glutamate-dopamine and nonglutamate-dopamine neurons, as well as the influence of glutamate or dopamine release machineries in glutamate-dopamine neurons in natural reward- and aversion-motivated behaviors, we developed a conceptual neural population model of glutamate-dopamine cotransmitting and nonglutamate-dopamine VTA neurons to illustrate how differences in transmitter output might influence behavior across learning. The model reflects the anatomical distinction that glutamate-dopamine neurons predominantly project to medial NAcc shell whereas nonglutamate-dopamine

Downloaded from https://www.science.org at University of Colorado Boulder on November 21, 2026

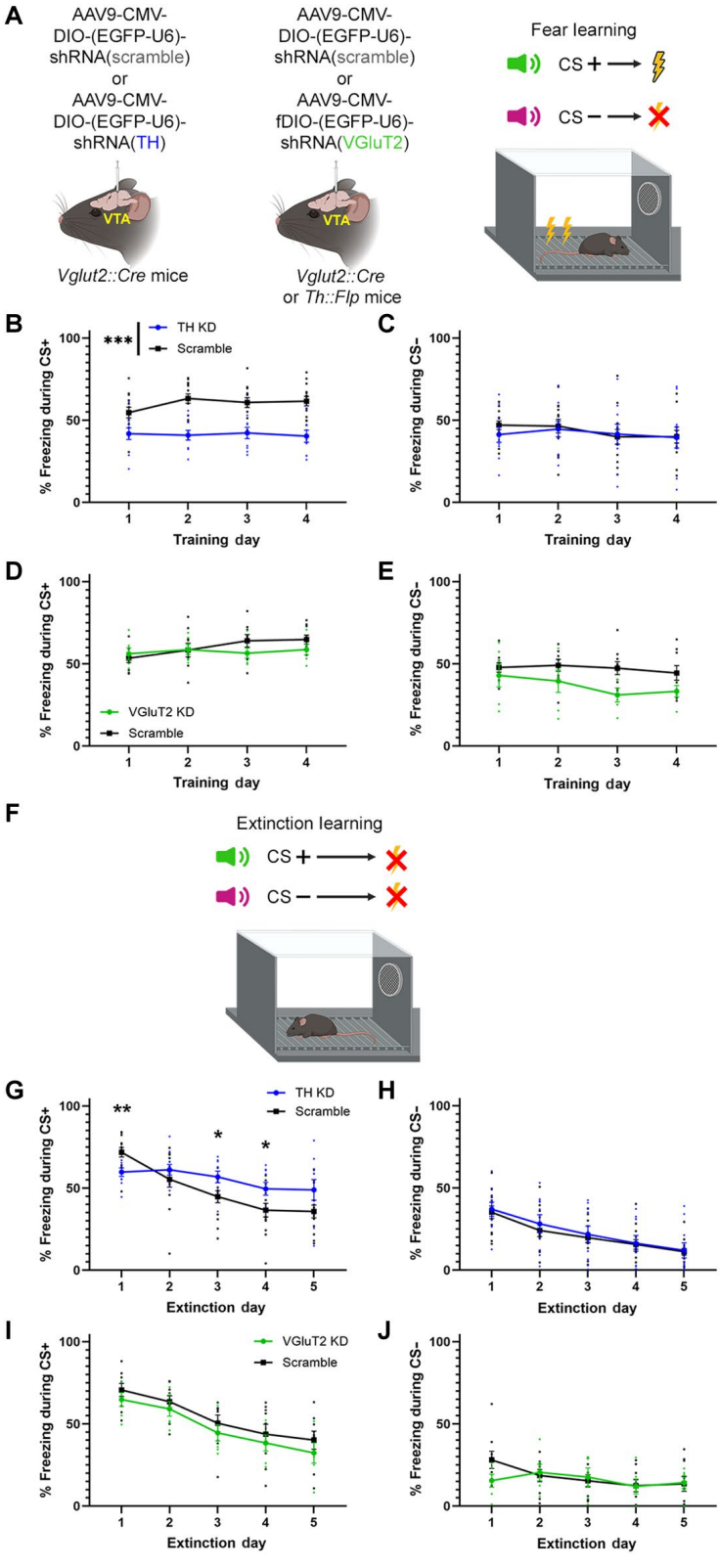


Fig. 9. Neurotransmitter-specific knockdown from VTA glutamate-dopamine neurons alters conditioned fear learning and extinction of conditioned fear. (**A**) Experimental setup. *Vglut2::Cre* mice were injected in the VTA with AAVs encoding Cre-dependent *Th* shRNA (TH KD) or scramble control shRNA (Scramble). *Th::Flp* mice were injected in the VTA with an AAV encoding Flp-dependent *Vglut2* shRNA (VGluT2 KD), and *Vglut2::Cre* mice received Cre-dependent scramble control (Scramble). Mice then underwent Pavlovian fear training. (**B** to **E**) Average (±SEM) percent of time spent freezing across days during the CS+ and CS− between (and) *Vglut2* knockdown and scramble control groups. Small symbols represent individual mice. (B) Average (±SEM) percent of time spent freezing across days during the CS+ for *Th* knockdown and scramble control groups. Two-way repeated measures ANOVA, main effect of *Th* knockdown $F(1,21) = 24.22$, $P < 0.001$. (C) Average (±SEM) percent of time spent freezing across days during the S- for *Th* knockdown and scramble control groups. Two-way repeated measures ANOVA, no main effects or interactions. For (B) and (C), $N = 10$ to 13 mice per group (14 male and 9 female). (D) Average (±SEM) percent of time spent freezing across days during the CS+ for *Vglut2* knockdown and scramble control groups. Two-way repeated measures ANOVA, no main effects or interactions. (E) Average (±SEM) percent of time spent freezing across days during the CS− *Vglut2* knockdown and scramble control groups. Two-way repeated measures ANOVA, no main effects or interactions. For (D) and (E), $N = 6$ to 9 mice per group (7 male and 8 female). (**F**) Mice were trained to associate the CS+ with no footshock delivery over five extinction sessions, and the CS− continued to be associated with no footshock delivery. (**G**) CS+ freezing across days between *Th* knockdown and scramble control groups. Two-way repeated measures ANOVA, day × group interaction $F(4,84) = 8.08$, $P < 0.001$, Šidák-adjusted pairwise comparisons day 1 $P = 0.006$, day 3 $P = 0.031$, day 4 $P = 0.038$. $N = 10$ to 13 mice per group (14 male and 9 female). (**H**) CS− freezing across days between *Th* knockdown and scramble control groups. Two-way repeated measures ANOVA, no main effects or interactions. $N = 10$ to 13 mice per group. (**I**) CS+ freezing across days between *Vglut2* knockdown and scramble control groups. Two-way repeated measures ANOVA, no main effects or interactions. $N = 6$ to 9 mice per group (7 male and 8 female). (**J**) CS− freezing across days between *Vglut2* knockdown and scramble control groups. Two-way repeated measures ANOVA, no main effects or interactions. $N = 6$ to 9 mice per group. $^*P < 0.05$, $^{**}P < 0.01$, and $^{***}P < 0.001$.

neurons target the NAcc core (*37*, *60*–*62*) (figs. S6, D and H, and S14A). In this conceptual model, the conditioned stimulus elicited striatal glutamate and/or dopamine release from glutamate-dopamine and nonglutamate-dopamine VTA neurons. Their transmitter outputs modulated a single action drive variable that biased action selection. After neuronal activity crossed a context-dependent threshold, actions were selected in the striatum. The outcome of the action fed back to the striatum and to the stimulus input circuits in proportion to the magnitude and probability of each outcome, shortening the latency to act across conditioning (fig. S14A). Our fixed parameter set aligned the simulated neural activity time series with our cell type–specific GCaMP recordings. Outcome-gated updates to neural stimulus-response relationships gradually updated per-day behavioral trajectories. After conditioning in an appetitive context, modeled nonglutamate-dopamine and glutamate-dopamine VTA neurons activated in response to the conditioned stimulus and the rewarding outcome. In an aversive context, only the glutamate-dopamine VTA neurons responded to the conditioned stimulus and aversive outcome (fig. S14B). We tested the consequences of removing glutamate or dopamine release from glutamate-dopamine neurons in silico. Parameters were fixed to produce response behavior quantitatively consistent with reward and shock feedback-trained control conditions (fig. S14, C to E; variables and parameters defined in table S2). Behavioral outputs of a simulated multiday block demonstrated an increase in the proportion of trials per day that resulted in CS+ hits in the rewarding

Downloaded from https://www.science.org at University of Colorado Boulder on November 21, 2026

context (fig. S14C) and a decrease in the CS+ hit latency (fig. S14D), as well as an increase in freezing in the aversive context (fig. S14E). Knockout conditions resulted in behavior qualitatively similar to that observed in experimental data. Simulated glutamate knockout from glutamate-dopamine neurons slowed the acquisition of CS+-guided reward-seeking (CS+ hit rate) but did not alter the asymptotic performance by the end of training. Simulated glutamate knockout also increased the latency to respond to the reward-predicting CS+. Simulated dopamine knockout reduced the probability of freezing responses to the shock-predicting CS+. Together, our model recapitulated both neural recordings and the contributions of glutamate and dopamine release toward Pavlovian reward- and aversion-based motivated behaviors using a simple neural population model of glutamate-dopamine and nonglutamate-dopamine VTA neurons.

DISCUSSION

Despite well-established heterogeneity in neuronal activity patterns of VTA dopamine neurons (*16*–*27*), it is unclear whether molecular heterogeneity is functionally relevant for the diverse array of motivation-related functions ascribed to VTA dopamine neurons. A primary molecular distinction between subpopulations of VTA dopamine neurons is the presence or absence of the VGluT2, the only mechanism for accumulation of glutamate into synaptic vesicles by VTA neurons (*38*–*40*, *51*). Leveraging INTRSECT vectors in Cre/Flp coexpressing mouse lines, we molecularly untangled the functions of glutamate-dopamine neurons from nonglutamate-dopamine neurons and glutamate-only neurons (nonGABAergic and nondopaminergic).

Key findings

Each VTA cell type had distinguishing single and multidimensional in vivo neuronal activity patterns as well as distinct single ex vivo electrophysiological properties (Fig. 10). Compared with glutamate-dopamine and glutamate-only neurons, key distinguishing features of nonglutamate-dopamine neurons were their suppression of neuronal activity during negative reward prediction error, cues predicting the absence of reward, and both aversive outcomes and cues that predict aversive outcomes. Glutamate-dopamine and glutamate-only neurons were activated by aversive outcomes and their predictors, congruent with other investigations of VTA glutamate neurons (*42*, *49*, *70*, *72*, *73*). Thus, a primary factor distinguishing the function of dopamine neuron subtypes was the direction of their response to negatively valenced events. Consistent with their selective activation by reward-related events, somatic optogenetic stimulation of nonglutamate-dopamine neurons supported reward and reinforcement. Glutamate-dopamine and glutamate-only neurons were activated by both aversive and rewarding stimuli and somatic optogenetic stimulation did not support reward or reinforcement. Nevertheless, in glutamate-dopamine neurons, dopamine and glutamate release machineries contributed to independent components of natural reward- and aversion-motivated behaviors. *Th* was required for associative learning about aversive outcomes without affecting nonassociative or natural aversive processing. *Vglut2* was required for reward- and exploration-related vigor without impinging upon associative reward learning, natural reward intake, or aversive responding. Given that glutamate-dopamine neurons distinctly showed a sustained activity pattern between a reward-predictive cue and reward delivery that has been previously hypothesized to support motivational states (*56*), it is possible that this motivational state involves glutamate release.

The behavioral functions of glutamate-only neurons remain unclear. Their lack of rewarding or aversive consequences after somatic optogenetic stimulation was similar to glutamate-dopamine neurons examined here as well as VTA glutamate-GABA neurons (*73*). We found that glutamate-only neurons are a distinct VTA neuronal subtype distinguished electrophysiologically by more hyperpolarized resting membrane potentials, faster firing rates, and reliable rebound firing patterns after hyperpolarization compared with glutamate-dopamine and nonglutamate-dopamine cell types. Subsets of glutamate-only neurons showed I_h and/or D_2/D_3 receptor sensitivity, features traditionally associated with a dopaminergic phenotype. Subsets of glutamate-only neurons have been observed to project locally to VTA dopamine neurons (*74*) and express the μ opioid receptor (*75*), suggesting further diversity within this subpopulation.

Neuronal signaling patterns from all dopamine neurons (without consideration for glutamate cotransmission) during both reward prediction error and aversive processing obscured subpopulation activity of the intermingling glutamate-dopamine and nonglutamate-dopamine neurons, highlighting the importance of segregating dopaminergic subtypes in functional assays. We also observed similar but not identical dopamine release dynamics in the NAcc after ChRmine stimulation of glutamate-dopamine and nonglutamate-dopamine axons. Some variability was observed in each subpopulation's evoked dopamine release dynamics and may reflect further diversity in the genetic characteristics of glutamate-dopamine and nonglutamate-dopamine neurons (*40*).

Despite their largely distinct (but partially overlapping) anatomical domains in the VTA, in vivo and ex vivo characteristics of VTA cell types could not be explained by anatomical location alone. We found that molecular cell type better explained in vivo behavior-related signaling dynamics than anatomical location within the sampled range. Nevertheless, there may be mediolateral gradients across and within cell types that were not identified. In contrast, multidimensional electrophysiological properties of VTA neurons were not reliably predicted by cell type or location, similar to investigations of electrophysiological properties of *Vglut2*$^+$/*Vgat*$^+$, *Vglut2*$^+$/*Vgat*$^-$, and *Vglut2*$^-$/*Vgat*$^+$ VTA neurons that also did not cluster according to cell type (*76*). These findings likely reflect further heterogeneity within the neuronal subsets described here as well as the influence of afferents that drive distinct patterns of behavior-related Ca^{2+} signaling.

A neural population model was developed that illustrates how glutamate-dopamine cotransmission could bias action selection across learning trials, informed by our in vivo recordings. The model recapitulated both neural recordings and the contributions of glutamate and dopamine release toward Pavlovian reward- and aversion-based motivated behaviors using a simple model of glutamate-dopamine and nonglutamate-dopamine VTA neurons. Greater behavioral and neurophysiological complexity would likely result from additional consideration of heterogeneity in glutamate-dopamine and nonglutamate-dopamine populations as well as distinct subcircuits involving different postsynaptic targets (*36*, *37*, *40*, *77*, *78*).

Electrophysiological properties

Ex vivo, one might predict that glutamate-dopamine neurons would have intermediate electrophysiological characteristics between glutamate-only and nonglutamate-dopamine neurons. In some measures, such as firing rate and action potential duration, this was the case. Glutamate-dopamine neurons were intermediate between the broad action potentials and slower firing rates of nonglutamate-dopamine neurons and the fast action potentials and elevated firing rates of glutamate-only

Downloaded from https://www.science.org at University of Colorado Boulder on November 21, 2026

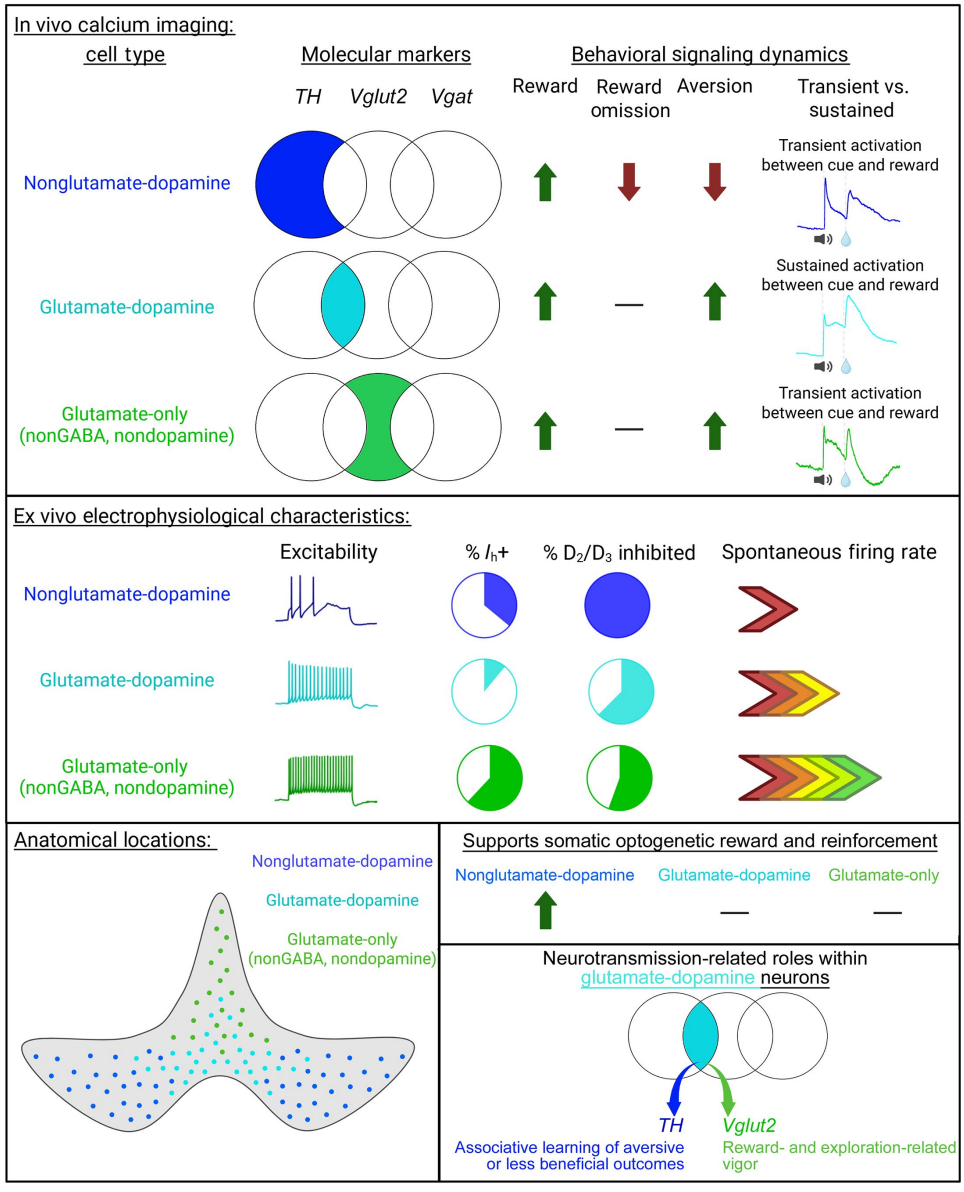


Fig. 10. Summary of major findings. We targeted mutually exclusive VTA populations of nonglutamate-dopamine neurons, glutamate-dopamine cotransmitting neurons, and glutamate-only (nonGABAergic and nondopaminergic) neurons. These populations exhibited distinct in vivo Ca^{2+} signaling dynamics in motivated behaviors and ex vivo electrophysiological properties. Nonglutamate-dopamine neurons were activated at reward and reward-predicting events as well as suppressed at reward omission and aversive stimuli and aversive predictors. Glutamate-dopamine and glutamate-only neurons were activated at both rewarding and aversive events. Glutamate-dopamine neurons exhibited sustained signaling between a cue and reward, in contrast with transient signaling in nonglutamate-dopamine and glutamate-only neurons. Glutamate-only neurons were more spontaneously active than dopaminergic subtypes, and a subset of glutamate-only neurons exhibited a hyperpolarization-induced current and D_2/D_3 receptor inhibition. Although their anatomical domains partially overlap, nonglutamate-dopamine neurons were predominantly found in the lateral VTA, glutamate-dopamine neurons were predominantly in the ventromedial VTA, and glutamate-only neurons were found near the VTA midline. In glutamate-dopamine cotransmitting neurons, dopamine and glutamate neurotransmission had distinct functional roles in motivated behaviors. Dopamine contributed to associative learning of aversive or less-beneficial outcomes and glutamate contributed to reward- and exploration-related vigor. NT, neurotransmitter.

neurons. However, in other measures, glutamate-dopamine neurons were similar to either nonglutamate-dopamine neurons or to glutamate-only neurons, but not the other. For example, both glutamate-dopamine neurons and nonglutamate-dopamine neurons largely lacked rebound firing after hyperpolarization, whereas glutamate-only neurons reliably showed rebound firing. In some properties, glutamate-dopamine neurons were distinct from both glutamate-only neurons and nonglutamate-dopamine neurons. For instance, we observed that a subset of glutamate-only neurons exhibited large I_h similar to nonglutamate-dopamine neurons, whereas glutamate-dopamine neurons largely lacked I_h. Together, glutamate-dopamine neurons had single physiological properties distinct from those of both glutamate-only and nonglutamate-dopamine neurons rather than an intermediate phenotype. Further, the identification of a subset of glutamate-only neurons with traditional electrophysiological markers of dopamine neurons, such as I_h and D_2/D_3 receptor inhibition, supports prior research demonstrating the unreliability of physiological criteria alone for identifying VTA dopamine neurons (*33*, *55*, *79*).

Sustained and transient signaling patterns

During the natural reward task, glutamate-dopamine neurons showed sustained signaling between the CS+ and reward, whereas nonglutamate-dopamine and glutamate-only neurons showed transient signaling. These data extend prior observations that sustained Pavlovian reward-related signaling patterns of VTA dopamine neurons occur in medial VTA, where glutamate-dopamine neurons predominate, and transient Pavlovian reward-related signaling patterns of VTA dopamine neurons have been detected in the lateral VTA, where nonglutamate-dopamine neurons predominate (*56*). Further, dopamine concentration remains elevated for longer durations after reward-predictive cues exclusively in the NAcc shell, where glutamate-dopamine neurons preferentially project, and not in the NAcc core, where nonglutamate-dopamine axons predominate (*80*, *81*). The

Downloaded from https://www.science.org at University of Colorado Boulder on November 21, 2026

transient activity pattern of nonglutamate-dopamine neurons between CS+ and reward likely allowed for their negative reward prediction error signaling (defined as a suppression below baseline) when an expected reward was omitted. Vice versa, the sustained activity pattern of glutamate-dopamine neurons likely prevented the possibility of producing a negative reward prediction error. However, glutamate-only neurons showed transient activity between CS+ and reward but did not signal negative reward prediction error when reward was omitted. These findings suggest that a transient activation pattern is necessary but not sufficient to produce a negative reward prediction error phenotype. Parallel signaling by sustained and transiently activated dopamine neurons has been hypothesized to enable proportional-differential encoding (*56*). Sustained activity in glutamate-dopamine neurons may support a behavioral state such as outcome expectation, whereas transient activity in nonglutamate-dopamine neurons may support rate-of-change processing, which together support an ability to change expectations on the basis of the presence or absence of the expected outcome. It is currently unknown how glutamate-dopamine neuron sustained activation patterns arise. Glutamate-dopamine neurons showed greater firing in a sustained manner compared with nonglutamate-dopamine neurons ex vivo, which may indicate that intrinsic physiological factors underlie a capacity for sustained activity. Likewise, the duration of NAcc dopamine release from glutamate-dopamine neurons scaled linearly with longer stimulation pulse trains, whereas nonglutamate-dopamine neurons scaled curvilinearly, peaking at a lower number of pulses. We previously observed that glutamate-dopamine neuronal activity scales with increases in reward value in duration but not in magnitude (*73*), suggesting that their duration-dependent signaling patterns may be behaviorally meaningful. However, it is unclear from fiber photometry experiments whether sustained Ca^{2+} signaling and dopamine release are exhibited by individual neurons, whether this is a population-level effect, or whether our results are explained by other factors [such as cell-type differences in reuptake through dopamine transporters (*82*) or network participation from local VTA interneurons or long-range circuits]. A key implication of our findings is that somatic activity patterns alone are insufficient to predict the behavioral consequences of glutamate-dopamine neuron activation because *Th* and *Vglut2* influenced distinct aspects of motivated behavior. In addition, excitable and sustained firing was observed in glutamate-only neurons, which had a transient Pavlovian reward-related activation pattern in vivo, in contrast with glutamate-dopamine neurons. Additional research will be necessary to determine the mechanism underlying sustained compared with transient signaling patterns of each VTA cell type.

Comparisons to overlapping populations and pathways

The VTA aversion-related signaling patterns we identified are consistent with the location of VTA neurons that are activated by noxious stimuli in the ventromedial VTA (*17*) where glutamate-dopamine neurons predominate, whereas VTA neurons inhibited by noxious stimuli are located in the lateral VTA (*17*, *19*), where nonglutamate-dopamine neurons predominate. Shock-excited VTA dopamine neurons have been hypothesized to show greater excitability than shock-inhibited dopamine neurons (*17*). We found greater excitability in the shock-excited glutamate-dopamine neurons compared with the shock-suppressed nonglutamate-dopamine neurons, supporting this hypothesis. A subset of D_2 receptor–expressing VTA dopamine neurons are excited by aversive stimuli through *N*-methyl-D-aspartate (NMDA) receptor signaling (*20*), suggesting that the subset of D_2-sensitive glutamate-dopamine neurons may also express NMDA receptors, giving rise to their aversion-related excitation. Given that glutamate-dopamine neurons preferentially innervate the NAcc medial shell, whereas nonglutamate-dopamine neurons preferentially innervate the NAcc core and lateral shell (*37*), our results additionally bolster the observations that aversive stimuli increase dopamine in the NAcc medial shell and decrease dopamine release in the NAcc core (*83*–*85*).

Similar motivation-related activation profiles and ex vivo electrophysiological characteristics have been reported in NAcc shell–projecting *Cck* dopaminergic VTA neurons (presumably glutamate-dopamine) and NAcc core–projecting *Crhr1* dopaminergic VTA neurons (*44*) (presumably nonglutamate-dopamine). However, *Cck* VTA neurons (presumably glutamate-dopamine) were suppressed below baseline at reward omission (*44*), which we did not observe in glutamate-dopamine neurons. Nonetheless, Elum and colleagues posit that *Cck* neurons encode goal-directed actions rather than predictive information, which is in alignment with our observed lack of negative reward prediction error signaling. Further, whereas in vivo electrophysiological properties such as firing rate did not differ between *Cck* and *Crhr1* cell types (*43*), our ex vivo recording indicated that glutamate-dopamine and nonglutamate-dopamine neurons differ in firing rate and other single electrophysiological properties. Thus, whereas *Cck* and *Crhr1* response characteristics may at least partially map onto glutamate-dopamine and nonglutamate-dopamine characteristics, respectively, these findings likely reflect an incomplete overlap of Cck^+ or $Crhr1^+$ populations with $Vglut2^+/Th^+$ or $Vglut2^-/Th^+$ populations.

Dissociable valence-related behavioral roles for glutamate and dopamine from cotransmitting neurons

We inferred from our knockdown experiments that glutamate release from glutamate-dopamine neurons contributed to reward- and exploration-related vigor without affecting associative reward learning or fear learning, natural reward intake, aversion-related vigor, or gross motor deficits. Congruent with this interpretation, VTA dopamine neurons that project to the NAcc shell (glutamate-dopamine neurons) may support motivational vigor in a previously learned reward task (*43*), suggesting a role in the attainment of rewards. Loss of *Vglut2* accelerated cued reward extinction learning, also supporting the interpretation that glutamate transmission influences reward-related vigor. However, because glutamate receptor antagonists block place aversion resulting from optogenetic activation of VTA glutamatergic axons in the NAcc shell (*36*), glutamate release likely plays a role in aversive processes not captured in the present experiments.

In contrast with Vglut2, *Th* knockdown resulted in deficits in suppressing responses to nonreward-predicting cues, cued reward extinction learning, and cued fear learning. The results were not explained by effects on nonassociative memory, anxiety-like behavior, reward-seeking under aversive contexts, innate threat avoidance, or natural aversive processing per se. We inferred that dopamine from glutamate-dopamine neurons supported associative learning about less beneficial or aversive outcomes. Our interpretation supports the finding that the NAcc shell, which glutamate-dopamine neurons heavily innervate, is involved in suppressing actions that are less likely to result in reward attainment (*86*). A possible departure from this pattern is that loss of *Th* impaired extinction of the freezing response to the previously shock-predictive CS+. Although the lack of

Downloaded from https://www.science.org at University of Colorado Boulder on November 21, 2026

shock in extinction is a presumably favorable outcome, extinction learning is contingent upon initial learning of the cue-shock association. It is therefore possible that the impairment in initial learning influenced associative learning or expression of learned fear responses in the extinction phase.

Our interpretations are partially aligned with reports that dopamine signaling drives optogenetically induced aversion and glutamate signaling drives optogenetically induced reward in VTA glutamatergic neurons. Loss of *Th* from VTA *Vglut2*$^+$ neurons reduces optogenetic real-time place avoidance of VTA *Vglut2*$^+$ projections to the NAcc shell, and loss of *Vglut2* from VTA *Vglut2*$^+$ neurons reduces optogenetic self-stimulation of VTA *Vglut2*$^+$ projections to the NAcc shell (*45*). However, we found that *Th* knockdown mice displayed intact active and passive avoidance to naturalistic threats and fear responses to nonassociative threats, and *Vglut2* knockdown mice successfully learned the Pavlovian reward task and had no deficits in natural reward consumption. These distinctions are likely due to several methodological differences such as naturally rewarding or aversive stimuli compared with optogenetically elicited reward or aversion, somatic compared with projection-specific stimulation, and knockdown method. Given that loss of *Vglut2* from dopamine neurons does not affect optogenetic self-stimulation of VTA dopamine neurons (*87*), it is also possible that glutamate release from dopamine neurons may support separate behaviors than glutamate release from all glutamate neurons together. Nevertheless, despite being cohort-matched, a key limitation of our *Vglut2* knockdown experiments in *TH::Flp* mice was a comparison to scramble controls in *VGluT2::Cre* mice, which may have influenced the observed results.

Valence signaling and salience signaling

Dopamine release from VTA has been implicated in both valence-dependent and valence-independent signaling of behaviorally meaningful events (*28*, *88*). Our somatic Ca^{2+} recordings of nonglutamate-dopamine neurons are consistent with bidirectional valence signaling involving increased activity during rewarding stimuli and decreased activity during aversive or less desirable stimuli. Our somatic Ca^{2+} recordings of glutamate-dopamine neurons appeared to be consistent with salience signaling. However, our knockdown experiments in glutamate-dopamine neurons identified dissociable roles for glutamate release and dopamine release in different aspects of motivated behavior. It is therefore possible that somatic activity of glutamate-dopamine neurons reflects apparent salience, whereas their distinct cotransmitters differentially influence valence-related behaviors through multiplexed signaling dynamics that were not captured in somatic Ca^{2+} signaling. At this time, it is unknown whether glutamate-dopamine neurons can independently fine-tune the release of either cotransmitter, whether context or experience may shape the formation and expression of such fine-tuning, or whether separate neurotransmitters are biased to separate projection targets, although many potential modalities have been described as both dependent (*89*–*91*) and independent (*92*–*96*) of somatic firing patterns.

Conclusion

On the basis of our results, we inferred that a key feature determining the motivation-related signaling characteristics and roles in natural reward- and aversion-motivated behaviors of VTA dopamine neurons was whether they released dopamine with or without glutamate cotransmission. Variability within these cell types likely indicates further heterogeneity in the populations described here. A major distinction among dopaminergic subtypes is that nonglutamate-dopamine neurons exhibited bidirectional valence-based signaling and supported somatic optogenetically elicited reward and reinforcement, whereas glutamate-dopamine neurons were unidirectionally activated at positive and negative valence events and did not support somatic optogenetically elicited reward or reinforcement. However, glutamate and dopamine release machineries in glutamate-dopamine cotransmitting neurons supported distinct behaviors, potentially indicating a capacity for multiplexed transmitter-specific influence on behaviorally meaningful events.

MATERIALS AND METHODS

Animals

Vglut2-ires::Cre mice (*Slc17a6*$^{tm2(cre)Lowl}$/J; Jax Stock no. 016963), *Th-2a::FlpO* mice (C57BL/6N-*Th*^{tm1Awar}/Mmmh; RRID:MMRRC_050618-MU), and *Vgat-ires::Cre* mice (*Slc32a1*$^{tm2.1(cre)Lowl}$/J; Jax Stock no. 016962) were bred at the University of Colorado Boulder. *Vglut2::Cre* and *Vgat::Cre* mice were crossed with *Th::Flp* mice to produce *Vglut2::Cre*/*Th::Flp* and *Vgat::Cre*/*Th::Flp* offspring, respectively. Mice were maintained in a colony room with a 12-hour light/dark cycle (lights on at 2200) with ad libitum access to food and water. All animal procedures were performed in accordance with the National Institutes of Health *Guide for the Care and Use of Laboratory Animals* and approved by the University of Colorado Boulder Institutional Animal Care and Use Committee.

Stereotactic surgery

Male and female mice (8 to 28 weeks of age) were anesthetized with 1 to 3% isoflurane and secured in a stereotactic frame (Kopf). For Ca^{2+} imaging experiments, INTRSECT vectors encoding GCaMP6m and sRGECO were used to target select neuronal populations (*59*, *97*). In *Vglut2::Cre*/*Th::Flp* mice, AAV8-Ef1-Con/Fon-GCaMP6m (Addgene no. 137119, 8.5×10^{12} titer, 400 nl) was injected into the VTA (AP −3.20 mm relative to bregma, ML 0.00 mm relative to midline, DV −4.34 mm from skull surface) to target glutamate-dopamine (*Vglut2*$^+$/*Th*$^+$) neurons. In *Vglut2::Cre*/*Th::Flp* mice, AAV8-Ef1-Coff/Fon-GCaMP6m (Addgene 137121, 7.0×10^{12} titer) was injected into the VTA (AP −3.23, ML +0.30, DV −4.34 mm; 400 nl) to target nonglutamate-dopamine (*Vglut2*$^-$/*Th*$^+$) neurons. In *Th::Flp* mice, AAV8-Ef1-Coff/Fon-GCaMP6m (Addgene 137121, 7.0×10^{12} titer) was injected into the VTA (AP −3.23, ML +0.30, DV −4.34 mm; 400 nl) to target all dopamine (*Th*$^+$) neurons regardless of cotransmission capabilities (without respect to Cre). In *Vgat::Cre*/*Th::Flp* mice, AAV8-nEF-(Cre-or-Flp)-Off-GCaMP6m (COFO-GCaMP6m; Neurophotonics, 5×10^{12} titer) was injected into the VTA (AP −3.20, ML 0.00, DV −4.34 mm; 350 nl) to target glutamate-only (*Vgat*$^-$/*Th*$^-$) neurons. In separate *Vglut2::Cre*/*Th::Flp* mice, AAV8-Ef1-Coff/Fon-GCaMP6m (Addgene 137121, 7.0×10^{12} titer) and AAV8-Ef1a-Con/Fon-sRGECO (Addgene 137126, 8.0×10^{12} titer) were coinjected in the VTA (AP −3.20, ML +0.10, DV −4.34 mm; 400 nl total) to target nonglutamate-dopamine (*Vglut2*$^-$/*Th*$^+$) and glutamate-dopamine (*Vglut2*$^+$/*Th*$^+$) neurons, respectively. Total injection volume and flow rate (100 nl/min) were controlled with a microinjection pump (Micro4; World Precision Instruments, Sarasota, FL). The syringe was left in place for an additional 10 min after injection to allow for virus diffusion, after which the syringe was slowly withdrawn to prevent spread by capillary action. Mice in photometry experiments were implanted with an optic fiber cannula (400 μm core diameter, 0.66 NA;

Downloaded from https://www.science.org at University of Colorado Boulder on November 21, 2026

Doric Lenses, Québec, Canada) dorsal to the VTA injection site (GCaMP in glutamate-dopamine and glutamate-only: AP −3.20, ML +1.00 angled at 10°, DV −4.20 mm; GCaMP in nonglutamate-dopamine and all dopamine: AP −3.23, ML +1.30 at 10°, DV −4.25 mm; combined GCaMP-sRGECO in nonglutamate-dopamine and glutamate-dopamine neurons: AP −3.20, ML +1.10 angled at 10°, DV −4.20 mm). Implants were secured to the skull with screws and dental cement. Mice recovered for 3 weeks before experimentation. To verify cell-type specificity of the INTRSECT vectors, male and female mice were injected with GCaMP-encoding AAVs as described above to target glutamate-dopamine neurons, nonglutamate-dopamine neurons, and glutamate-only neurons. After 3 weeks, mice were perfused for in situ hybridization as described below.

For ex vivo electrophysiology experiments, *Vglut2::Cre*/*Th::Flp* mice were injected in the VTA (AP −3.2, ML 0.00, DV −4.34 mm) with Con/Fon-eYFP (Addgene 55650, 5.3×10^{12} titer, 350 nl) to target glutamate-dopamine neurons and, in the same surgery, were injected in the VTA (AP −3.23, ML +0.30, DV −4.34 mm) with Coff/Fon-mCherry (Addgene 137134, 4.8×10^{12} titer, 350 nl) to target nonglutamate-dopamine neurons. To target glutamate-only neurons, *Vgat::Cre*/*Th::Flp* mice were injected in the VTA (AP −3.24, ML 0.00, DV −4.32 mm) with COFO-ChRmine-oScarlet (UNC Neurotools, 3.1×10^{12} titer, 350 nl). After 3 weeks, mice were shipped to George Washington University for whole-cell recordings.

For in vivo optical stimulation and dopamine sensor photometry experiments, male and female *Vglut2::Cre*/*Th::Flp* mice were injected in the NAcc (AP +1.28, ML +0.75, DV −4.50 mm) with pan-neuronal AAV-hSyn-GRAB_DA1h (Addgene no. 113050, 5.0×10^{12} titer, 400 nl). In the same surgery, mice received either AAV8-nEF-Con/Fon-ChRmine-oScarlet (Addgene 137159, 9.0×10^{12} titer, 400 nl) in the VTA (AP −3.25, ML 0.00, DV −4.30 mm) to target glutamate-dopamine neurons or AAV8-nEF-Coff/Fon-ChRmine-oScarlet (Addgene 137160, 9.0×10^{12} titer, 400 nl) in the VTA (AP −3.22, ML +0.30, DV −4.30 mm) to target nonglutamate-dopamine neurons. As a control, *Vglut2::Cre* mice received identical injections of AAV-hSyn-GRAB_DA1h in the NAcc but received AAV8-hSyn-DIO-mCherry (Addgene no. 50459, 8.3×10^{12} titer, 400 nl) in the VTA (AP −3.25, ML 0.00, DV −4.30 mm). All mice were implanted with an optic fiber cannula (400 μm core diameter, 0.66 NA; Doric Lenses, Québec, Canada) dorsal to the NAcc injection site (AP +1.28, ML +0.75, DV −4.30 mm). Implants were secured to the skull with screws and dental cement. Mice were allowed to recover for 3 weeks before experiments were performed.

For real-time place conditioning and self-stimulation experiments, male and female *Vglut2::Cre*/*TH::Flp* mice were injected in the VTA with AAV8-nEF-Con/Fon-ChRmine-oScarlet (Addgene 137159, 9.0×10^{12} titer, 400 nl) in the VTA (AP −3.25, ML 0.00, DV −4.30 mm) to target glutamate-dopamine neurons or AAV8-nEF-Coff/Fon-ChRmine-oScarlet (Addgene 137160, 9.0×10^{12} titer, 400 nl) in the VTA (AP −3.22, ML +0.30, DV −4.30 mm) to target nonglutamate-dopamine neurons. Male and female *Vgat::Cre*/*TH::Flp* mice were injected in the VTA with AAV8-hSyn-COFO-ChRmine-oScarlet (UNC Neurotools, 3.1×10^{12} titer, 350 nl) (AP −3.22, ML +0.30, DV −4.30 mm). As controls, male and female *Vgat::Cre*/*TH::Flp* mice were injected in the VTA with AAV8-hSyn-COFO-oScarlet (Deisseroth lab, 5×10^{12} titer, 400 nl) or AAV5-hSyn-DIO-EGFP (Addgene 50457, 5×10^{12} titer, 400 nl) and male and female *Vglut2::Cre*/*TH::Flp* mice were injected in the VTA with either AAV8-EF1a-Coff/Fon-mCherry or AAV8-EF1a-Con/Fon-EYFP. All mice were implanted with fiber optics (200 μm) dorsal to VTA (−3.2 AP, 1.0 ML at 10°, DV −4.0). Implants were secured to the skull with screws and dental cement. Mice were allowed to recover for 3 weeks before experiments were performed.

To knock down neurotransmission capabilities from VTA cell types, we used Cre- or Flp-inducible AAV2/9 vectors that encode a recombinase-inducible EGFP and a U6 promoter upstream of an shRNA with a complementary sequence to the mRNA transcript of the target gene of interest. The control vector encoded a scrambled shRNA sequence not complementary to any transcript. Vectors were either AAV9-CMV-DIO-(U6-EGFP)-shRNA(Th), AAV9-CMV-DIO-(U6-EGFP)-shRNA(Vglut2), AAV9-CMV-DIO-(U6-EGFP)-shRNA(Vgat), or AAV9-CMV-DIO-(U6-EGFP)-shRNA(Scramble). shRNA sequences were 5′-GGCAAAGTTATCAAGGAGAAA-3′ (for *Vglut2*), 5′-GTGCAGCCCTACCAAGATCAA-3′ (for *Th*), 5′-GCATCATCGTGTTCAGCTACA-3′ (for *Vgat*), and 5′-CCTAAGGTTAAGTCGCCCTCG-3′ (scrambled control).

To test the specificity and effectiveness of Cre-dependent vectors, *Vglut2::Cre* mice were injected with either AAV9-CMV-DIO-(U6-EGFP)-shRNA(Th) (BrainVTA PT-6772), AAV9-CMV-DIO-(U6-EGFP)-shRNA(Vgat) (3, BrainVTA PT-6765), AAV9-CMV-DIO-(U6-EGFP)-shRNA(Vglut2) (BrainVTA PT-5655), or AAV9-CMV-DIO-(U6-EGFP)-shRNA(Scramble) (BrainVTA PT-2644) in the VTA (AP −3.20, ML 0.00, DV −4.34 mm, 1.0 to 2.0×10^{12} titer, 400 nl). TH::Flp mice were injected with AAV9-CMV-fDIO-(U6-EGFP)-shRNA(Vglut2) in the VTA as described. After 4 weeks, tissue was collected and prepared for histological analysis as described below.

In neurotransmitter knockdown behavioral experiments, we knocked down *Th* from glutamate-dopamine neurons by injecting AAV9-CMV-DIO-(U6-EGFP)-shRNA(Th) (BrainVTA PT-6722, 2.0×10^{12} titer, 350 nl) in the VTA (AP −3.20, ML 0.00, DV −4.34) of *Vglut2::Cre* mice. Alternatively, we knocked down *Vglut2* from glutamate-dopamine neurons by injecting AAV9-CMV-fDIO-(U6-EGFP)-shRNA(Vglut2) (BrainVTA PT-8351, 2.88×10^{12} titer, 350 nl) in the VTA (AP −3.20, ML 0.00, DV −4.30) of *Th::Flp* mice. As a control, we injected AAV9-CMV-DIO-(U6-EGFP)-shRNA(Scramble) (BrainVTA PT-2644, 2.0×10^{12} titer) unilaterally (AP −3.20, ML 0.00, DV −4.34; 350 nl) or bilaterally in the VTA (AP −3.20, ML ±0.30, DV −4.34; 250 nl per hemisphere) of *Vglut2::Cre* mice. Control mice were compared with experimentally manipulated mice within their respective cohorts. Experimenters were blinded to experimental conditions.

Pavlovian reward conditioning

Mice were food restricted to 85% free-feeding body weight and were brought daily to behavior chambers (Med-Associates) outfitted with a reward magazine. A syringe pump (Med-Associates) was equipped to deliver 20 μl of sucrose to the reward magazine. To acclimate mice to the reward magazine, mice were administered on the first day 30 uncued presentations of 8% sucrose solution on a variable-interval 60-s schedule. In subsequent daily sessions, mice were trained to consume 8% sucrose in a Pavlovian conditioning task. The task consisted of 30 presentations (trials) of a 10-s conditioned stimulus (CS+: 6 kHz tone) that coterminated with sucrose reward delivery (US: 1.5 s, onset 8.5 s after CS+ onset). The task also included 30 trials that presented a 10-s conditioned stimulus (CS−: white noise) that delivered no sucrose. Trials were delivered on a variable-interval 90-s schedule and cues were programmed for randomized order presentation. Reward port entries were detected by infrared beam break. If a reward

Downloaded from https://www.science.org at University of Colorado Boulder on November 21, 2026

port entry occurred during the CS+ or CS−, it was considered a CS+ hit or CS− hit, respectively. Reward port entries outside the CS+ or CS− were considered uncued entries. For GCaMP experiments, mice trained for a minimum of 9 days, until they reached 3 consecutive days with more than 90% CS+ hits and less than 64% CS− hits. For at least one training day, mice wore dummy tethers on their optic fiber cannula to acclimate them to the recording patch cable. In the subsequent recording session, the paradigm was the same as training except that there were 41 CS+ and 41 CS− trials, and 11% of total trials were CS error (CSe) trials in which the CS+ was presented but did not result in sucrose delivery to measure the neuronal response to prediction error. For knockdown experiments, mice trained for 14 days as described. After training, knockdown mice then began 5 days of extinction training involving 30 CS+ presentations without sucrose delivery on a variable-interval 90-s schedule.

Pavlovian fear conditioning

Ad libitum fed mice were brought for 4 days to behavior chambers outfitted with rod flooring that was electrically connected to a shock generator (Med-Associates). The task consisted of 10 presentations (trials) of a 10-s conditioned stimulus (CS+: 10 kHz tone) that co-terminated with footshock delivery (US: 0.50 mA, 0.5 s, onset 9.5 s after CS+ onset). The task also included 10 trials that presented a 10-s conditioned stimulus (CS−: clicking) that delivered no footshock. Trials were delivered on a variable-interval 90-s schedule, and cues were programmed for randomized order presentation. For GCaMP and combined GCaMP-sRGECO experiments, Ca^{2+} sensors were recorded on the fourth day. For knockdown experiments, mice trained for 4 days as described. After training, knockdown mice began 5 days of extinction training involving 10 CS+ presentations without footshock and 10 CS− presentations on a variable-interval 90-s schedule. Knockdown mice were video recorded with ANY-Maze (Stoelting) or a custom video capture software. Total seconds of freezing, defined as the absence of movement except for breathing and postural adjustments, was scored from videos during the CS+ and CS− cues. Cue discrimination was defined by the average daily (CS+ freezing – CS− freezing) / (CS+ freezing + CS− freezing). On the rare occasion of hardware failure during video recording, the daily average consisted of trials where video was recorded.

Uncued aversive signaling

Ad libitum fed mice were brought on a single day of testing to behavior chambers outfitted with rod flooring that was electrically connected to a shock generator (Med-Associates). During the GCaMP6m and combined GCaMP-sRGECO recordings, mice were administered uncued footshocks of 0.25-, 0.50-, 0.75-, and 1.00-mA intensities (0.5 s). The presentation of shock levels was randomized on a variable-interval 60-s schedule. After the delivery of three shocks per level, the shock generator was disconnected from the rod flooring, and three 0.00-mA "shocks" were delivered on a variable-interval 60-s schedule. For all shocks, including 0.00 mA, shock delivery was accompanied by an audible click.

Ca^{2+} imaging

GCaMP6m was excited at 465 nm, sRGECO (where applicable) was excited at 560 nm, and 405 nm was used as the isosbestic control. Amplitude-modulated signals from the three light-emitting diodes (LEDs) were reflected off dichroic mirrors and coupled into an optic fiber at 20 to 40 μW. Signals from GCaMP, sRGECO, and the isosbestic control channel were returned through the same optic fiber and acquired with femtowatt photo-receivers (Newport, Irvine, CA), digitized at 1 kHz, and recorded by a real-time signal processor [Tucker-Davis Technologies (TDT)]. Analysis of the recorded Ca^{2+} signal was performed using custom-written MATLAB scripts. Signals (465, 560, and 405 nm) were downsampled (10×) and peri-event time histograms (PETHs) were created trial-by-trial between −10 and +20 s surrounding conditioned stimulus (CS+, CS−) onsets. For each trial, data were detrended by regressing the isosbestic control signal (405 nm) on the GCaMP signal (465 nm) and generating a predicted 405-nm signal using the linear model generated during the regression. The predicted 405-nm channel was subtracted from the 465-nm signal to remove movement, photo-bleaching, and fiber bending artifacts (dF). The sRGECO signal (560 nm) was detrended by regressing a linear best-fit line from the trial and subtracting this line from the 560-nm signal. For combined GCaMP and sRGECO recordings in Pavlovian fear conditioning, excitation was triggered from 20 s before CS+ or CS− onset until 20 s after CS+ or CS− offset. Baseline-normalized *z*-scores were taken from −6 to −3 s before CS+ or CS− onset and from 0 to 2 s after CS+ or CS− onset (*70*, *75*). For cued outcome analyses, such as response to reward or shock, normalized *z*-scores were taken 0 to 2 s after each event onset. In cases of nonevents (nonreward in CS− trials and nonshock in CS− trials), the time of the outcome during CS+ trials was imposed and the normalized *z*-scores were taken from 0 to 2 s after each nonevent. For reward omission in CSe trials, normalized *z*-scores were taken at the time corresponding to 1 to 3 s after reward offset in CS+ trials. Within each cell type, the subject- and group-averaged normalized *z*-scores at each cue and outcome were compared with the averaged normalized *z*-scores at the corresponding baseline. When cue- or outcome-related activity was greater than baseline, we calculated the maximum subject-average normalized *z*-score (maximum normalized dF) over the same baseline, cue, and event epochs to identify activation peaks. When cue- or outcome-related activity was lower than baseline, we calculated the minimum subject-average normalized *z*-score (minimum normalized dF) to identify suppressions in activity. To analyze GCaMP activity according to recording location, the mediolateral position of the tip of the optic fiber was manually measured in millimeters from the midline. In categorical analyses, optic fibers proximal to 0.40 mm from midline were considered medial, whereas fibers distal to 0.40 mm from midline were considered lateral.

UMAP projections and cluster analysis

Data were processed for dimensionality reduction and visualized through a UMAP technique (*98*–*101*). The analysis was performed in Python using the library umap-learn (https://umap-learn.readthedocs.io/en/latest). We quantified silhouette scores with the library scikit-learn to examine the quality of the data's clustering. Each dataset (behavior-related GCaMP responses and electrophysiological properties) was categorized by cell type (glutamate-only, glutamate-dopamine, and nonglutamate-dopamine) or recording location (medial VTA and lateral VTA; boundary = ±0.40 mm from midline) to examine whether the data's quantitative clustering was better explained by anatomical location or cell-type identity. We performed the UMAP analysis and calculated the silhouette scores independently in each dataset. The GCaMP dataset was analyzed on 21 variables and 28 mice. To examine cluster quality among only dopaminergic subtypes, we repeated the analysis after removing glutamate-only recordings (21 variables and 17 mice).

Downloaded from https://www.science.org at University of Colorado Boulder on November 21, 2026

For the electrophysiological dataset, we analyzed variables from whole-cell recordings and excluded recorded cells that were missing data for any variable. The analysis was performed on 17 variables and 55 recorded cells. Raw electrophysiological data were used for UMAP analysis, but *z*-scored data were used for heatmap visualization across the diverse variables. The UMAP parameters (n_neighbors = 10, min_dist = 0.1, "correlation" metric for GCaMP, and "Euclidean" metric for electrophysiological) were optimized for these datasets.

ChRmine stimulation and $GRAB_{DA}$ recordings

Ad libitum fed mice were tail restricted by gauze tape and placed inside a Plexiglas container (*49*). The purpose of tail restriction was to minimize locomotor behavior that may feed back onto recorded accumbal dopamine signals but still allow for full body movement. Light (589 nm; 10 mW) was delivered through the recording fiber at 1, 5, 10, 20, or 30 pulses (10 ms pulse width, 20 Hz) once per minute for a total of five stimuli per pulse number condition. The pulse number was randomly ordered, and 5 min of no stimulation was given between pulse number conditions. $GRAB_{DA}$ was excited at 465 nm with an amplitude-modulated signal from an LED reflected off dichroic mirrors and coupled into an optic fiber. Signals from $GRAB_{DA}$ were returned through the same optic fiber and acquired with a femtowatt photo-receiver (Newport, Irvine, CA), digitized at 1 kHz, and recorded by a real-time signal processor (TDT). Analysis of the recorded $GRAB_{DA}$ signal was performed using custom-written MATLAB scripts. Signal (465 nm) was downsampled (10×) and PETHs were created trial-by-trial between −10 and +20 s surrounding the onset of stimulation trains. For each trial, data were detrended by fitting a first-order regression over the entire trial and subtracting the first-order fit from the 465-nm channel data (dF). To assess changes in the magnitude dopamine transmission, maximum baseline-normalized *z*-scores (normalized dF) were taken from −5 to −3 s before stimulation train onset and maximum stimulation *z*-scores were taken from 0 to 2 s after stimulation train onset. To assess changes in the duration of dopamine transmission, the decay time to half-maximum was calculated by the time point after 0 s at which the normalized signal returned to half of the maximum observed value induced by stimulation (*73*). In mCherry control mice, no peaks above baseline were observed in $GRAB_{DA1h}$ fluorescence after 589-nm stimulation, so half-maximum analysis was not performed.

Real-time place conditioning

Mice were placed in a Stoelting AnyBox with conditioned place preference insert. Mice were plugged into optical fibers and allowed to traverse the arena on all days. On the first day, no light stimulation was delivered. The daily session duration was 20 min, with minutes 0 to 10 having a random outer-chamber designated the stimulation chamber and minutes 10 to 20 having the opposite outer-chamber designated the stimulation chamber. When mice were within the stimulation chamber, 589-nm light was delivered to the VTA, and when mice were outside the stimulation chamber, no light was delivered. The time spent in each stimulation chamber was averaged daily. Stimulation frequency (5, 10, 20, or 40 Hz) was randomly assigned over days but was always 5-ms pulse duration, 10 to 15 mW, and 589-nm light controlled by AnyMaze software.

Self-stimulation

Mice were placed in a Stoelting AnyBox with open field insert. Mice were plugged into optical fibers and allowed to traverse the open field for 45 min. Two squares demarcated by white electrical tape were placed between the center and perimeter of the field [3 inch by 3 inch (7.62 cm by 7.62 cm)] with one designated as active square and the other as inactive square. On the first day, no light stimulation was delivered. Entries into the active square resulted in a 1-s train of 589 nm light (40 Hz, 5 ms pulse width, 10 to 12 mW). Training commenced over 3 days before reversing the active and inactive squares. Specifically, entries into the previous inactive square resulted in light delivery, whereas entries into the previous active square had no consequence.

Free sucrose consumption

Mice were food restricted to 85% free-feeding body weight and were brought daily to behavior chambers (Med-Associates) outfitted with a bottle containing 8% sucrose for 60 min. Licks were determined by a lickometer (Med-Associates). Reward intake was defined as the free consumption of 8% sucrose on the third day of free consumption.

Open field locomotor behavior

Ad libitum fed mice were placed in an open field (Any-Box, Stoelting, 40.5 cm by 40.5 cm, walls 35 cm high) and video recorded at 30 Hz using ANY-Maze software for 15 min. Distance traveled, number of immobile episodes, and total immobile time were calculated (ANY-Maze). In ANY-Maze, the slider for immobility detection sensitivity was set to 65% and the minimum immobile period was 2000 ms. For center zone analysis, the center zone was defined as 25% of the total arena surface area. Center zone measures were normalized to total distance traveled within subjects.

Gait assessment

Ad libitum fed mice were placed on a Plexiglas catwalk channel [28.5 cm by 4 cm, side walls 8 cm high, approximately 2 feet (60.96 cm) above the ground] and video recorded from below as they traversed across (QuickTime, 30 Hz). Gait regularity was determined by analysis of paw placement sequences using the six normal step sequence patterns (NSSPs) (*102*, *103*). Paw placements were notated by a frame-by-frame review of catwalk video recordings. Notation began with the first step taken once all paws were in frame and ended when one of the paws reached the distal end of the catwalk. One of six NSSPs (*102*) was then assigned to each paw placement sequence. For a sequence to qualify as an NSSP, the following constraints were applied. First, an NSSP required a minimum of four and fewer than eight paw placements. Second, half-length sequences were included where there was a clear demonstration of uniformity of gait broken by only one irregular step, except at the beginning of a trial where consistency could not be determined by <4 paw placements. Third, NSSPs could begin with any paw placement of the cycle. Last, the RI was not negatively influenced if mice changed from one NSSP to another without intervening paw placements, so long as each sequence contained at least four paw placements (*102*). After NSSPs were assigned to each paw sequence, the RI was used to quantify ambulatory coordination

$$\mathrm{RI} = \frac{\mathrm{NSSP} \cdot 4}{\mathrm{PP}} \cdot 100\,\%$$

where NSSP is the number of valid NSSP sequences and PP is the total number of paw placements. Coordination was defined as the exclusive use of NSSPs during uninterrupted locomotion (*102*, *103*). Thus, an RI score of 100% indicates regular interlimb coordination, that no irregular steps were made, and that the trial consisted entirely of continuous sequences of NSSPs. An RI score of less than

Downloaded from https://www.science.org at University of Colorado Boulder on November 21, 2026

100% indicates some loss of coordination. To measure the latency to cross the catwalk, the number of frames from the start of crossing to the end of crossing was divided by the video frame rate to calculate latency time in seconds. The start of crossing was defined as the frame immediately before all paws entered the viewing plane, and the end of crossing was defined as the frame immediately before the nose reached the end of the catwalk. Mice were given two or three trials and only the trial with the shortest latency was scored.

RotaRod motor assessment

Ad libitum fed mice were placed on the horizontal, rotating rod of a RotaRod apparatus (IITC Life Sciences). The rod's rotations per minute increased at a constant rate from 4 to 16 RPM over the course of 5 min. Mice received one training session consisting of three 5-min trials with 20 min of rest between trials. On the following day, mice were given three trials that ended when the mouse fell off the rod, with 20 min rest in between trials. Fall latency was measured and averaged across the three trials.

Tail immersion test

Ad libitum fed mice were briefly restrained in a restraint tube (Kent Scientific). Approximately 60% of distal tail was placed in 50°C heated water, and the latency to remove the tail was determined. If the mouse did not remove the tail after 10 s, the mouse was not analyzed (one mouse).

Novel object recognition test

Ad libitum fed mice were placed in an open field (AnyBox, Stoelting, 40.5 cm by 40.5 cm, walls 35 cm high) together with two identical copies of an object, termed the familiar object. Familiar objects were either a plastic bottle (Uxcell, 150 ml, 9 cm height × 5 cm diameter, filled with brown paper towels to decrease translucency and adorned with colored tape to increase visual complexity) or a block of interlocking plastic bricks (MEGA BLOKS, Mattel, 9.5 cm by 3 cm by 6.5 cm). Bottle and brick objects were selected for similarity in size, material, and complexity. Objects were positioned in the back left and front right corners of the apparatus 7 cm from the left or right wall and 7 cm from the back or front wall and were secured to the floor with adhesive hook and loop tape (3M). Mice were allowed to explore the familiar objects for 10 min, then were returned to the home cage for 40 min. Meanwhile, both familiar objects were removed. A third identical copy of the familiar object was placed in either the back left or front right corner. A novel object (either the bottle if the familiar object was the brick or the brick if the familiar object was the bottle) was placed in the opposite corner. The familiar object and location of the novel object were randomized across subjects. After the 40-min timeout, mice were returned to the apparatus and were allowed to explore the familiar object and the novel object for 10 min. The familiarization and novel phases were tracked using ANY-Maze software, which calculated the time mice spent investigating each object. When the mouse's head was within 25 mm and oriented toward an object, investigation was scored. Investigation was not scored when the mouse's center point overlapped with the object in the visual field, which indicated that the animal had climbed on top of the object. The orientation angle was set to 90°. Mice were removed from analysis if the total investigation time was less than 20 s in either stage. To determine whether mice could discriminate between the familiar and novel object, the discrimination score was calculated as

$$\text{Discrimination} = \left| \frac{N-F}{N+F} \right|$$

where N is time spent investigating the novel object in the novel phase, F is the time spent investigating the familiar object in the novel phase, and vertical bars represent absolute value (*104*).

Visual loom and visual sweep paradigms

Ad libitum fed mice were placed in an open field (AnyBox, Stoelting, 40.5 cm by 40.5 cm, walls 35 cm high) together with a shelter in the corner of the box. After at least 8 min of acclimation, when mice entered the trigger zone near the center of the apparatus and were facing away from the shelter, the visual sweep or loom stimulus was presented upon a gray background on an overhead monitor (35 cm above the apparatus). The sweep stimulus was a black silhouette of a raptor (29.6° of visual angle) that moved from one side of the monitor to the other over 3 s. The loom stimulus was a black disc that expanded at a diameter of 2° of visual angle to 20° in 250 ms and remained at that size for 250 ms (*69*). The expanding black disc was repeated 15 times with 500-ms pauses. For both paradigms, one trial per mouse was performed. From ANY-Maze-recorded videos, we hand scored the latency until mice performed a freezing response, total duration of freezing, and the latency until mice entered the shelter in the 30 s after onset of the stimulus animation. The latency to re-exit the shelter was also scored. Individual freezing bouts shorter than 500 ms were not scored. If no freezing response was made in 30 s after stimulus onset, the freezing duration was not examined further. If no shelter entry was made in 30 s after stimulus onset, the escape latency and re-exit latency were not examined further. The trial ended after shelter re-exit or 5 min after stimulus offset, whichever was sooner. Exact counts of trials resulting in only freezing, only escaping, or freezing followed by escaping were used to statistically compare the distributions of behavior between treatment groups.

Sucrose shock

Mice were food restricted to 85% free-feeding body weight and were brought daily to behavior chambers (Med-Associates) outfitted with a bottle containing 8% sucrose and rod flooring that was electrically connected to a shock generator (Med-Associates). Licks were determined by a lickometer (Med-Associates). Mice received one acclimation day with 1 hour access to sucrose, after which they received 10-min daily access to sucrose for at least 6 days and until stability criteria were reached (3 consecutive days with <20% variability in number of licks from the 3-day average). Mice were then given one test session with 18-m access to sucrose, during which 10 noncontingent footshocks (0.20 mA) were delivered through the rod flooring at randomized intershock intervals. Intershock intervals ranged from 50 to 150 s. Footshock durations were presented in increasing order: 0.1, 0.2, 0.3., 0.4, 0.5, 0.6, 0.7, 0.8, 0.9, and 1.0 s. ANY-Maze software tracked animals' movements from above. Freezing detection in ANY-Maze was set to level 3 and the minimum immobile period was 500 ms. Mice were assessed for freezing behavior and number of licks at baseline (before the first shock) and in each intershock interval, as well as the latency to return to licking after each shock. Percent of time freezing and number of licks were normalized to the intershock interval duration. Using survival analysis, we also analyzed the shock duration at which each mouse's licking

Downloaded from https://www.science.org at University of Colorado Boulder on November 21, 2026

behavior reached a breakpoint. A death was scored at the intershock interval after which the normalized number of licks dropped below 50% of licks at baseline and did not rise above 50% in any subsequent intershock intervals. For lick latency analysis, intershock intervals in which mice did not lick were scored as the maximum intershock interval (150 s).

Light-dark box

Tests were performed in a two-chambered apparatus (Light/Dark Box, Stoelting, 40.5 cm by 40.5 cm, walls 35 cm high) equipped with tunable adhesive LED strip lights around the top perimeter of the light side. Room lights were turned off and the LED strip lights were adjusted until the illumination at the entrance to the light side measured approximately 600 lux. Ad libitum fed mice were placed into the dark side of the apparatus and an opaque lid was immediately placed over the dark side. ANY-Maze software tracked the animal's location in the light side and calculated the latency to the first exit from the dark side, total number of exits from the dark side, total time spent in the dark side, average duration of visits to the light side, maximum duration of visits to the light side, total distance traveled in the light side, and average walking speed in the light side. The trial ended after 5 min. One trial was performed per mouse.

Histology

Mice were anesthetized with isoflurane and perfused transcardially with phosphate buffer followed by 4% (w/v) paraformaldehyde in 0.1 M phosphate buffer, pH 7.3. Brains were extracted, postfixed overnight in the same fixative and cryoprotected in 18% sucrose in phosphate buffer at 4°C. Coronal sections containing the VTA or NAcc (30 μm) were taken on a cryostat, mounted to gelatin-coated slides, and imaged for GFP or oScarlet and optical fiber cannula placement depending on experimental condition on a Zeiss Axioscope, a Nikon A1R microscope, or an Olympus VS200 slide scanner. Experimenters were blinded to experimental conditions.

In situ hybridization and immunohistochemistry

Mice were anesthetized with isoflurane and perfused transcardially with RNase-free phosphate buffer and RNase-free 4% (w/v) paraformaldehyde in 0.1 M phosphate buffer, pH 7.3. VTA sections (14 μm) were mounted onto Fisher SuperFrost Plus slides, and RNAscope in situ hybridization was performed according to the manufacturer's instructions. Briefly, sections were treated with heat and protease digestion and hybridized with target probes for mouse *Slc17a6* (*Vglut2*) mRNA (ACDBio no. 319171, 1:50) and *Slc32a1* (*Vgat*) mRNA (ACDBio no. 319191, 1:50). *Vglut2* mRNA was hybridized with an Opal650 label probe (Akoya Biosciences FP1496001KT, 1:750) and *Vgat* mRNA was hybridized with an Opal570 label probe (Akoya Biosciences FP1488001KT, 1:750). Sections were immunolabeled with mouse anti-GFP (Clontech Labs 3P 632381, 1:100) and donkey anti-mouse Alexa Fluor 488 (Jackson ImmunoResearch 715545150, 1:200) to amplify viral fluorophore (GCaMP or shRNA-EGFP) expression and with rabbit anti-TH (Abcam ab112, 1:100) and donkey anti-rabbit DyLight 405 (Jackson ImmunoResearch 711475152, 1:200) to label TH. Slides were coverslipped in Prolong Diamond mountant (Thermo Fisher Scientific) and imaged on a Nikon A1R confocal (20×) with z-stacked images in 3-μm steps at 512 × 512 pixel resolution. Manual cell counts in Adobe Photoshop were performed to identify $mRNA^{+/-}$ neurons (at least three puncta per soma) and/or $TH^{+/-}$ neurons among GFP^{+} somata.

Slice preparation for electrophysiology

After 1 week of acclimation to George Washington University, acute slices were prepared as previously described (*75*) from mice anesthetized with ketamine (100 mg/kg) and dexmedetomidine (0.25 mg/kg). Mice were perfused with 34°C NMDG ringer: 92 mM NMDG, 2.5 mM KCl, 1.2 mM NaH_2PO_4, 30 mM $NaHCO_3$, 20 mM Hepes, 25 mM glucose, 5 mM sodium ascorbate, 2 mM thiourea, 3 mM sodium pyruvate, 10 mM $MgSO_4$, and 0.5 mM $CaCl_2$ (*92*). After perfusion, brains were rapidly dissected and horizontal slices (220 mM) were prepared in warmed NMDG ringer using a vibratome. Slices were incubated for 1 hour at 34°C in oxygenated Hepes holding solution: 86 mM NaCl, 2.5 mM KCl, 1.2 mM NaH_2PO_4, 35 mM $NaHCO_3$, 20 mM Hepes, 25 mM glucose, 5 mM sodium ascorbate, 2 mM thiourea, 3 mM sodium pyruvate, 1 mM $MgSO_4$, and 2 mM $CaCl_2$ (*105*) and were held in the same solution at room temperature until use.

Electrophysiology

Electrophysiological recordings were performed using a Sutterpatch integrated patch amplifier. Midbrain slices were continuously perfused at 1.5 to 2 ml/min with artificial cerebrospinal fluid (ACSF) (28 to 32°C) containing the following: 126 mM NaCl, 21.4 mM $NaHCO_3$, 2.5 mM KCl, 1.2 mM NaH_2PO_4, 2.4 mM $CaCl_2$, 1.0 mM $MgSO_4$, and 11.1 mM glucose. Potassium gluconate internal solution was used for all recordings and contained the following (mM): 35 K-gluconate, 10 Hepes, 4 KCl, 4 Mg-ATP, and 0.3 Na_3-GTP. Junction potential was not corrected for. Cell types were identified by eYFP, tdTomato, or oScarlet fluorescence. Capacitance was measured using Sutterpatch software upon break-in. Input resistance was calculated using Ohm's law and the voltage responses to a series of hyperpolarizing current steps. Steps that induced a sag were excluded from calculation of input resistance. I_h was measured in voltage clamp. Cells were held at −50 mV and were subjected to a series of 500 ms hyperpolarizing voltage steps ranging from −10 to −50 mV. I_h was determined by the mean current at the end of the 500-ms step subtracted from the mean leak current at the onset of the step. Cells were considered I_h+ if they exhibited a current >25 pA in response to a 50-mV step. Spontaneous action potentials were collected in whole-cell current clamp mode. Action potential properties were measured using Sutterpatch's action potential analysis module. Properties of between 10 and 50 action potentials (depending on firing rate of cell) collected shortly after break-in were averaged from each cell. Although bursting in slices was rare, action potentials in bursts were not included in analysis of action potential properties. Evoked action potentials were measured in response to escalating depolarizing 500-ms current injections (increments of 25 pA). Cell-attached recordings were obtained in the loose-patch configuration (*106*). Baseline firing rate was determined over a 30-s period at the end of 3 min of stable firing. For recordings examining responses to D_2/D_3 receptor agonism, 1 μM quinpirole (*32*) was added to the bath after a 5-min baseline of steady firing, and firing rate was measured again over a 30-s period 10 min after quinpirole addition.

Neural population model of VTA-striatum in reward/shock feedback task

Guided by our cell type–specific recordings, we used a minimal population model comprising nonglutamate-dopamine and glutamate-dopamine units, slow filtering of inputs, and a single action-drive variable. We next detail the state-update equations. As identified in our Ca^{2+} imaging experiments, we incorporated a population of

Downloaded from https://www.science.org at University of Colorado Boulder on November 21, 2026

purely dopamine-expressing neurons u_t^d from the VTA and a coexpressing population u_t^{gd} that releases glutamate and dopamine. These were each driven by the stimulus and feedback according to the differential equation ($\dot{u} = \frac{du}{dt}$: time derivative)

$$\dot{u}_t^d = -\frac{u_t^d}{\tau_u} + \left(w_t^{di} \cdot \dot{I}_t + w_t^{dss}\right) \cdot I_t + w_t^{df} \cdot \delta_{tf}$$

and

$$\dot{u}_t^{gd} = -\frac{u_t^{gd}}{\tau_u} + \left(w_t^{gdi} \cdot \dot{I}_t + w_t^{gdss}\right) \cdot I_t + w_t^{gdf} \cdot \delta_{tf}$$

where $\tau_u = 10$ s is the slow decay timescale of activity in both neural populations established by either neuromodulation or slow short-term synaptic plasticity (*107*, *108*). The conditioned stimulus input $I_t = H_t - H_{tf}$ is a square wave lasting until the potential feedback time $tf = 10$ s, generating both instantaneous w_t^{xi} and steady-state w_t^{xss} responses. Feedback $r_t = (\delta_{tf}, \chi_t)$ potentially generated at the $t = tf$ was either reward $\chi_t = \chi_{\text{rew}}$ or shock $\chi_t = \chi_{\text{shock}}$ and triggered reweighting of the input/feedback weights w_t^{xf}

$$\dot{w}_t^{xy} = -\frac{w_t^{xy}}{\tau_p} + \left(\left[\chi_t = \chi_{\text{rew}}\right] \cdot \overline{w}_t^{xyr} + \left[\chi_t = \chi_{\text{shock}}\right] \cdot \overline{w}_t^{xys}\right) \cdot \delta_{tf}$$

where reward compared with shock feedback drove the long-term weight toward different steady-state values, parameterized in the reward context as $\overline{w}_t^{dir} = 0.208$, $\overline{w}_t^{dssr} = 0.0160$, $\overline{w}_t^{dfr} = 0.0128$, $\overline{w}_t^{gdir} = 0.176$, $\overline{w}_t^{gdssr} = 0$, $\overline{w}_t^{gdfr} = 0.0096$, and $\tau_p = 25{,}000$ s, and in the shock context as $\overline{w}_t^{dis} = 0.566$, $\overline{w}_t^{dsss} = 0.404$, $\overline{w}_t^{dfs} = 0.242$, $\overline{w}_t^{gdis} = -0.0808$, $\overline{w}_t^{gdsss} = 0$, $\overline{w}_t^{gdfs} = 0$, and $\tau_p = 1000$ s to qualitatively match time series of our neural population recordings. Synaptic release by these neural populations was given by the evolution equations

$$\tau_s \cdot \dot{s}_t^{d1} = -s_t^{d1} + w_s \cdot u_t^d$$

$$\tau_s \cdot \dot{s}_t^{d2} = -s_t^{d2} + w_s \cdot u_t^{gd}$$

$$\tau_s \cdot \dot{s}_t^{g} = -s_t^{g} + w_s \cdot u_t^{gd}$$

with timescales $\tau_s = 10$ s and synaptic scaling $w_s = 0.3$. The total dopamine driving the action selection circuit in striatum was $s_t^{dtot} = s_t^{d1} + s_t^{d2}$. Dopamine and glutamate were weighted and noise was added to account for stochasticity so the action variable evolves as

$$\dot{a}_t = w_t^d \cdot s_t^{dtot} + w_t^g \cdot s_t^g + \sigma \cdot \xi_t$$

Given the learned context $c \in \{\chi_{\text{rew}}, \chi_{\text{shock}}\}$, if a_t crosses the decision threshold θ before $t = tf$, then either a nose poke or freeze response was generated at the first time $a_t \geq \theta$. A rapid learning rule used feedback to train the neurotransmitter weights $w_t^d \to 0.3$ and $w_t^g \to 0.4$ and the noise amplitude and choice threshold according to the context, so if $c = \chi_{\text{rew}}$, $\sigma = 0.707$, and $\theta \to 0.6$ and $c = \chi_{\text{shock}}$, then $\sigma = 0.224$ and $\theta \to 2.5$. For glutamate knockout experiments in the reward context and dopamine knockout experiments in the shock context, we set $w_t^g \to 0$ $(w_t^d \to 0.2)$.

Testing model on numerical knockout experiments and significance measures

To simulate 10 different subjects each, we ran 10 realizations each of the four different task conditions: (i) 50/50 rewarded control; (ii) rewarded glutamate knockout; (iii) shock control; and (iv) shock dopamine knockout. All trainable weights were initialized to zero at the beginning of a block. Each simulated day contained 20 sequential trials, and 20 simulated days were run per block. Each trial lasted 40 s with a 10-s conditioned stimulus time and 30-s postchoice time. Evolution equations were solved using the Euler-Maruyama method with $dt = 0.01$ s. We recorded whether a choice was made on each trial and if so, the reaction time, using these to compute the mean and SE each day across subjects for each block. The 10 subject means were used to compute the Euclidean pairwise distance between choice fractions and reaction times between control and knockout conditions. This was compared with a distribution of distances computed from 10^4 shuffled versions of the dataset to compute *P* values for these statistics in the two blocks.

Statistical tests

GCaMP behavior and neuronal experiments, GRAB_{DA} experiments, and knockdown experiments were statistically analyzed in SPSS (IBM) or Prism (GraphPad), and figures were generated in Prism and Photoshop (Adobe). For all tests, α was set to 0.05 (data file S1).

To compare training-related differences before GCaMP recording, two-way repeated measures analyses of variance (ANOVAs) compared days of training and cell-type group for percent CS+ hits and CS− hits. To identify cell type–specific GCaMP signaling changes, repeated measures ANOVAs compared differences between baseline, cue, and outcome epochs for each cell type. Maximum or minimum normalized *z*-scores were used for analyses as described above. After significant effects of epoch, we prioritized determining differences in neuronal activity between baseline and cue or baseline and outcome. Therefore, simple contrast tests were used. In prediction error trials, *t* tests compared minimum normalized *z*-scores between baseline and reward omission. To assess whether signaling was transient or sustained, paired *t* tests compared maximum CS+ *z*-score with the prereward or preshock outcome (−2 to 0 s before outcome). To assess aversion scaling, two-way repeated measures ANOVAs compared *z*-scores 0 to 2 s after shock within cell types across independent variables of current and epoch. Šidák-adjusted pairwise comparisons were performed upon significant main effects or interaction. To determine whether the cell type–specific patterns of behavior-related activation could be explained by anatomical recording location, these analyses were repeated identically after mice were recategorized according to medial or lateral recording fiber position irrespective of cell type. To assess correlations between anatomical recording location and GCaMP signaling dynamics, separate linear regressions compared the mediolateral recording fiber coordinate with *z*-scores at behavioral events. For GRAB_{DA} experiments, two-way repeated measures ANOVAs compared maximum *z*-score after optogenetic pulses across epoch and pulse number for each cell type–specific projection. Šidák-adjusted pairwise comparisons followed up significant main effects of epoch or pulse number and interaction. Repeated measures ANOVAs compared decay time with half-maximum *z*-score across pulse numbers for each cell type–specific projection. Šidák-adjusted pairwise comparisons were performed upon significant effects of pulse number. For real-time place conditioning experiments, mixed ANOVAs with frequency as a within-subjects factor and group as a between-subjects factor were used. For self-stimulation experiments,

Downloaded from https://www.science.org at University of Colorado Boulder on November 21, 2026

mixed ANOVAs with day as a within-subjects factor and group as a between-subjects factor were used. For both real-time place conditioning and self-stimulation experiments, Šidák-adjusted pairwise comparisons were performed upon significant main effects or interactions. For knockdown Pavlovian reward or fear behavioral experiments, two-way repeated measures or mixed model ANOVAs compared variables of interest across days and groups. Šidák-adjusted pairwise comparisons were performed upon significant main effects or interactions. For other knockdown comparisons between two groups alone (such as free sucrose licks), independent samples *t* tests were conducted. When the assumption of normal distribution was not met as determined by a Shapiro-Wilk test, a nonparametric Mann-Whitney *U* test was used. Homogeneity of variance was confirmed in all comparisons with *F* tests. To compare the survival curves of licking behavior in intershock intervals between knockdown and control mice, a Mantel-Cox log-rank test was used. To compare the number of trials resulting in different responses to the visual sweep and visual loom stimuli between knockdown and control mice, Fisher's exact test was used. For all ANOVAs, if the assumption of sphericity was not met (Mauchley's test), the Greenhouse-Geisser correction was used. For all *t* tests or nonparametric Mann-Whitney *U* tests, two-tailed tests were used. Electrophysiological data were analyzed using Sutterpatch software and GraphPad Prism. Repeated measures were analyzed using a two-way repeated measures ANOVA or mixed-effect model followed by Dunnett's multiple comparison test. Action potential half-width, AHP size, and firing rate were measured by a one-way ANOVA or Welch ANOVA (when SDs were unequal) followed by a Tukey's test.

Supplementary Materials

The PDF file includes:
Figs. S1 to S14
Tables S1 and S2
Legend for data file S1

Other Supplementary Material for this manuscript includes the following:
Data file S1
MDAR Reproducibility Checklist

REFERENCES AND NOTES

1. M. Morales, E. B. Margolis, Ventral tegmental area: Cellular heterogeneity, connectivity and behaviour. *Nat. Rev. Neurosci.* **18**, 73–85 (2017).
2. H. Jeong, A. Taylor, J. R. Floeder, M. Lohmann, S. Mihalas, B. Wu, M. Zhou, D. A. Burke, V. M. K. Namboodiri, Mesolimbic dopamine release conveys causal associations. *Science* **378**, eabq6740 (2022).
3. M. J. Sharpe, C. Y. Chang, M. A. Liu, H. M. Batchelor, L. E. Mueller, J. L. Jones, Y. Niv, G. Schoenbaum, Dopamine transients are sufficient and necessary for acquisition of model-based associations. *Nat. Neurosci.* **20**, 735–742 (2017).
4. M. J. Sharpe, G. Schoenbaum, Evaluation of the hypothesis that phasic dopamine constitutes a cached-value signal. *Neurobiol. Learn. Mem.* **153**, 131–136 (2018).
5. K. C. Berridge, T. E. Robinson, What is the role of dopamine in reward: Hedonic impact, reward learning, or incentive salience? *Brain Res. Rev.* **28**, 309–369 (1998).
6. W. Schultz, Predictive reward signal of dopamine neurons. *J. Neurophysiol.* **80**, 1–27 (1998).
7. W. Schultz, P. Dayan, P. R. Montague, A neural substrate of prediction and reward. *Science* **275**, 1593–1599 (1997).
8. J. D. Salamone, A. Wisniecki, B. B. Carlson, M. Correa, Nucleus accumbens dopamine depletions make animals highly sensitive to high fixed ratio requirements but do not impair primary food reinforcement. *Neuroscience* **105**, 863–870 (2001).
9. J. D. Salamone, M. Correa, S. M. Mingote, S. M. Weber, Beyond the reward hypothesis: Alternative functions of nucleus accumbens dopamine. *Curr. Opin. Pharmacol.* **5**, 34–41 (2005).
10. E. J. Nestler, W. A. Carlezon Jr., The mesolimbic dopamine reward circuit in depression. *Biol. Psychiatry* **59**, 1151–1159 (2006).
11. Y. Niv, N. D. Daw, D. Joel, P. Dayan, Tonic dopamine: Opportunity costs and the control of response vigor. *Psychopharmacology* **191**, 507–520 (2007).
12. A. B. Barron, E. Søvik, J. L. Cornish, The roles of dopamine and related compounds in reward-seeking behavior across animal phyla. *Front. Behav. Neurosci.* **4**, 163 (2010).
13. P. W. Glimcher, Understanding dopamine and reinforcement learning: The dopamine reward prediction error hypothesis. *Proc. Natl. Acad. Sci. U.S.A.* **108**, 15647–15654 (2011).
14. S. Waddell, Reinforcement signalling in *Drosophila*; dopamine does it all after all. *Curr. Opin. Neurobiol.* **23**, 324–329 (2013).
15. R. A. Wise, Dopamine, learning and motivation. *Nat. Rev. Neurosci.* **5**, 483–494 (2004).
16. J. C. Horvitz, Mesolimbocortical and nigrostriatal dopamine responses to salient non-reward events. *Neuroscience* **96**, 651–656 (2000).
17. F. Brischoux, S. Chakraborty, D. I. Brierley, M. A. Ungless, Phasic excitation of dopamine neurons in ventral VTA by noxious stimuli. *Proc. Natl. Acad. Sci. U.S.A.* **106**, 4894–4899 (2009).
18. E. S. Bromberg-Martin, M. Matsumoto, O. Hikosaka, Dopamine in motivational control: Rewarding, aversive, and alerting. *Neuron* **68**, 815–834 (2010).
19. B. Mileykovskiy, M. Morales, Duration of inhibition of ventral tegmental area dopamine neurons encodes a level of conditioned fear. *J. Neurosci.* **31**, 7471–7476 (2011).
20. L. S. Zweifel, J. P. Fadok, E. Argilli, M. G. Garelick, G. L. Jones, T. M. K. Dickerson, J. M. Allen, S. J. Y. Mizumori, A. Bonci, R. D. Palmiter, Activation of dopamine neurons is critical for aversive conditioning and prevention of generalized anxiety. *Nat. Neurosci.* **14**, 620–626 (2011).
21. M. P. Saddoris, J. A. Sugam, G. D. Stuber, I. B. Witten, K. Deisseroth, R. M. Carelli, Mesolimbic dopamine dynamically tracks, and is causally linked to, discrete aspects of value-based decision making. *Biol. Psychiatry* **77**, 903–911 (2015).
22. A. Eban-Rothschild, G. Rothschild, W. J. Giardino, J. R. Jones, L. De Lecea, VTA dopaminergic neurons regulate ethologically relevant sleep–wake behaviors. *Nat. Neurosci.* **19**, 1356–1366 (2016).
23. Y. S. Jo, G. Heymann, L. S. Zweifel, Dopamine neurons reflect the uncertainty in fear generalization. *Neuron* **100**, 916–925.e3 (2018).
24. B. Engelhard, J. Finkelstein, J. Cox, W. Fleming, H. J. Jang, S. Ornelas, S. A. Koay, S. Y. Thiberge, N. D. Daw, D. W. Tank, I. B. Witten, Specialized coding of sensory, motor and cognitive variables in VTA dopamine neurons. *Nature* **570**, 509–513 (2019).
25. J. Y. Choi, H. J. Jang, S. Ornelas, W. T. Fleming, D. Fürth, J. Au, A. Bandi, E. A. Engel, I. B. Witten, A comparison of dopaminergic and cholinergic populations reveals unique contributions of VTA dopamine neurons to short-term memory. *Cell Rep.* **33**, 108492 (2020).
26. J. C. R. Grove, L. A. Gray, N. La Santa Medina, N. Sivakumar, J. S. Ahn, T. V. Corpuz, J. D. Berke, A. C. Kreitzer, Z. A. Knight, Dopamine subsystems that track internal states. *Nature* **608**, 374–380 (2022).
27. C. Solié, B. Girard, B. Righetti, M. Tapparel, C. Bellone, VTA dopamine neuron activity encodes social interaction and promotes reinforcement learning through social prediction error. *Nat. Neurosci.* **25**, 86–97 (2022).
28. M. G. Kutlu, J. E. Zachry, P. R. Melugin, S. A. Cajigas, M. F. Chevee, S. J. Kelly, B. Kutlu, L. Tian, C. A. Siciliano, E. S. Calipari, Dopamine release in the nucleus accumbens core signals perceived saliency. *Curr. Biol.* **31**, 4748–4761.e8 (2021).
29. S. Lammel, B. K. Lim, R. C. Malenka, Reward and aversion in a heterogeneous midbrain dopamine system. *Neuropharmacology* **76**, 351–359 (2014).
30. S. Ikemoto, Dopamine reward circuitry: Two projection systems from the ventral midbrain to the nucleus accumbens-olfactory tubercle complex. *Brain Res. Rev.* **56**, 27–78 (2007).
31. S. Lammel, A. Hetzel, O. Hackel, I. Jones, B. Liss, J. Roeper, Unique properties of mesoprefrontal neurons within a dual mesocorticolimbic dopamine system. *Neuron* **57**, 760–773 (2008).
32. E. B. Margolis, J. M. Mitchell, J. Ishikawa, G. O. Hjelmstad, H. L. Fields, Midbrain dopamine neurons: Projection target determines action potential duration and dopamine D_2 receptor inhibition. *J. Neurosci.* **28**, 8908–8913 (2008).
33. S. Lammel, D. I. Ion, J. Roeper, R. C. Malenka, Projection-specific modulation of dopamine neuron synapses by aversive and rewarding stimuli. *Neuron* **70**, 855–862 (2011).
34. T. S. Hnasko, G. O. Hjelmstad, H. L. Fields, R. H. Edwards, Ventral tegmental area glutamate neurons: Electrophysiological properties and projections. *J. Neurosci.* **32**, 15076–15085 (2012).
35. S. Lammel, B. K. Lim, C. Ran, K. W. Huang, M. J. Betley, K. M. Tye, K. Deisseroth, R. C. Malenka, Input-specific control of reward and aversion in the ventral tegmental area. *Nature* **491**, 212–217 (2012).
36. J. Qi, S. Zhang, H. L. Wang, D. J. Barker, J. Miranda-Barrientos, M. Morales, VTA glutamatergic inputs to nucleus accumbens drive aversion by acting on GABAergic interneurons. *Nat. Neurosci.* **19**, 725–733 (2016).
37. S. Mingote, A. Amsellem, A. Kempf, S. Rayport, N. Chuhma, Dopamine-glutamate neuron projections to the nucleus accumbens medial shell and behavioral switching. *Neurochem. Int.* **129**, 104482 (2019).
38. T. Yamaguchi, W. Sheen, M. Morales, Glutamatergic neurons are present in the rat ventral tegmental area. *Eur. J. Neurosci.* **25**, 106–118 (2007).

Downloaded from https://www.science.org at University of Colorado Boulder on November 21, 2026

39. T. Yamaguchi, H. L. Wang, X. Li, T. H. Ng, M. Morales, Mesocorticolimbic glutamatergic pathway. *J. Neurosci.* **31**, 8476–8490 (2011).
40. X. Li, J. Qi, T. Yamaguchi, H. L. Wang, M. Morales, Heterogeneous composition of dopamine neurons of the rat A10 region: Molecular evidence for diverse signaling properties. *Brain Struct. Funct.* **218**, 1159–1176 (2013).
41. D. H. Root, S. Zhang, D. J. Barker, J. Miranda-Barrientos, B. Liu, H. L. Wang, M. Morales, Selective brain distribution and distinctive synaptic architecture of dual glutamatergic-GABAergic neurons. *Cell Rep.* **23**, 3465–3479 (2018).
42. D. H. Root, D. J. Barker, D. J. Estrin, J. A. Miranda-Barrientos, B. Liu, S. Zhang, H. L. Wang, F. Vautier, C. Ramakrishnan, Y. S. Kim, L. Fenno, K. Deisseroth, M. Morales, Distinct signaling by ventral tegmental area glutamate, GABA, and combinatorial glutamate-GABA neurons in motivated behavior. *Cell Rep.* **32**, 108094 (2020).
43. G. Heymann, Y. S. Jo, K. L. Reichard, N. McFarland, C. Chavkin, R. D. Palmiter, M. E. Soden, L. S. Zweifel, Synergy of distinct dopamine projection populations in behavioral reinforcement. *Neuron* **105**, 909–920.e5 (2020).
44. J. E. Elum, E. R. Szelenyi, B. Juarez, A. D. Murry, G. Loginov, C. A. Zamorano, P. Gao, G. Wu, S. Ng-Evans, J. X. Yee, X. Xu, S. A. Golden, L. S. Zweifel, Distinct dynamics and intrinsic properties in ventral tegmental area populations mediate reward association and motivation. *Cell Rep.* **43**, 114668 (2024).
45. S. M. Warlow, S. M. Singhal, N. G. Hollon, L. Faget, D. S. Dowlat, V. Zell, A. C. Hunker, L. S. Zweifel, T. S. Hnasko, Mesoaccumbal glutamate neurons drive reward via glutamate release but aversion via dopamine co-release. *Neuron* **112**, 488–499.e5 (2024).
46. K. R. Tovar, G. L. Westbrook, Amino-terminal ligands prolong NMDA receptor-mediated EPSCs. *J. Neurosci.* **32**, 8065–8073 (2012).
47. C. E. Vaaga, M. Borisovska, G. L. Westbrook, Dual-transmitter neurons: Functional implications of co-release and co-transmission. *Curr. Opin. Neurobiol.* **29**, 25–32 (2014).
48. N. Uchida, Bilingual neurons release glutamate and GABA. *Nat. Neurosci.* **17**, 1432–1434 (2014).
49. D. J. McGovern, A. Ly, K. L. Ecton, D. T. Huynh, E. D. Prevost, S. C. Gonzalez, C. J. McNulty, A. R. Rau, S. T. Hentges, T. L. Daigle, B. Tasic, M. V. Baratta, D. H. Root, Ventral tegmental area glutamate neurons mediate nonassociative consequences of stress. *Mol. Psychiatry* **29**, 1671–1682 (2024).
50. M. F. Barbano, H. Wang, S. Zhang, A. V. Shevelkin, K. J. Yu, C. T. Richie, B. Liu, S. Hahn, R. Ye, M. Morales, VTA monosynaptic connections by local glutamate and GABA neurons and their distinct roles in behavior. *Nat. Commun.* **16**, 8500 (2025).
51. T. Yamaguchi, J. Qi, H. L. Wang, S. Zhang, M. Morales, Glutamatergic and dopaminergic neurons in the mouse ventral tegmental area. *Eur. J. Neurosci.* **41**, 760–772 (2015).
52. M. Morales, D. H. Root, Glutamate neurons within the midbrain dopamine regions. *Neuroscience* **282**, 60–68 (2014).
53. D. H. Root, C. A. Mejias-Aponte, S. Zhang, H. L. Wang, A. F. Hoffman, C. R. Lupica, M. Morales, Single rodent mesohabenular axons release glutamate and GABA. *Nat. Neurosci.* **17**, 1543–1551 (2014).
54. D. H. Root, H.-L. Wang, B. Liu, D. J. Barker, L. Mód, P. Szocsics, A. C. Silva, Z. Maglóczky, M. Morales, Glutamate neurons are intermixed with midbrain dopamine neurons in nonhuman primates and humans. *Sci. Rep.* **6**, 30615 (2016).
55. E. B. Margolis, H. Lock, G. O. Hjelmstad, H. L. Fields, The ventral tegmental area revisited: Is there an electrophysiological marker for dopaminergic neurons? *J. Physiol.* **577**, 907–924 (2006).
56. J. W. de Jong, Y. Liang, J. P. H. Verharen, K. M. Fraser, S. Lammel, State and rate-of-change encoding in parallel mesoaccumbal dopamine pathways. *Nat. Neurosci.* **27**, 309–318 (2024).
57. S. J. Gershman, J. A. Assad, S. R. Datta, S. W. Linderman, B. L. Sabatini, N. Uchida, L. Wilbrecht, Explaining dopamine through prediction errors and beyond. *Nat. Neurosci.* **27**, 1645–1655 (2024).
58. M. P. Saddoris, F. Cacciapaglia, R. M. Wightman, R. M. Carelli, Differential dopamine release dynamics in the nucleus accumbens core and shell reveal complementary signals for error prediction and incentive motivation. *J. Neurosci.* **35**, 11572–11582 (2015).
59. L. E. Fenno, C. Ramakrishnan, Y. S. Kim, K. E. Evans, M. Lo, S. Vesuna, M. Inoue, K. Y. M. Cheung, E. Yuen, N. Pichamoorthy, A. S. O. Hong, K. Deisseroth, Comprehensive dual-and triple-feature intersectional single-vector delivery of diverse functional payloads to cells of behaving mammals. *Neuron* **107**, 836–853.e11 (2020).
60. S. Zhang, J. Qi, X. Li, H. L. Wang, J. P. Britt, A. F. Hoffman, A. Bonci, C. R. Lupica, M. Morales, Dopaminergic and glutamatergic microdomains in a subset of rodent mesoaccumbens axons. *Nat. Neurosci.* **18**, 386–392 (2015).
61. J. F. Poulin, G. Caronia, C. Hofer, Q. Cui, B. Helm, C. Ramakrishnan, C. S. Chan, D. A. Dombeck, K. Deisseroth, R. Awatramani, Mapping projections of molecularly defined dopamine neuron subtypes using intersectional genetic approaches. *Nat. Neurosci.* **21**, 1260–1271 (2018).
62. J. N. Tomaio, Y. Li, O. Ghazy, G. H. Pavia, S. Fleury, A. Bilder, J. Nacimba, I. Castillo, W. Hilaire, A. Balogun, L. Abhilash, Y. S. Kim, C. Ramakrishnan, L. E. Fenno, K. Deisseroth, S. Mingote, Aging-related vulnerability in dopamine–glutamate neurons weakens entorhinal dopamine signaling and underlies novelty discrimination deficits. Research Square [Preprint]; https://www.researchsquare.com/article/rs-9321992/v1(2026).
63. A. Matarasso, I. R. Reyes, E. Seaholm, A. Cheeyandira, M. J. Seibert, S. Jagalur, S. C. Piantadosi, L. Li, Y. Li, D. Weinshenker, M. R. Bruchas, Stimulus-dependent dopamine dynamics from locus coeruleus axons. *Cell Rep.* **45**, 117729 (2026).
64. J. Taniguchi, R. Melani, L. Chantranupong, M. J. Wen, A. Mohebi, J. Berke, B. Sabatini, N. Tritsch, Comment on 'Accumbens cholinergic interneurons dynamically promote dopamine release and enable motivation'. bioRxiv 573485 [Preprint] (2024); https://doi.org/10.1101/2023.12.27.573485.
65. H. Y. Liang, Z. J. Chen, H. Xiao, Y. H. Lin, Y. Y. Hu, L. Chang, H. Y. Wu, P. Wang, W. Lu, D. Y. Zhu, C. X. Luo, nNOS-expressing neurons in the vmPFC transform pPVT-derived chronic pain signals into anxiety behaviors. *Nat. Commun.* **11**, 2501 (2020).
66. M. M. Zhang, A. Q. Geng, K. Chen, J. Wang, P. Wang, X. T. Qiu, J. X. Gu, H. W. Fan, D. Y. Zhu, S. M. Yang, Q. Y. Chen, Z. X. Zhou, B. Y. Fan, Y. Bai, K. K. Xing, J. M. Feng, J. D. Wang, Y. Chen, Y. C. Lu, Y. Liang, P. Cao, B. K. Kaang, M. Zhuo, Y. Q. Li, T. Chen, Glutamatergic synapses from the insular cortex to the basolateral amygdala encode observational pain. *Neuron* **110**, 1993–2008.e6 (2022).
67. Y. C. Li, F. C. Zhang, D. Li, R. X. Weng, Y. Yu, R. Gao, G. Y. Xu, Distinct circuits and molecular targets of the paraventricular hypothalamus decode visceral and somatic pain. *Neuron* **112**, 3734–3749.e5 (2024).
68. Y. Hu, Y. Feng, H. Luo, X.-N. Zhu, S. Chen, K. Yang, Z. Deng, M. Luo, W. Du, Q. Wang, S. Wang, K. Wei, J. Hu, Y. Wang, Dissociation-related behaviors in mice emerge from the inhibition of retrosplenial cortex parvalbumin interneurons. *Cell Rep.* **44**, 115086 (2024).
69. M. Yilmaz, M. Meister, Rapid innate defensive responses of mice to looming visual stimuli. *Curr. Biol.* **23**, 2011–2015 (2013).
70. D. J. McGovern, A. M. Polter, D. H. Root, Neurochemical signaling of reward and aversion to ventral tegmental area glutamate neurons. *J. Neurosci.* **41**, 5471–5486 (2021).
71. G. De Franceschi, T. Vivattanasarn, A. B. Saleem, S. G. Solomon, Vision guides selection of freeze or flight defense strategies in mice. *Curr. Biol.* **26**, 2150–2154 (2016).
72. D. H. Root, D. J. Estrin, M. Morales, Aversion or salience signaling by ventral tegmental area glutamate neurons. *iScience* **2**, 51–62 (2018).
73. D. J. McGovern, A. Phillips, A. Ly, E. D. Prévost, L. Ward, K. Siletti, Y. S. Kim, L. E. Fenno, C. Ramakrishnan, K. Deisseroth, M. V. Baratta, C. P. Ford, D. H. Root, Salience signaling and stimulus scaling of ventral tegmental area glutamate neuron subtypes. *J. Neurosci.* **45**, e1073242025 (2025).
74. H. L. Wang, J. Qi, S. Zhang, H. Wang, M. Morales, Rewarding effects of optical stimulation of ventral tegmental area glutamatergic neurons. *J. Neurosci.* **35**, 15948–15954 (2015).
75. D. J. McGovern, A. M. Polter, E. D. Prevost, A. Ly, C. J. McNulty, B. Rubinstein, D. H. Root, Ventral tegmental area glutamate neurons establish a mu-opioid receptor gated circuit to mesolimbic dopamine neurons and regulate opioid-seeking behavior. *Neuropsychopharmacology* **48**, 1889–1900 (2023).
76. J. Miranda-Barrientos, I. Chambers, S. Mongia, B. Liu, H. L. Wang, G. E. Mateo-Semidey, E. B. Margolis, S. Zhang, M. Morales, Ventral tegmental area GABA, glutamate, and glutamate-GABA neurons are heterogeneous in their electrophysiological and pharmacological properties. *Eur. J. Neurosci.* **54**, 4061–4084 (2021).
77. N. Chuhma, S. Mingote, H. Moore, S. Rayport, Dopamine neurons control striatal cholinergic neurons via regionally heterogeneous dopamine and glutamate signaling. *Neuron* **81**, 901–912 (2014).
78. N. Chuhma, S. Mingote, L. Yetnikoff, A. Kalmbach, T. Ma, S. Ztaou, A.-C. Sienna, S. Tepler, J.-F. Poulin, M. Ansorge, R. Awatramani, U. J. Kang, S. Rayport, Dopamine neuron glutamate cotransmission evokes a delayed excitation in lateral dorsal striatal cholinergic interneurons. *eLife* **7**, e39786 (2018).
79. C. P. Ford, G. P. Mark, J. T. Williams, Properties and opioid inhibition of mesolimbic dopamine neurons vary according to target location. *J. Neurosci.* **26**, 2788–2797 (2006).
80. F. Cacciapaglia, M. P. Saddoris, R. M. Wightman, R. M. Carelli, Differential dopamine release dynamics in the nucleus accumbens core and shell track distinct aspects of goal-directed behavior for sucrose. *Neuropharmacology* **62**, 2050–2056 (2012).
81. D. A. Sackett, M. P. Saddoris, R. M. Carelli, Nucleus accumbens shell dopamine preferentially tracks information related to outcome value of reward. *eNeuro* **4**, ENEURO.0058-17.2017 (2017).
82. S. J. Cragg, M. E. Rice, DAncing past the DAT at a DA synapse. *Trends Neurosci.* **27**, 270–277 (2004).
83. P. W. Kalivas, P. Duffy, Selective activation of dopamine transmission in the shell of the nucleus accumbens by stress. *Brain Res.* **675**, 325–328 (1995).
84. J. W. de Jong, S. A. Afjei, I. Pollak Dorocic, J. R. Peck, C. Liu, C. K. Kim, L. Tian, K. Deisseroth, S. Lammel, A neural circuit mechanism for encoding aversive stimuli in the mesolimbic dopamine system. *Neuron* **101**, 133–151.e7 (2019).
85. A. Badrinarayan, S. A. Wescott, C. M. Vander Weele, B. T. Saunders, B. E. Couturier, S. Maren, B. J. Aragona, Aversive stimuli differentially modulate real-time dopamine transmission dynamics within the nucleus accumbens core and shell. *J. Neurosci.* **32**, 15779–15790 (2012).

Downloaded from https://www.science.org at University of Colorado Boulder on November 21, 2026

86. S. B. Floresco, The nucleus accumbens: An interface between cognition, emotion, and action. *Ann. Rev. Psychol.* **66**, 25–52 (2015).
87. D. V. Wang, T. Viereckel, V. Zell, A. Konradsson-Geuken, C. J. Broker, A. Talishinsky, J. H. Yoo, M. H. Galinato, E. Arvidsson, A. J. Kesner, T. S. Hnasko, A. Wallen-Mackenzie, S. Ikemoto, Disrupting glutamate co-transmission does not affect acquisition of conditioned behavior reinforced by dopamine neuron activation. *Cell Rep.* **18**, 2584–2591 (2017).
88. G. C. Lopez, L. D. Van Camp, R. F. Kovaleski, M. D. Schaid, V. N. Sherathiya, J. M. Cox, T. N. Lerner, Region-specific nucleus accumbens dopamine signals encode distinct aspects of avoidance learning. *Curr. Biol.* **35**, 2433–2443.e5 (2025).
89. N. Chuhma, W. Y. Choi, S. Mingote, S. Rayport, Dopamine neuron glutamate cotransmission: Frequency-dependent modulation in the mesoventromedial projection. *Neuroscience* **164**, 1068–1083 (2009).
90. H. Hirai, K. Konno, M. Yamasaki, M. Watanabe, T. Sakaba, Y. Hashimotodani, Distinct release properties of glutamate/GABA co-transmission serve as a frequency-dependent filtering of supramammillary inputs. *eLife* **13**, RP99711 (2024).
91. E. Svensson, J. Apergis-Schoute, G. Burnstock, M. P. Nusbaum, D. Parker, H. B. Schiöth, General principles of neuronal co-transmission: Insights from multiple model systems. *Front. Neural Circuits* **12**, 117 (2019).
92. M. E. Rice, S. J. Cragg, Nicotine amplifies reward-related dopamine signals in striatum. *Nat. Neurosci.* **7**, 583–584 (2004).
93. R. Cachope, Y. Mateo, B. N. Mathur, J. Irving, H. L. Wang, M. Morales, D. M. Lovinger, J. F. Cheer, Selective activation of cholinergic interneurons enhances accumbal phasic dopamine release: Setting the tone for reward processing. *Cell Rep.* **2**, 33–41 (2012).
94. J. H. Shin, M. F. Adrover, V. A. Alvarez, Distinctive modulation of dopamine release in the nucleus accumbens shell mediated by dopamine and acetylcholine receptors. *J. Neurosci.* **37**, 11166–11180 (2017).
95. S. Threlfell, T. Lalic, N. J. Platt, K. A. Jennings, K. Deisseroth, S. J. Cragg, Striatal dopamine release is triggered by synchronized activity in cholinergic interneurons. *Neuron* **75**, 58–64 (2012).
96. P. F. Kramer, S. G. Brill-Weil, A. C. Cummins, R. Zhang, G. A. Camacho-Hernandez, A. H. Newman, M. A. G. Eldridge, B. B. Averbeck, Z. M. Khaliq, Synaptic-like axo-axonal transmission from striatal cholinergic interneurons onto dopaminergic fibers. *Neuron* **110**, 2949–2960.e4 (2022).
97. L. E. Fenno, J. Mattis, C. Ramakrishnan, M. Hyun, S. Y. Lee, M. He, J. Tucciarone, A. Selimbeyoglu, A. Berndt, L. Grosenick, K. A. Zalocusky, H. Bernstein, H. Swanson, C. Perry, I. Diester, F. M. Boyce, C. E. Bass, R. Neve, Z. J. Huang, K. Deisseroth, Targeting cells with single vectors using multiple-feature Boolean logic. *Nat. Methods* **11**, 763–772 (2014).
98. L. McInnes, J. Healy, J. Melville, Umap: Uniform manifold approximation and projection for dimension reduction. arXiv:1802.03426 [stat.ML] (2018).
99. A. Narayan, B. Berger, H. Cho, Assessing single-cell transcriptomic variability through density-preserving data visualization. *Nat. Biotechnol.* **39**, 765–774 (2021).
100. J. Healy, L. McInnes, Uniform manifold approximation and projection. *Nat. Rev. Methods Primers* **4**, 82 (2024).
101. S.-J. Bouchard, J. Boutin, M. Lévesque, V. Breton-Provencher, System-wide dissociation of reward and aversive dopaminergic signals. bioRxiv 656467 [Preprint] (2025); https://doi.org/10.1101/2025.05.27.656467.
102. F. P. Hamers, A. J. Lankhorst, T. J. van Laar, W. B. Veldhuis, W. H. Gispen, Automated quantitative gait analysis during overground locomotion in the rat: Its application to spinal cord contusion and transection injuries. *J. Neurotrauma* **18**, 187–201 (2001).
103. G. C. Koopmans, R. Deumens, W. M. M. Honig, F. P. T. Hamers, H. W. M. Steinbusch, E. A. J. Joosten, The assessment of locomotor function in spinal cord injured rats: The importance of objective analysis of coordination. *J. Neurotrauma* **22**, 214–225 (2005).
104. L. M. Lueptow, Novel object recognition test for the investigation of learning and memory in mice. *J. Vis. Exp.* **2017**, 55718 (2017).
105. J. Ting, T. Daigle, Q. Chen, G. Feng, Patch-clamp methods and protocols. *Methods Mol. Biol.* **1183**, 1–21 (2014).
106. C. S. Nunemaker, R. A. DeFazio, S. M. Moenter, A targeted extracellular approach for recording long-term firing patterns of excitable cells: A practical guide. *Biol. Proced. Online* **5**, 53–62 (2003).
107. R. N. Lippert, A. L. Cremer, S. Edwin Thanarajah, C. Korn, T. Jahans-Price, L. M. Burgeno, M. Tittgemeyer, J. C. Brüning, M. E. Walton, H. Backes, Time-dependent assessment of stimulus-evoked regional dopamine release. *Nat. Commun.* **10**, 336 (2019).
108. G. Mongillo, O. Barak, M. Tsodyks, Synaptic theory of working memory. *Science* **319**, 1543–1546 (2008).

Acknowledgments: We thank L. Watkins (University of Colorado Boulder) for assistance with gait and motor analyses and R. Rowe (University of Colorado Boulder) for the use of her slide scanner. Additional imaging was performed at the University of Colorado Boulder BioFrontiers Institute's Advanced Light Microscopy Core (RRID: SCR_018302). Laser scanning confocal microscopy was performed on a Nikon A1R microscope supported by NIST-CU Cooperative Agreement award number 70NANB15H226. GraphPad Prism, Adobe Photoshop, and BioRender.com were used to generate figures and schematics. **Funding:** This work was supported by National Institutes of Health, National Institute on Drug Abuse grant DA047443 (D.H.R.); National Institutes of Health, National Institute of Mental Health grant MH130576 (D.H.R.); National Institutes of Health, National Institute of Mental Health grant MH137472 (D.H.R.); National Institutes of Health, National Institute of Mental Health grant MH122712 (A.M.P.); National Institutes of Health, National Institute on Drug Abuse grant DA062470-01A1 (E.D.P.); a State of Colorado Institute for Cannabis Research grant (D.H.R.); and a University of Colorado ABNexus grant (D.H.R.). The content is solely the responsibility of the authors and does not necessarily represent the official views of the National Institutes of Health. The funders had no role in study design, data collection and analysis, decision to publish, or preparation of the manuscript. **Author contributions:** Conceptualization: E.D.P. and D.H.R. Methodology: E.D.P., D.H.R., J.B., A.M.P., Z.P.K., S.F., Y.S.K., L.E.F., C.R., and K.D. Software: D.H.R., Z.P.K., and F.S.d.S. Formal analysis: E.D.P., D.H.R., A.M.P., F.S.d.S., and Z.P.K. Investigation: E.D.P., L.A.W., D.A., G.A.A., S.K.I., K.F., M.D., J.P., K.P., A.M.P., and S.F. Visualization: E.D.P., D.H.R., F.S.d.S., A.M.P., and Z.P.K. Supervision: D.H.R. and A.M.P. Writing—original draft: E.D.P. and D.H.R. Writing—review and editing: E.D.P., D.H.R., A.L., J.B., A.M.P., Z.P.K., and F.S.d.S. **Competing interests:** Y.S.K., L.E.F., and K.D. are inventors on US Patent US20230064644A1 held by Stanford University that covers INTRSECT vectors. All other authors declare that they have no competing interests. **Data, code, and materials availability:** All data needed to evaluate the conclusions in the paper are present in the paper or the Supplementary Materials. All viral vectors used are commercially available except for AAVs encoding COFO-oScarlet, which can be provided by K.D. with a material transfer agreement. The data have been uploaded to doi:10.25452/figshare.plus.33065138. MATLAB code for reproducing model time series and statistical tests is available at Zenodo (https://doi.org/10.5281/zenodo.20046374).

Submitted 26 November 2025
Accepted 29 July 2026
Published 18 August 2026
10.1126/scisignal.aee2028

Downloaded from https://www.science.org at University of Colorado Boulder on November 21, 2026

Science Signaling

Distinct properties of glutamate-dopamine, nonglutamate-dopamine, and glutamate-only ventral tegmental area neurons

Emily D. Prévost, Lucy A. Ward, Daniel Alas, Giulia A. Aimale, Sara K. Ikenberry, Katie Fox, Melissa Deming, Julianne Pelletier, Annie Ly, Jayson Ball, Zachary P. Kilpatrick, Kailyn Price, Abigail M. Polter, Fabio Simões de Souza, Suzanne Fulgham, Yoon Seok Kim, Lief E. Fenno, Charu Ramakrishnan, Karl Deisseroth, and David H. Root

Sci. Signal. **19** (951), eaee2028. DOI: 10.1126/scisignal.aee2028

Editor's summary

The dopaminergic neurons in the ventral tegmental area (VTA) of the brain regulate learning and behavioral adaptations in response to rewarding and aversive events. They are often analyzed as a single population or by their location in the VTA. Using intersectional genetic strategies to target neurons in VTA that transmit dopamine or glutamate alone or together, Prévost *et al.* found that the neurotransmitters released reliably correlated with the neurons' behavioral functions and signaling dynamics. In VTA neurons that cotransmitted dopamine and glutamate, dopamine synthesis and glutamate vesicular packaging were involved with aversion- and reward-based learning, respectively. These findings provide molecular definitions of the dopaminergic VTA neurons that regulate motivated behavior. —Wei Wong

View the article online

https://www.science.org/doi/10.1126/scisignal.aee2028

Permissions

https://www.science.org/help/reprints-and-permissions

Use of this article is subject to the Terms of service

Science Signaling (ISSN 1937-9145) is published by the American Association for the Advancement of Science. 1200 New York Avenue NW, Washington, DC 20005. The title *Science Signaling* is a registered trademark of AAAS.

Copyright © 2026 The Authors, some rights reserved; exclusive licensee American Association for the Advancement of Science. No claim to original U.S. Government Works

Downloaded from https://www.science.org at University of Colorado Boulder on November 21, 2026